Enhancing efficiency of TCO-less tandem dye sensitized solar cells by architecture optimization

DISSERTATION
FOR THE DEGREE OF
DOCTOR OF PHILOSOPHY

AJAY KUMAR BARANWAL

SUPERVISOR

PROF. SHUZI HAYASE

DIVISION OF GREEN ELECTRONICS
GRADUATE SCHOOL OF LIFE SCIENCE AND SYSTEMS ENGINEERING
KYUSHU INSTITUTE OF TECHNOLOGY

January 2016

Abstract

Extensive use of fossil fuels to circumvent our current energy needs and their limited availability along with climate change due to greenhouse effect lead to the serious thinking about the logical implementation of renewable energy resources. Photovoltaic technologies enables us the direct utilization of solar energy in the form of electrical energy. The clean energy generation using renewable energy resource must be accomplished considering the cost effectiveness with existing power generating technologies. Dye sensitized solar cells (DSSCs), kind of excitonic solar cells have attained the rampant popularity among the existing solar cells due to its ease of fabrication and cost effective nature. DSSCs have achieved comparable photoconversion efficiency as that of amorphous Si solar cell and are on the verge of commercialization.

Apart from focus being directed to achieve the cost effectiveness and stability, further enhancement in the power conversion efficiency is inevitable to compete with traditional silicon based solar cells. In order to enhance photoconversion efficiency, tandem DSSCs has been approached where the two different cells having complementary absorption spectra are mechanically stacked. This thesis work is directed to avoid and alter the precious transparent conductive oxide (TCO) glass being commonly used in the conventional tandem device architectures aiming towards the fabrication of photon flux efficient novel tandem DSSCs architectures in combination with near infra-red (NIR) photon harvesting novel sensitizers. To begin with this compilation, focus has been centralized on the energy thrust promoted existing and current research status for solar cells in general and next generation solar cells in particular. The trend has followed the first ever demonstrated practical solar cell from bell lab to mature Si solar cell technology. The technology enhancement pave the way for thin film solar cell research. Diverse application of solar cell for indoor and outdoor applications have necessitated the flexible solar cell research. Dye sensitized solar cells (DSSCs) possess these properties and have drawn attention due to its environmental friendly properties. Limitation to achieve high performance for DSSCs are outlined along with the discussion about the need for extending the photon harvesting window.

The photoconversion efficiency of DSSCs can be increased beyond the limit of a single cell by stacking multiple DSSCs with the complementary light absorption followed by photon harvesting. Conventional series connected and mechanically stacked tandem DSSCs bearing four TCO glass plates fabricated and its functioning was verified with external power conversion efficiency of 6.28% under simulated solar irradiation. Aiming towards reduction of fabrication cost, a novel tandem device architecture was proposed by stacking top cell TCO-DSSC and TCO-less back contact bottom cell DSSCs. This TCO-less bottom-cell DSSC was consisted of flexible and protected SUS metal mesh coated with dye adsorbed nanoporous TiO_2 functioning as photoanode. The model sensitizing dyes D131 and N719 were utilized as photosensitizers for top cell and bottom cell respectively. The fabricated tandem device architecture have shown the practicality in terms of increased optical transmission (around 20%) at bottom cell by avoiding the intermediate TCO glass. To enable the flexible processing and more economical tandem device architecture, bottom cell counter electrode was also replaced with flexible titanium (Ti) foil leading to the enhanced photoconversion efficiency of 7.10 % which is not only better than individual cell but the conventional mechanically stacked four TCO base tandem DSSCs also.

After the demonstration of proof-of concept using model dyes for TCO-less tandem DSSCs having capability of photon harvesting mainly in the visible region of solar spectrum, effort as directed to enhance the photon harvesting window by utilizing NIR light harvesting axially ligated Si-phthalocyanine dye in the TCO-less bottom cell. Efficient photoconversion was demonstrated having photon harvesting up to 900 nm. Conventional tandem DSSCs using four TCO glass was first fabricated using this NIR dye for the bottom cell in combination with N719 for the top cell with the efficiency of 6.58%. In order to provide the flexibility to the tandem DSSCs, ITO-PET film having similar resistivity and enhanced transparency compared to ITO glass was utilized for the top cell. This flexible film has been incorporated to mechanically stack this top cell DSSC with TCO-less back contact bottom DSSCs using Ti foil as counter electrode aiming towards the flexible TCO-less tandem DSSCs architecture. This resulting flexible tandem TCO-less DSSCs exhibited enhanced optical transmission (around 30%) and external power conversion efficiency of 7.19%.

Table of Contents

Chapter 1

Introduction

1.1 Motivation:

Solar irradiation is the single most generous energy source on our planet earth. From ancient era, human life solely relied upon renewable form of solar energy by taking advantage of indirect form like biomass, wind and direct form like lightning or heat. At the beginning of 20th century with the rise of civilized society lead spurt in demand of energy, fossil fuel like oil, gas and coal came into picture [1]. Fossil fuel energy resources inherit a very high energy density and possess flexibility in transportation and storage capacity making them viable to meet 80% of world energy demand by 2040 [2]. On the other hand in coming future with the ever increase in population, total energy requirement engendered consumption will forge world energy demand projection very intense. Considering the similar population growth and standard of human being, the world energy consumption rate is expected to grow and is projected to double from 13.5 TW in 2001 to 27 TW by 2050 and to triple of 43 TW by 2100 [3]. It has been estimated that the fossil energy resources could support a 25 to 30 TW energy consumption rate globally for at least several centuries [3]. The continued fossil energy resource utilization generates environmental issue such as global warming, water supply, land use, thermal pollution and their adverse impact on weather and climate cannot be ignored. As a result, these concerns have led to encouragement for research for advancement in alternate green energy technology which are renewable and clean energy resources. Different kind of renewable energy resources have been well documented like solar energy, wind energy, geothermal energy and hydroelectric energy as shown in Fig. 1 [4].

Among all known renewable energy resources, solar energy is by far the largest exploitable resource, enriching more energy in 1 hour to the earth than all of the energy consumed by humans in an entire year. Moreover solar energy is abundant and clean in nature, placing it very high promising energy resource. It has been estimated that world's land and ocean surface receives

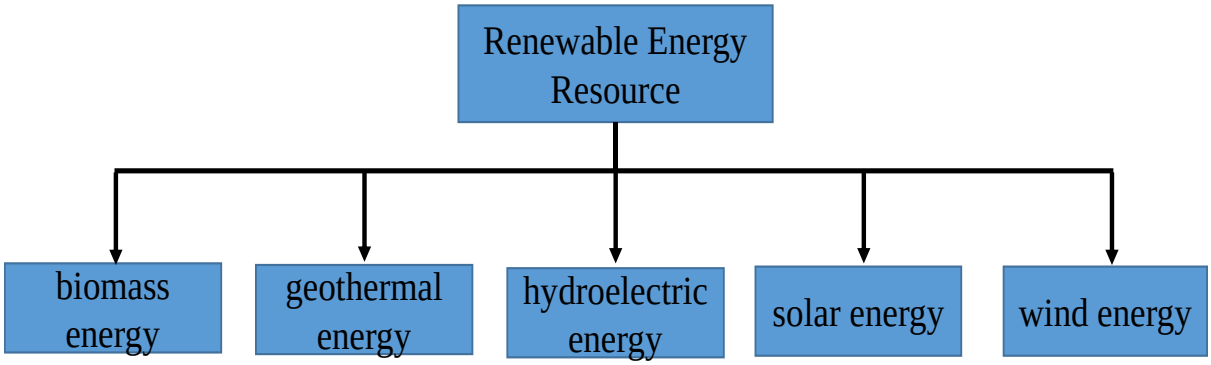

Figure 1. Different kind of renewable energy resources.

6500 TW sunlight if all can be used to power photovoltaics and is available freely [5-8]. Photovoltaics effect is phenomenon under which solar energy is being converted to electricity directly using semiconducting materials. In 1954, Bell lab first unveiled the practical solar cell which eventually lead to modern solar cell technology [9]. It was the year 1956 when PV module (together connected various solar cell) with increased power output from watts (W) to megawatts (MW) were available commercially. Table 1 shows the comparison of different renewable sources over worldwide power available, power in high energy locations, power in likely developable locations and current power delivered as electricity [8]. Globally 6500 TW solar power is available and currently only 0.0013 TW is being exploited. However the probable developing locations have the capacity to generate 340 TW solar power and concentrated solar power demonstrate 240 TW capacity. Even though hydroelectric energy current delivered power exceed all other power sources but have been already exploited a lot and no further harvesting potential is feasible. Geothermal energy lies below deep inside the earth and is not practical to extract. Wave power exploration is possible near costal area and accomplishing it not a practically possible approach. Overall there is enough feasibly viable solar power supply practicable to world in comparison to other existing energy technology empowering it obvious choice for future energy demand. Depending upon the manufacturing process and techniques, type of absorbing materials used, the solar cell technologies can be broadly classified as according to Fig. 2.

Table 1. Available power worldwide in energy resources [8].

Energy Technology	Wind	Wave	Geothermal	Hydroelectric	Tidal	Solar PV	Concentrated Solar Power
Power world wise (TW)	1700	>2.7	45	1.9	3.7	***6500***	**4600**
Power in high Energy locations (TW)	72-170	2.7	2	<1.9	0.8	***1300***	**920**
Power in likely-developable locations (TW)	40-85	0.5	0.07-0.14	1.6	0.02	***340***	**240**
Current Power delivered as electricity (TW)	0.02	0.000002	0.0065	0.32	0.00006	***0.0013***	**000046**

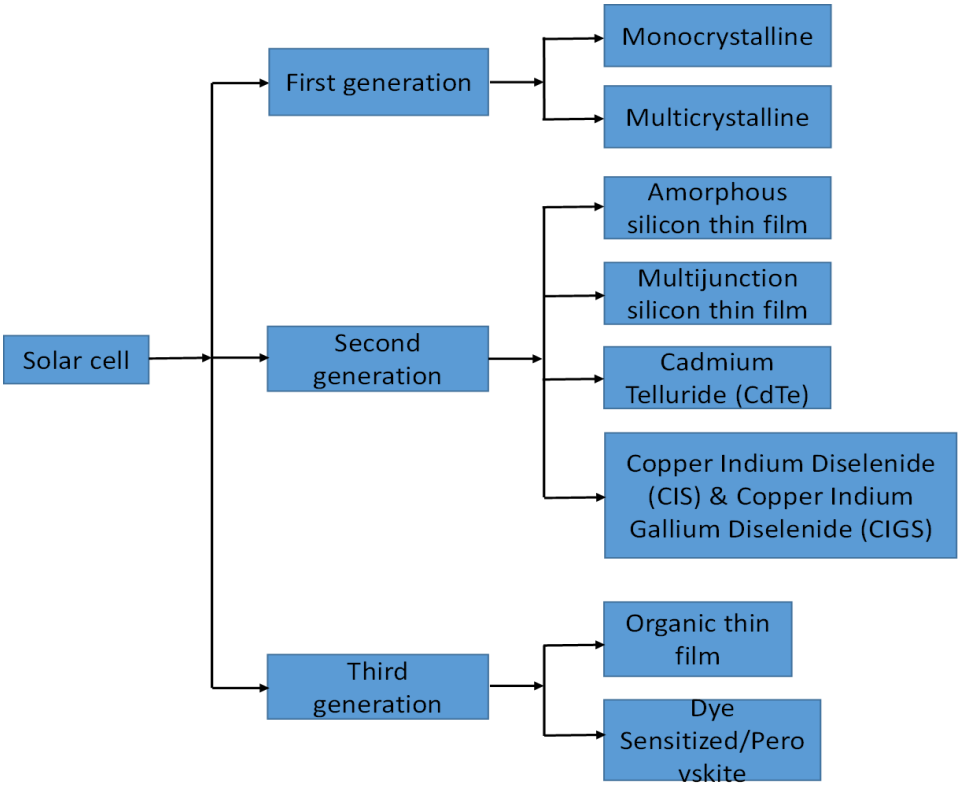

Figure 2. Classification of various solar cell technology.

1.2 Photovoltaic technologies:

The different generation solar cells have their significant advantages and their specification have been enlisted in Table 2.

Table 2. Different kind of solar energy specification [10-15].

Solar cell	Advantages	Disadvantages	Status	Efficiency/ Type
Crystalline silicon	High efficiencies	large amount Si wafer is needed, vacuum process needed	Mature technology, long established at industrial scale	(25.6%)/ Semiconductor
Multi junction gallium-indium phosphide (GaInP), gallium arsenide (GaAs) and germanium (Ge)	Traditionally used in space, have highest efficiencies	Crystalline layer production and expensive	At research stage, trend towards increased terrestrial applications in combination with light concentrators	(30-40%)/ Semiconductor
Thin Film	Conventional Si solar cell uses wafers of hundred micrometers thicker due to extinction coefficient limitation. Thin film technology enables nanometers across active layer for light harvesting and the fabrication process is governed by simple printing technique enabled by vacuum process and sputtering system. Dye sensitized solar cells, Organic solar cells, employs the dyes or molecules of nanometers thick and have shown potential towards future industrial applications. The fabrication process of these prospective solar cells does not need ultra-pure materials making it cost effective alternate viable source.			
Nano and Amorphous Si	Has found application as thin film unlike crystalline solar cell	Have shown comparably lower efficiency	Stability is an issue and degrades with light/moisture	(10.2%)/ Semiconductor
Cadmium Telluride (CdTe)	Performances are good at lower light levels	Cadmium is toxic material	Mature technology	(21.0%)/ Semiconductor
Copper Indium Gallium Diselenide (CIGS)	Better efficiency among thin film solar cells. Shows better resistance to heat than Si solar panel. The active layer can be in polycrystalline form	Cost of fabrication is high than polycrystalline Si, CdTe solar cell	At industrial scale	(20.5%)/ Semiconductor

Solar cell	Advantages	Disadvantages	Status	Efficiency/ Type
Dye sensitized solar cell	Good performance at low light intensity and acceptance of wide angle	Solvent & electrolyte electrochemical system	Moving from development to deployment	(14%)/ The process is very similar to photosynthesis
Organic solar cell	Potentially known cheapest solar cell	Have poor efficiency, poor stability	Research stage	(11%)/ Uses organic semiconductors
Perovskite solar cell	Rapid efficiency growth	Poor stability, Pb is toxic material	Not mature technology and at research stage	(20.1%)/ uses organo-inorganic semiconductor

1.3 Flexible solar cell:

With the rise in scale of industrialization, flexible solar cells are attaining interest and viability. The interest on flexible solar panels can be traced to the era of space missions in the 1960s (Crabb & Treble, 1967; Ray, 1967). At the meantime, flexible power sources capable of providing power in the 1 to 50-kW range with the advent of compact, reliable, and lightweight was an issue. To address these issues, the large area of R&D of solar cells were devoted on study of flexible solar cell [16]. Energy is obligation of time and indoor and outdoor application of electronic devices need to be independent by generating their own energy. Flexible devices places themselves suitable to diverse acceptance owing to its flexible usage. Flexible solar modules are light weight and possesses the faster payback time than conventional PV modules [17]. They can be classify by following three categories.

Si flexible solar cell:

Crystalline Si solar cell have achieved considerable market share due to its high abundance, broad spectral absorbance and mature technology [18]. By exploring these advantages in 2006, Berge and Werner et al have achieved a considerable efficiency of 14.6%. They employed the epitaxial growth and layer transfer process (ELTRAN) and fabricated the flexible solar cell of 150 nm diameter, sandwiched in two plastic sheets [19]. However the process and photovoltaic performance was highly dependent towards substrate in use for growth and transfer. By taking advantage of properties of porous silicon as a substrate, Solexel have demonstrated a record 20.1% efficiency, with 156 mm^2 flexible c-Si solar cell in 2012 [20]. With etch release approach device fabrication processes 14.9% efficiency has been achieved for hexagonal shaped silicon segments

of 14μm thickness [21]. Using simple exfoliated method and by using 3 μm thicker mono crystalline Si, IBM have reported 4.3% efficiency [22]. The obtained efficiency was considered be low due to low thickness of Si. Saha et al have increased the Si thickness across 25 μm and with utilizing Si foil the efficiency reported was 14.9% [23].

Amorphous Si solar cell have the property of greater resistance to heat and development process proclaims less prone to brokage. Fuji Electric have developed a-Si:H/a-SiGe:H based tandem solar cells on polyimide plastic substrate with 9% stabilized efficiency on large area scale of 40*80 cm^2 [24]. A triple junction ultra-light weight a-Si:H/a-SiGe:H/a-SiGe:H solar cell with efficiency 9.84% and with specific power 1200 W/kg, using roll-roll process on 25μm plastic substrate has been reported by Unisolar [25].

Flexible Compound Solar cells:

Flexible CdTe solar cells:

They have shown ease of manufacturing process and by employing this architecture, First solar have manufactured the solar panel with 1$/MW. Recently in 2014, First solar achieved 21% module efficiency on 1.06cm^2 aperture area for CdTe thin film solar cell [26]. In 1990 the attempts were initiated and on metallic molybdenum foil substrate, CdTe solar cell have been fabricated with 7.8% efficiency. In 2013 utilizing flexible metal foil substrates 11.5% efficiency has been demonstrated [27]. Latter on using polyimide substrate a well-known polymer for flexible devices, 13.8% record efficiency has been achieved in superstrate configuration [28].

Flexible CIGS solar cells:

CIGS solar panels are popular among 2nd generation thin film solar cells. In 1993 International Solar Electronic Technology demonstrated the first flexible CIGS solar cell on Mo substrates with 8.3% efficiency [29]. By continuous and considerable efforts, in 2010 AIST (Japan) were capable to attain the module efficiency of 14% on Mo substrate [30]. Apart from Mo foil, metal foils has shown considerable flexibility and temperature acceptability in fabrication of flexible devices [31]. In 2012 using mild steel foil as substrate the reported certified efficiency was 17.6% [32]. Utilizing Al foil, Nanosolar, a US based company has obtained the efficiency of 17.1%. Yagioka et al have reported a considerable efficiency of 17.9% on flexible Ti foil [33]. Up to date

the maximum attained flexible CIGS efficiency has been reported on polyimide polymer substrate with 18.7% [34].

Flexible GaAs solar cells:

GaAs solar cells are specifically used in space applications. Sharp Corporation has first demonstrated paper like InGaP/GaAs solar cells on flexible metal film with 29.4% efficiency [35-36]. Japan Aerospace Exploration agency (JAXA) in 2012 demonstrated a large area (26.6 cm^2) InGaP/GaAs solar cells, laminated with polymer film and obtained efficiency was 20.4% [37].

Flexible organic solar cells:

Organic solar cells have attracted a lot of attention due to economical alternative of Si solar cell. Traditionally Indium Tin oxide (ITO) glass has been used in the fabrication of organic solar cells. The flexible organic solar cell has been fabricated by the usage of ITO-PET substrate, ITO-PEN film, PET film with PEDOT:PSS, Graphene, Carbon nanotube. The transparency and conductivity issues has been simultaneously resolved by the silver nanowire and copper nanowire. Utilizing these transparent electrodes 2-5% efficiency has been achieved [38-46]. The flexible dye sensitized solar cells (DSSCs) are fabricated and their performance have been summarized in Table 3.

Table 3. The performance of flexible DSSC comparison

Device Description	**η (%)**	**Comments**	**Ref**
Ti/TiO_2/N719/electrolyte/Pt/ITO	7.2	Ti metal foil as a substrate	48
StS/ITO/TiO_2/N719/electrolyte/Pt/ITO	8.6	Stainless steel was coated treated with ITO before TiO_2 treatment	49
PEN/ITO/TiO_2/N719/electrolyte/Pt/ITO	8.1	Using doctor blade method and compression as a post deposition treatment. Uses water based low temp TiO_2 paste	50
PEN/ITO/TiCl4/TiO_2/N719/electrolyte/Pt/ITO	7.5	CIP compression on TiO_2 paste. $TiCl_4$ treated	51
PEN/ITO/TiO_2/N719/electrolyte/electrolyte/Pt/ITO	6.3	CIP compression was utilized on TiO_2 in ethanol	52

1.4 Dye sensitized solar cells (DSSCs):

The research on solar cell have achieved a rapid growth and is evident from the number of publications available (around 20,000) in 2014 itself (web of science, by putting keyword "solar cell"). In 1893 the French scientist Becquerel, has invented the photovoltaic effect according to which incident light upon a semiconductor material generates the voltage difference [47]. The generation of electric current or voltage is the property of material. In 1991, O Regan and Gratzel firstly demonstrated the dye stained solar cell known as DSSCs [56]. Among the three generation solar cells, DSSCs have drawn attention due to its diverse user friendly properties and high optoelectronic conversion efficiency [53-54]. Intense work have been carried out in the meantime and in 2011 the Texas Instrument have predicted the DSSCs as the world strongest candidate for indoor application module [55].

1.4.1 Architecture with energy diagram of dye sensitized solar cells:

The simple architecture DSSC consist of transparent conductive glass (TCO glass), n type semiconductor, light harvesting medium called sensitizer or dye, electrolyte and counter electrode for dye regeneration. DSSCs working principle have been mimicking the similar process of natural photosynthesis. DSSC architecture is shown in Fig. 3 and energy diagram by Fig. 4.

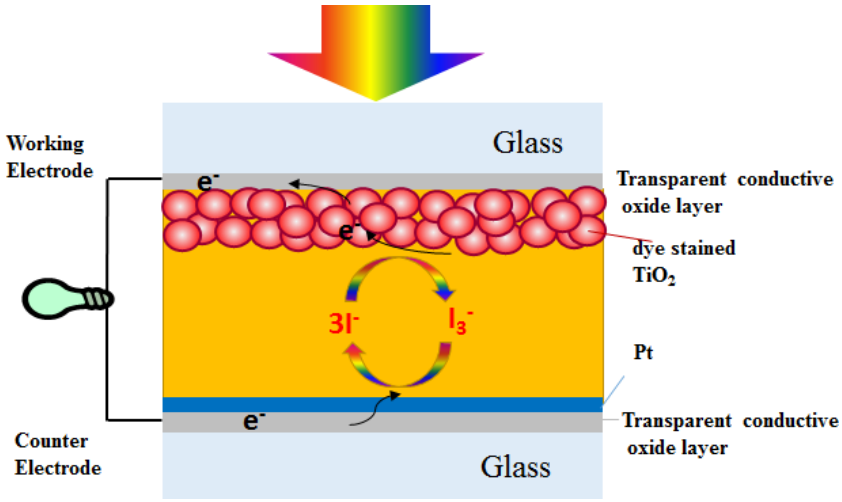

Figure 3. Schematic representation of the components and basic operating principle of DSSC.

1.4.2 Working principle of dye sensitized solar cells:

Upon incident of light on the dye absorbed photoanode layer, dye molecules get excited to form electron-hole pair. At the interface between dyes sensitized semiconductor and electrolyte, charge separation takes place and electron is energetically favored by TiO_2 semiconductor (most commonly used). In contrast to silicon solar cells, DSSCs charge conduction is entirely due to majority charge carriers and conduction takes place by diffusion process. Collected electron at TiO_2 layer is withdrawn at TCO layer and are diffused to outer circuit. Typically TiO_2 nanoparticles are utilized on TCO layer to form high surface area with mesoporous layer. The high surface area TiO_2 is prime and essential for high amount dye loading and is responsible towards light absorption. The nanoparticles employed in DSSCs makes the difference from Si solar cell that it must possess minimum defect level to avoid the electron recombination. The TiO_2 nanoparticles with better interconnectivity and bigger pore size makes the electrolyte diffusion very smoother. However all these properties are interconnected with each other and with lowering in nanoparticle size its surface area increases making decrement in pore size. This generates more grain boundary and can induce more defect levels. The electrons from outer circuit are collected to counter electrode and the regeneration of oxidized dye takes place by catalytic redox shuttle (generally I^-/I^{3-}) layer employed.

1.4.3 Kinetics involved in dye sensitized solar cell:

The main processes involved in the DSSC working along with energy band diagram is shown in Fig. 4. The DSSCs performance is mainly governed by the kinetics of charge dynamic processes involved at the interface of TiO_2, dye and electrolyte. The performance involved can be written in following form:

$$TiO_2/D + h\nu \rightarrow TiO_2/D^* \quad (1)$$

$$TiO_2/D^* \rightarrow TiO_2/D^+ + e_{cb} \quad (2)$$

$$TiO_2/D^+ + e_{cb} \rightarrow TiO_2/D \quad (3)$$

$$2TiO_2/D^+ + 3\,I^- \rightarrow 2TiO_2/D + I_3^- \quad (4)$$

$$2I_3^- + e_{(Pt)} \rightarrow 3/2\,I^- \quad (5)$$

$$I_3^- + 2e_{cb} \rightarrow 3I^- \quad (6)$$

Figure 4 represents the photochemical perspective of the working of DSSC, illustrating the sequence of electron motion and charge motion processes which make the photovoltaic device function. In addition to forward electron and charge motion, this Fig. 4 also shows a variety of competing loss pathways shown by long dotted line. This loss pathways comprises decay of excited dye state to ground state and injected electrons led charge recombination with dye cation and redox shuttle. Every charge transfer step results in an enhanced spatial separation of electrons and holes, which is supposed to increase the life time expectancy of charge separated state. The same functionality make it a close parallel to natural photosynthesis process where energy conversion efficiency is determined by the extent of kinetic competition behavior of various forward and backward electron transfer pathways [57].

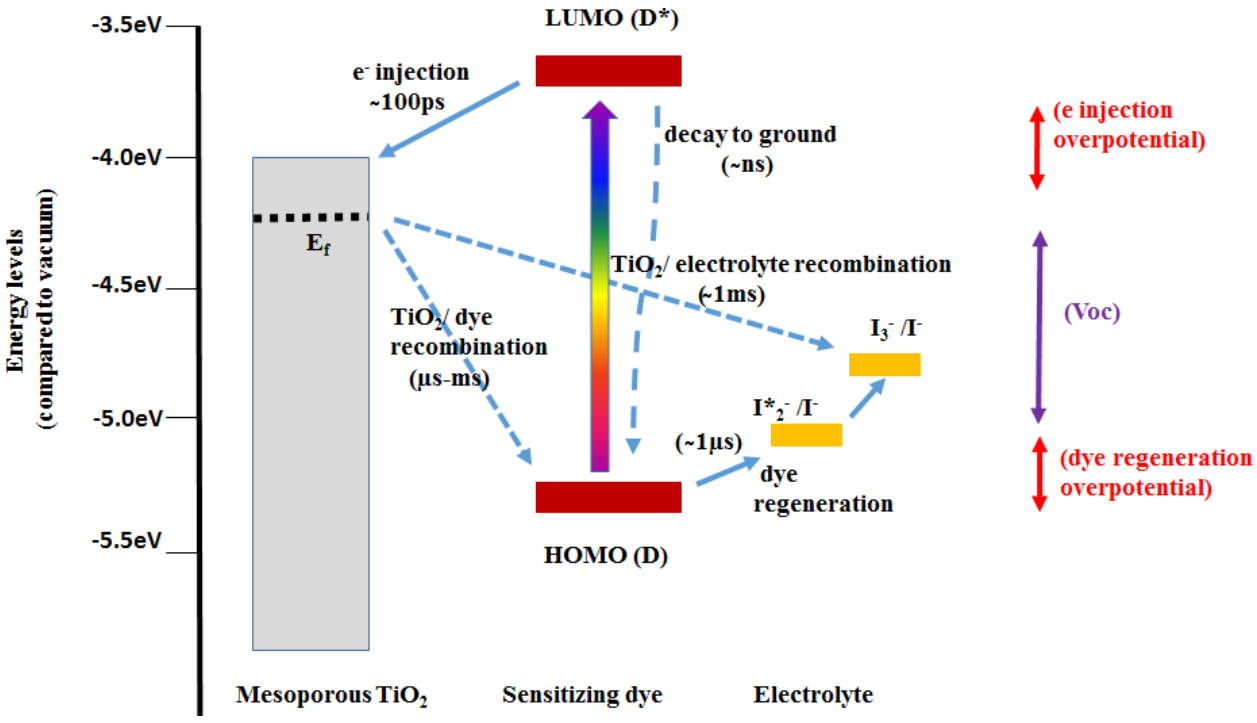

Figure 4. State diagram representation of the kinetics of DSSC function [60-62].

The electron injection dynamics from excited dye state to the TiO_2 conduction band are dependent on the relative energy to the dye excited state oxidation potential. Thus this injection in turn depends on the potential determining ions in electrolyte (e.g. Li^+). The high performance DSSC requires the dye regeneration rate be sufficient and the rate of reduction of dye cation exceeds the rate of recombination of injected electrons with these dye cations. The rate of reduction of dye cation i.e. regeneration of dye exceeds that of dye cation recombination with injected back electrons. This recombination reaction has shown to be dependent upon fermi level of mesoporous film, and therefore cell voltage and light intensity [58-59]. The regeneration behavior have found the dependency towards electrolyte viscosity, iodine concentration and dye structure also [57].

The kinetics of DSSCs charge collection and separation are related to energetic losses as discussed above and are the reason behind the device output voltage (Voc) being significantly less than its optical band gap. Apart from the material composition, the energy losses incurred also depend upon the device operating condition [57].

1.5 Back contact TCO-less dye sensitized solar cell:

Dye sensitized solar cells (DSSCs or Gratzel cell) were first introduced in 1991 by Gratzel and groups as an alternative solar energy resource. Their prospective development have shown the competence as one of promising next generation solar cells. The DSSCs application as photovoltaic devices are most sought towards indoor application having good performance with low light intensity and wide angle variation. The major components involved in DSSCs fabrication are photo anode, redox shuttle and counter electrode. The TCO glass constitutes an important role in holding the dye stained mesoporous layer and in demonstrated Gratzel cell the light is incident from TCO layer. A lot of investigations has been performed to further improve the efficiency with robustness. The photon illumination is incident on TCO glass to energize the dye molecules employed and this employed TCO glass bears the free charge carriers, known to be barrier towards photon transmission. On the other hand rigid and brittle nature of TCO glass generates difficulty in handling purposes. TCO glass constitutes one of important components of DSSCs fabrication and towards fabrication economy it contributes around 16% cost burden [63]. It has been reported that at industrialization scale with rise in production power capacity from 1 MW_{peak}/year to 4 MW_{peak}/year, the TCO layer cost burden contribution will exceeds to 24% [63]. For industrial

aspects the rise in cost contribution of TCO layer is considered as hindrance and efforts are needed to resolve it.

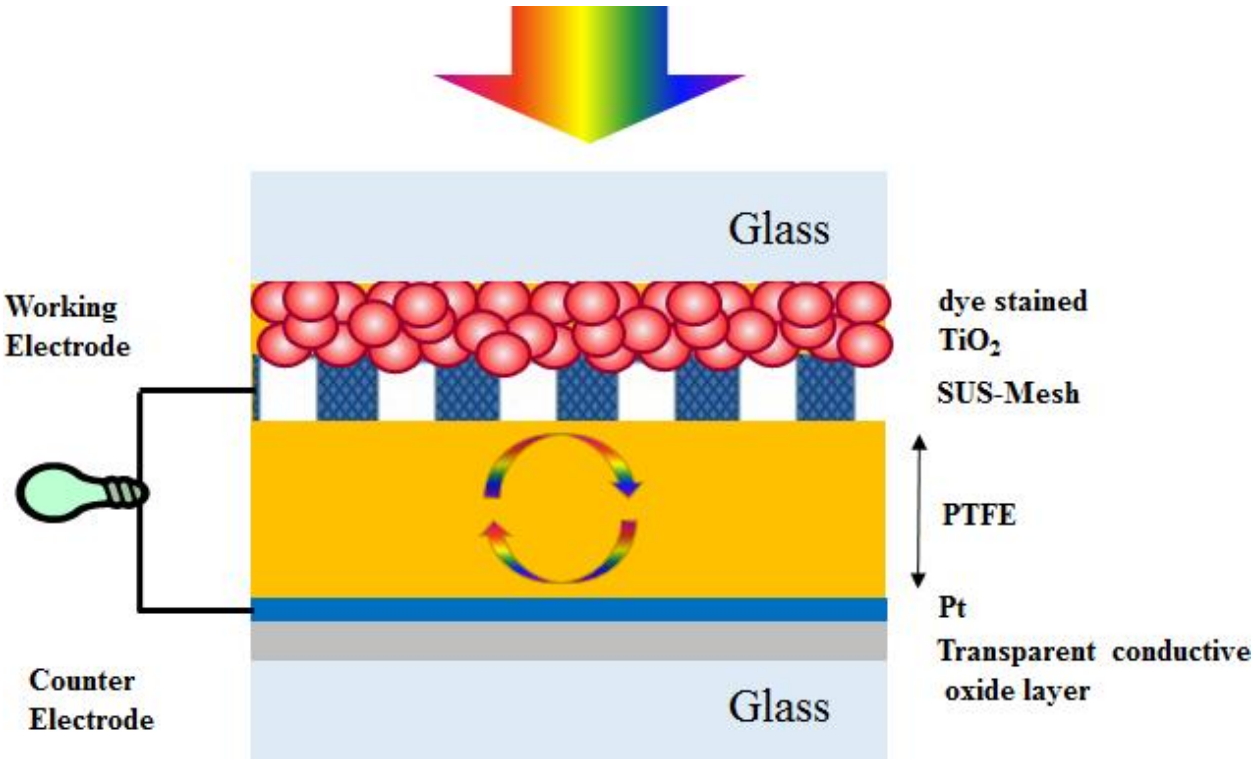

Figure 5. The schematic of back contact TCO-less dye sensitized solar cell.

To address these issues, Fuke et al have published the back contact DSSC architecture where the electrode contact with TiO_2 film is on opposite side of light illumination and naming it back contact structure. Here the photon incidence is directly on dye stained TiO_2 passing through the glass only and providing light efficient TCO-less DSSC structure [64]. The electron extraction process was maintained by vacuum processed Ti, deposited on TiO_2 surface. Latter on Kashiwa et al have published all metal TCO-less back contact DSSC making it completely free of TCO layers [65]. The fabrication process utilizes the active layer of mixture of tetrapod ZnO and nanoparticle TiO_2. For charge extraction the sputtered Titanium (Ti) layer was formed on TiO_2 and ZnO active layer mixture. The tetrapod ZnO properties were utilized to get the straight holes in sputtered Ti

layer which was essential for dye staining and electrolyte insertion. The beauty of this report lies that the obtained efficiency of TCO-less back contact DSSC was similar to that of conventional TCO based DSSCs. In 2014 Zaman et al have utilized the light efficient and economical back contact structure with steel SUS-mesh as electron collecting grid by incorporating Co electrolyte (Fig. 5) [66]. The efficient TCO-less back contact DSSCs architecture has been exploited in many different ways by the fabrication of fiber DSSCs or by cylinder DSSCs [67-68]. The TCO-less back contact DSSCs architectures have pave the way to fabricate the light efficient and economical high performance DSSCs towards futuristic application.

1.6 Efficiency limitation of dye sensitized solar cells:

DSSCs have offered considerable economic and environmental advantages compared to conventional photovoltaic devices owing to easier manufacturing in relatively inexpensive with environment friendly and energy efficient manner [69]. To further achieve a wide spread use of DSSCs, it is imperative to enhance the energy conversion efficiency to greater extent.

The DSSCs efficiency has been provided by following Equation

η = Jsc*Voc*FF/Ir, where Jsc, Voc, FF and Ir are the short circuit density(mA/cm^2), open circuit voltage (Voc), Fill Factor and irradiated light intensity per unit area (mW/cm^2).

Among these photovoltaic parameters, Voc depends upon the potential gap of TiO_2 fermi level and redox shuttle. The theoretical possible maximum value of FF can be 1. These two factors pay a strong role towards DSSCs efficiency determination and has been highly studied. The short circuit current (Jsc) under illumination can be expressed as following

$J_{sc} = q_e \int_{\lambda_{\min}}^{\lambda_{\max}} I_{photon}(\lambda) IPCE(\lambda) d\lambda$, here q_e is electronic charge and $IPCE(\lambda)$ is incident monochromatic photon to electron conversion efficiency given by

$$IPCE(\lambda) = \eta_{LHE} \eta_{inj} \eta_{cc}$$

Where η_{LHE} is light harvesting efficiency, η_{inj} is electron injection efficiency from excited dye state to TiO_2 and η_{cc} is charge collection efficiency at the electrodes. It has been shown in Fig. 4 and to achieve η_{inj} unity, (~0.2V) over potential ($-\Delta G$) are needed between TiO_2 conduction band

and dye lowest unoccupied molecular orbital (LUMO) level for sufficient electron injection [70]. For oxidized dye regeneration (~0.3V) over potential ($-\Delta G$) is needed between highest occupied molecular orbital (HOMO) and redox potential [71,72]. In present scenario the high efficient DSSCs over 10% have found the value of η_{inj} and η_{cc} close to one [73]. Therefore the approach to enhance the light harvesting efficiency (η_{LHE}) is needed and may be attained by enhancing the short circuit current (J_{sc}).

Pathway to higher efficient dye sensitized solar cells:

The approach to increase the light harvesting efficiency is by increasing J_{sc} and can be achieved by either enhanced molar extinction coefficient (ε) of dye employed or increasing the dye uptake and increasing the optical path length by extending the absorption spectra. While considering IPCE of 100% integrated from UV region to band edge for 800nm and 920nm onset of dye IPCE edge employed, the Jsc value is 27.3mA/cm^2 and 34.7mA/cm^2 respectively. In order to harvest the broader wavelength photon, the narrow band gap dye is needed and the simultaneous maintenance of over potential at corresponding dye HOMO level and LUMO level is essential. This lead the serious limitation in balancing the over potential at redox shuttle level and TiO_2 level generating poor Voc. To increase the dye uptake, TiO_2 thickness can be improved but with high thickness the charge recombination among the electrons of TiO_2 and redox shuttle will increase making the poor Voc output performance.

Considering the 100% utilization of absorbed photons within 1127 wavelength band gap onset and with 0.1 eV necessary over potential for electron injection and dye regeneration, It has been reported that the theoretical efficiency of DSSCs are as high as 33% with the calculated Jsc 46mA/cm^2 and considering FF 0.8 with Voc 0.9 V [74]. The theoretical efficiency of DSSCs can be increased by interconnecting several DSSCs making it multi-junction structure.

1.7 Tandem dye sensitized solar cells:

To drive the S-Q band upward for covering the broader spectrum, tandem structure has been proposed which contains different band gap light harvesting materials in corresponding sub cells (Fig. 6). Ideally these subcells should connect optically and electrically either in series or parallel with decreasing order of band gap. According to Kirchhoff's law, series type of connection

implies the voltage output of connected cell will be the sum of individual subcells. The series connected tandem cell Jsc is highly influenced towards minimum Jsc of individual subcells and the FF of individual subcells play the crucial role in determining the tandem cell performance. Interconnection of cells can be stacked mechanically or monolithic and the latter structure pose the adaptation of individual cells and their interconnection with a recombination or tunnel layer making it complex in fabrication. In Fig. 7, a mechanically stacked tandem DSSC has been shown schematically, where top cell harvests the lower wavelength photon and remaining long wavelength photon unharvested by top cell are available to bottom cells. The architecture consists of four superfluous TCO glass making it prone to photon transmission loss sensitive and affecting towards photon intensity availability at bottom cell. Based upon this structure various reports has been published [75-80].

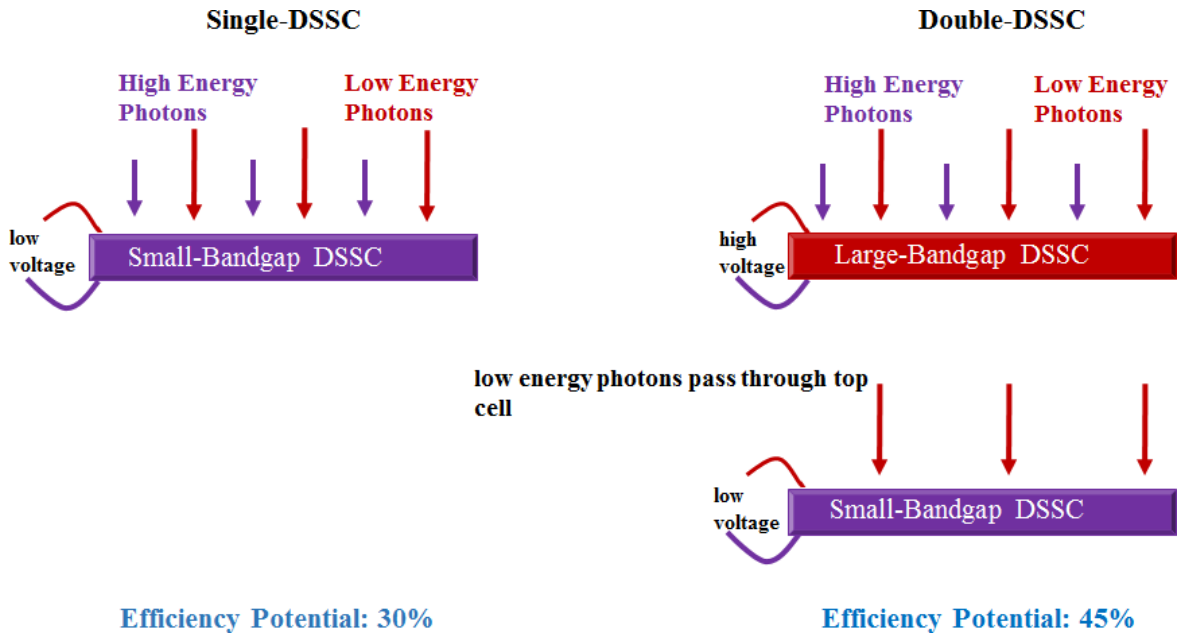

Figure 6. Advantages of tandem DSSCs: A single DSSC covering large wavelength region generates a low voltage from the available solar spectrum and A tandem architecture consist a large band gap DSSC to absorb the high-energy photons, generating the larger voltage from these photons in combination with the small band gap DSSC [74, 91].

1.7.1 Existing limitation and overcome of tandem dye sensitized solar cells:

Usage of superfluous TCO glass renders the optical transmission loss reaching at bottom cell. To resolve the intermediate loss transmission issue, n-p tandem DSSCs with TiO_2 as top cell photoanode and NiO as bottom cell photocathode has been reported. Though the fabricated tandem DSSCs architecture was economical by avoiding intermediate plates and consisting only two TCO glass, the obtained efficiency was not considerable good enough due to energy level difference available between the iodine redox shuttle potential and NiO valence band [81-82]. To improve the energy level difference between NiO valence band and redox shuttle the thiolate/disulfide base-

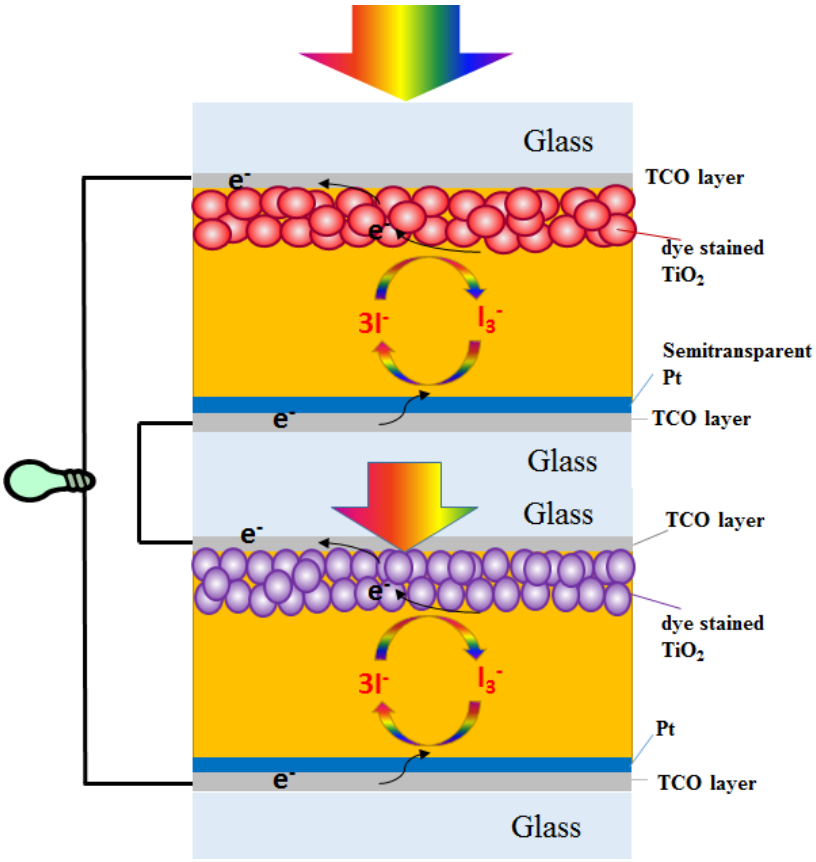

Figure 7. The schematic and architecture of TCO based Tandem dye sensitized solar cell.

d redox shuttle has been utilized and the pn tandem cell efficiency was 1.33%, slightly better than previous report [83]. The tandem cell concept has been demonstrated with architecture (Fig. 8) by employing the engineering of intermediate layer. The intermediate layer has been substituted with Pt-Ti mesh or Pt mesh. In all cases the proof of concept has been provided but the tandem cell performance was hindered due to transparency of intermediate layer [84-86]. To enhance the tandem cell performance by controlling the intermediate layer photon intensity at bottom cell the structural modification has been performed by inserting floating electrode (Fig. 9). The structure has flexibility and bottom cell achieves maximum possible photon. Though tandem cell Voc was greater than the individual subcell Voc, the leakage of electrolyte among the cell deeply affected the performance [87-88].

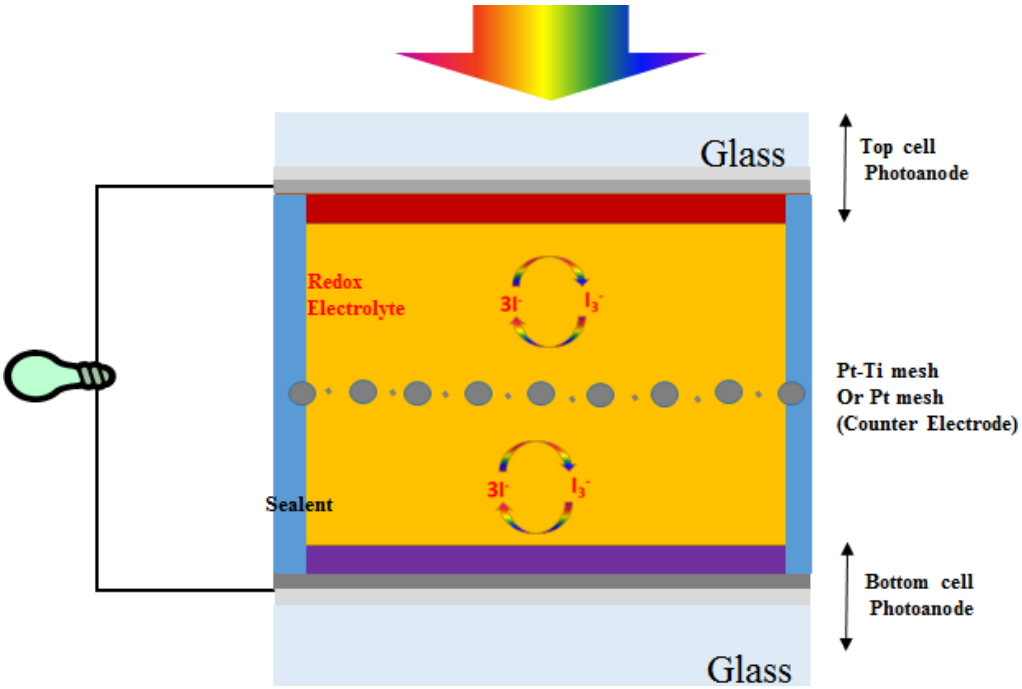

Figure 8. Structure of Tandem DSSCs with Pt-Ti or Pt mesh as intermediate layer.

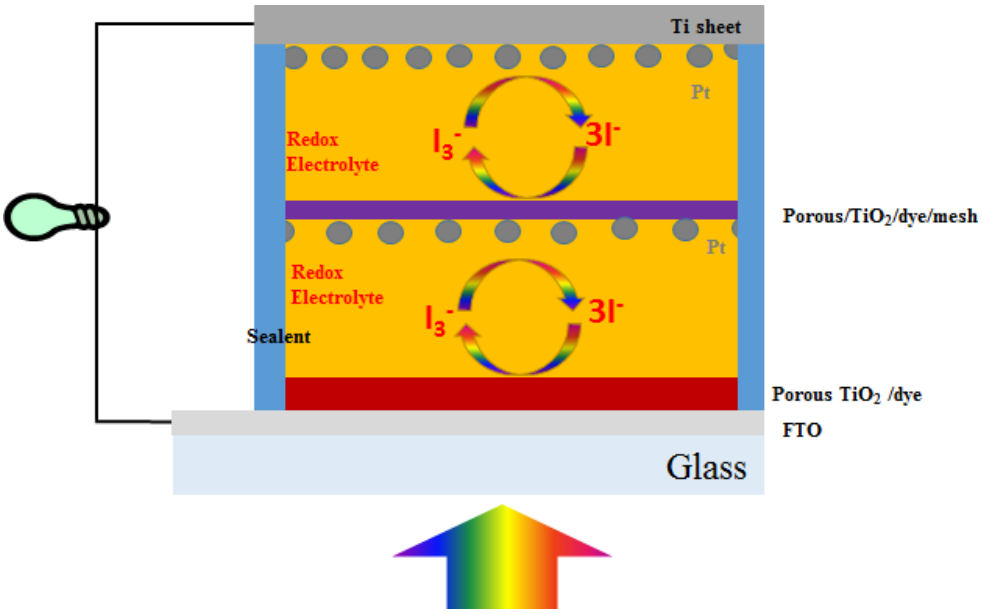

Figure 9. Structure of Tandem DSSCs with floating electrode.

1.8 TCO-less tandem dye sensitized solar cells:

The TCO-less dye sensitized solar cells (TCO-less DSSC) is a concept towards economical and light efficient fabrication of DSSC. Utilizing the merits of this architecture the TCO-less cylinder tandem structure has been fabricated on a glass rod. The architecture consisted of Glass/dye coated TiO_2/ porous Ti layer/ gel film electrode/ Ti counter electrode. The glass rod was stained with two different dye in different area connected by copper wire and the proof of concept was provided [89]. In other published report, taking advantage of combined effect of TCO-less tandem DSSC and light splitting wave guide, the architecture instrumented have shown the proof of concept however the reported efficiency was around 2%. Figure 10 is considering the publications going on since 1991 in TCO and TCO-less DSSCs architectures. It is considered that the about 201 publications of Tandem DSSCs has been explored and unexplored TCO-less tandem DSSCs (about 7 publications only) need a lot of attention for further research bearing economical and comparable energy harvesting properties.

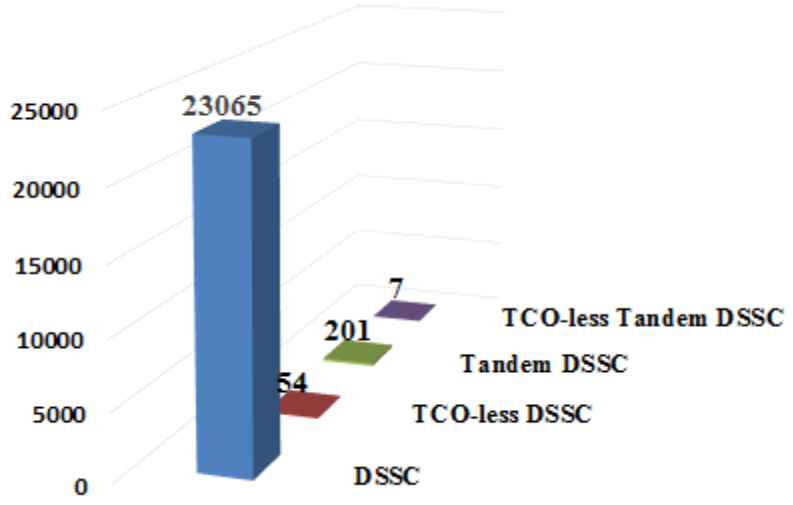

Figure 10. The number of published report from 1991 on Web of Science using the key word mentioned (accessed on 17 Nov 2015).

1.9 Challenges and ideas to overcome:

Tandem DSSCs demonstrations are needed to enhance the photoharvesting spectra of DSSCs. Most sought and studied four TCO Tandem DSSCs have shown the limitation towards bottom cells performance. Intermediate plates of TCO Tandem DSSCs are responsible towards the transmission loss affecting the bottom cell performance. Several approach have been followed to enhance the bottom cell performance by utilizing the transparent Pt nanoparticles on Titanium sheet (Pt/Ti sheet) as intermediate layer. These intermediate layers could not succeed in better light transmission towards high performance bottom cell DSSC. Other approach to improve obstacles faced by intermediate layer has been approached by floating electrode architecture could not succeeded well. The optical limitation induced by intermediate plate, possibly can be avoided by stack of TCO DSSC and TCO-less DSSC. The plausible architecture has been drawn in Fig. 11. In this mechanically stacked tandem structure the intermediate plate induced obstacle has been deprived to some extent with avoid of one TCO plate. The succession of Tandem DSSCs lies with panchromatic harvesting covering NIR wavelength region also. Phthalocyanine dyes are known

towards the NIR light harvesting properties. The major challenges to impasse this dye are solubility and aggregation issues. The incorporation of proposed architecture with modified Phthalocyanine dye can lead a novel approach towards tandem DSSC realization.

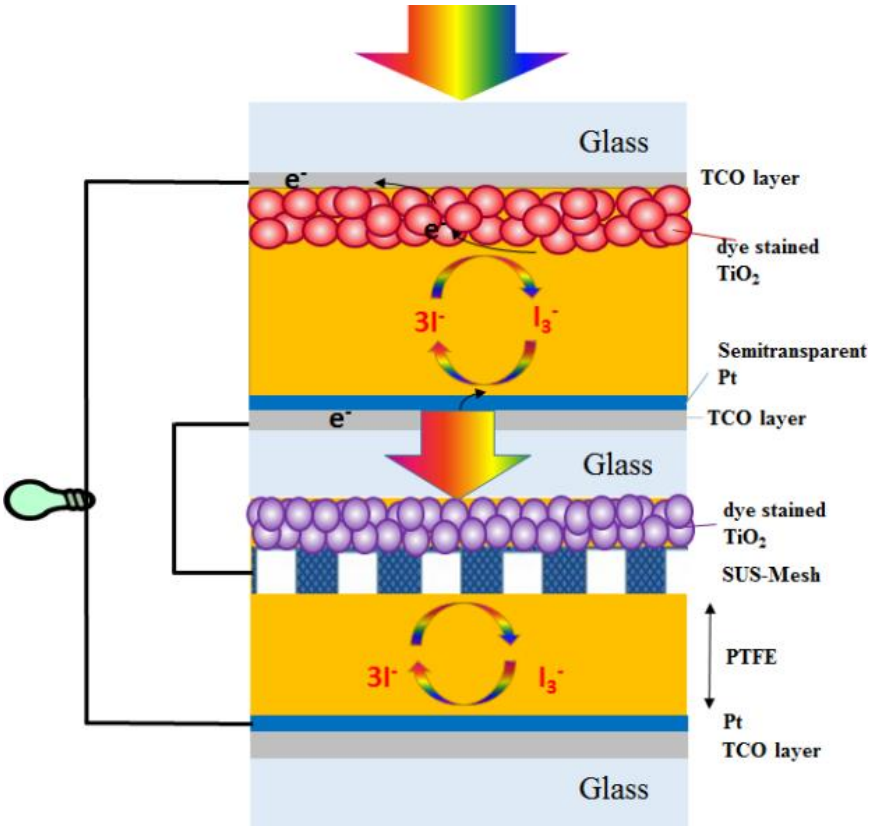

Figure 11. The schematic and architecture of Tandem dye sensitized solar cells with TCO-less back contact bottom electrode. [90]

References:

1. BP Statistical Review of World Energy June 2010. BP, London 2010.
2. International Energy Outlook 2013.
3. N. S. Lewis and D. G. Nocera, *PNAS*, 2006, **103**, 15729.
4. www.myenergygateway.com (accessed on 8/12/2015).
5. A. Hagfeldt, G. Boschloo, L. Sun, L. Kloo, and H. Pettersson, *Chemical reviews*, 2010, **110**,6595.
6. R. F. Service, *Science* (Washington, D.C.), 2005, **309**, 548.
7. J. Potočnik, *Science*, 2007, **315**, 810-811.
8. M. Z. Jacobson and M. A. Delucchi, *Energy Policy*, 2011, **39**, 1154.
9. D. M. Chapin, C. S. Fuller, G. L. Pearson, *Journal of Applied Physics*, 1954, **25**, 676.
10. D. L. Staebler and C. R. Wronski, *Applied Physics Letters*, 1977, **31**, 292.
11. http://www.solar-facts-and-advice.com/CIGS-solar-cell.html/accessed on (8/9/2015).
12. S. Mathew, A. Yella, P. Gao, R. H. Baker, B. F. E. Curchod, N. A. Astani, I. Tavernelli, U. Rothlisberger, M. K. Nazeeruddin and M. Gratzel, *Nature Chemistry*, 2014, **6**, 242.
13. M. A. Green, K. Emery, Y. Hishikawa, W. Warta and E. D. Dunlop, Solar cell efficiency tables (version 45), *Progress in Photovoltaics: Research and Applications*, 2015, **23**, 1.
14. Nature special report, thin films: ready for their close-up? Vol. 453/558-559,31 July 2008.
15. W. S. Yang, J. H. Noh, N. J. Jeon, Y. C. Kim, S. Ryu, J. Seo, S. Il Seok, *Science***,** 2015**,** **348**, 1234.
16. B.W. D Andrade, A.Z. Kattamis, and P.F. Murphy, Handbook of flexible organic electronics: Material, manufacturing and Applications.
17. Q. Lin, H. Huang, Y. Jing, H. Fu, P. Chang, D. Li, Y. Yao, and Z. Fan, *Journal of Materials Chemistry C*, 2014, **2**, 1233.
18. R. M. Swanson, *Progress in Photovoltaics: Research and Applications*, 2006, **14**, 443.
19. C. Berge, M. Zhu, W. Brendle, M. Schubert and J. Werner, *Solar Energy Materials and Solar Cells*, 2006, 90, 3102.
20. NREL, http://www.nrel.gov/ncpv/images/efficiency_chart.jpg,2013.

21. J. L. Cruz-Campa, M. Okandan, P. J. Resnick, P. Clews, T. Pluym, R. K. Grubbs, V. P. Gupta, D. Zubia and G. N. Nielson, *Solar Energy Materials and Solar Cells*, 2011, **95**, 551.

22. S. W. Bedell, D. Shahrjerdi, B. Hekmatshoar, K. Fogel, P. A. Lauro, J. A. Ott, N. Sosa and D. Sadana, *IEEE Journal of Photovoltaics*, 2012, **2**, 141.

23. S. Saha, M. M. Hilali, E. U. Onyegam, D. Sarkar, D. Jawarani,R. A. Rao, L. Mathew, R. S. Smith, D. Xu and U. K. Das, *Applied Physics Letters*, 2013, **102**, 163904.

24. S. Guha and J. Yang, *IEEE Transactional Electron Devices*, 1999, **46**, 2080.

25. A. Banerjee, X. Xu, K. Beernink, F. Liu, K. lord, G. DeMaggio, B. Yan, T. Su, G. Pietka and C. Worrel, *35th IEEE PVSC*, 2010,p. 002651.

26. C. R. Osterwald, M. W. Wanlass, T. Moriarty, M. A. Steiner, K. Emery, 10th International Conference on Concentrator Photovoltaic Systems, Albuquerque, New Mexico, 7- 9 April, 2014.

27. L. Kranz, C. Gretener, J. Perrenoud, R. Schmitt, F. Pianezzi, F. La Mattina, P. Bl¨osch, E. Cheah, A. Chiril˘a and C. M. Fella, *Nature Communication*, 2013, **4**, 2306.

28. EPMA, www.epma.ch/plugin/template/epma/*/110807, 2011.

29. B. Basol, V. Kapur, A. Halani and C. Leidholm, *Solar Energy Materials and Solar Cells*, 1993, **29**, 163.

30. S. Niki, M. Contreras, I. Repins, M. Powalla, K. Kushiya, S. Ishizuka and K. Matsubara, *Progress in Photovoltaics*, 2010, **18**, 453.

31. EMPA, www.empa.ch/plugin/template/empa/*/110807, 2011.

32. R. Wuerz, A. Eicke, F. Kessler, S. Paetel, S. Efimenko and C. Schlegel, *Solar Energy Materials and Solar Cells*, 2012, **100**,132.

33. T. Yagioka, *Appllied Physics Express*, 2009, **2**, 2201.

34. A. Chiril˘a, S. Buecheler, F. Pianezzi, P. Bloesch, C. Gretener, A. R. Uhl, C. Fella, L. Kranz, J. Perrenoud and S. Seyrling, *Nature Materials*, 2011, **10**, 857.

35. T. Takamoto, T. Agui, H. Washio, N. Takahashi, K. Nakamura, O. Anzawa, M. Kaneiwa, K. Kamimura, K. Okamoto and M.Yamaguchi, *31st IEEE PVSC*, 2005, p. 519.

36. T. Takamoto, M. Kaneiwa, M. Imaizumi and M. Yamaguchi, *Progress in Photovoltaics: Research & Applications*, 2005, **13**, 495.

37. C. Morioka, K. Shimazaki, S. Kawakita, M. Imaizumi, H. Yamaguchi, T. Takamoto, S. Sato, T. Ohshima, Y. Nakamura and K. Hirako, *Progress in Photovoltaics*, 2011, **19**, 825.

38. M. W. Rowell, M. A. Topinka, M. D. McGehee, H. Prall, G. Dennler, N. S. Sariciftci, L. Hu and G. Gruner, *Applied Physics Letters*, 2006, **88**, 233506.

39. S. Pang, Y. Hernandez, X. Feng and K. M¨ullen, *Advanced Materials*, 2011, **23**, 2779.

40. Y. Wang, X. Chen, Y. Zhong, F. Zhu and K. P. Loh, *Applied Physics Letters*, 2009, **95**, 063302.

41. Y. H. Kim, C. Sachse, M. L. Machala, C. May, L. M¨uller- Meskamp and K. Leo, *Advanced Functional Materials*, 2011, **21**, 1076.

42. Y. Galagan, J. J. M. Rubingh, R. Andriessen, C. Fan, P. W. M. Blom, S. C. Veenstra and J. M. Kroon, *Solar Energy Materials and Solar Cells*, 2011, **95**, 1339.

43. W. Gaynor, G. F. Burkhard, M. D. McGehee and P. Peumans, *Advanced Materials*, 2011, **23**, 2905.

44. H. Wu, L. Hu, M. W. Rowell, D. Kong, J. J. Cha, J. R. McDonough, J. Zhu, Y. Yang, M. D. McGehee and Y. Cui, *Nano Letters*, 2010, **10**, 4242.

45. M. Kaltenbrunner, M. S. White, E. D. Głowacki, T. Sekitani, T. Someya, N. S. Sariciftci and S. Bauer, *Nature Communications*, 2012, **3**, 770.

46. G. Li, V. Shrotriya, J. S. Huang, Y. Yao, T. Moriarty, K. Emery and Y. Yang, *Nature Materials*, 2005, **4**, 864.

47. A. E. Becquerel, On electric effects under the influence of solar radiation, CR Acad. Sci, **9**, 711-4.

48. S. Ito, N.-L C. Ha, G. Rothenberger, P. Liska, P. Comte, S. M. Zakeeruddin, P. Pechy, M. K. Nazeeruddin, M. Gratzel, *Chemical Communication*, 2006, **4004-4006**.

49. H. J. Snaith, A. J. Moule, C. Klein, K. Meerholz, R. H. Friend and M. Gratzel, *Nano Letters*, 2007, **7**, 3372.

50. T. Yamaguchi, N. Tobe, D. Matsumoto, T. Nagai and H. Arakawa, *Solar Energy Materials and Solar Cells*, 2010, **94**, 812.

51. F. Huang, D. Chen, Q. Li, R. A. Caruso and Y.-B. Cheng, *Applied Physics Letters*, 2012, **100**, 123102.

52. H. C. Weerasinghe, P. M. Sirimanne, G. P. Simon and Y.-B. Cheng, *Progress in Photovoltaics: research and Applications*, 2012, **20**, 321.

53. M. Ye, X. Wen, M. Wang, J. Iocozzia, N. Zhang, C. Lin and Z. Lin, *Materials Today*,00,**00**,2014.

54. F. Bella, C. Gerbaldi, C. Barolo and M. Gratzel, Aqueous dye-sensitized solar cells, *Chemical Society Review*, 2015, **44**, 3431.

55. www.gcell.com/dye-sensitized-solar-cells/accessed on 18/09/2015.

56. S. Mathew, A Yella, P. Gao, R. H.-Baker, B. F. E. Curchod, N. A.-Astani, I. Tavernelli, U. Rothlisberger, M. K. Nazeeruddin and M. Grätzel, *Nature Chemistry*, 2014, **6**, 242.

57. A. Listorti, B. O. Regan and J. R. Durrant, *Chemistry of Materials*, 2011, **23**, 3381.

58. N.G. Park, S. H. Chang, J. V.D. Lagemaat, K. J. Kim and A. J. frank, *Bulletin of Korean, Chemical Society*, 2000, **21**, 985.

59. D. F. Watson and G. J. Meyer, *Coord. Chemical Reviews*, 2004, **248**, 1391.

60. A. Listorti, B. O. Regan and J. R. Durrant, *Chemistry of materials*, 2011, **23**, 3381.

61. S. Holmberg, A. Perebikovsky, L. Kulinsky and M. Madou, *Micromachines*, 2014, **5**, 171.

62. A. B. F. Martinson, T. W. Hamann, M. J. Pellin, and J. T. Hupp, *Chemistry A Europian Journal*, 2008, **14**, 4458.

63. J. M. Kroon, N. J. Bakker, H. J. P. Smit, K. R. Thampi, P. Wang, S. M. Zakeeruddin, M. Gratzel, A. Hinsch, S. Hore, U. Wurfel, R. Sastrawn, J. R. Durrant, E. Palomares, H. Pettersson, T. Gruszecki, J. Walter, K. Skupien and G. E. Tulloch, *Progress in Photovoltaics: Research and Applications*, 2007, **15**, 1.

64. N. Fuke, A. Fukui, Y. Chiba, R. Komiya, R. Yamanaka, and L. Han, *Japanese Journal of Applied Physics*, 2007, **46**, L420.

65. Y. Kashiwa, Y. Yoshida, and S. Hayase, *Applied Physics Letters*, 2008, **92**, 033308.

66. M. Z. Molla, N. Mizukoshi, H. Furukawa, Y. Ogomi, S. S. Pandey, T. Ma and S. Hayase, *Progress in Photovoltaics: Research and Applications*, 2015, **23**, 1100.

67. J. Usagawa, S. S. Pandey, S. Hayase, M. Kono and Y. Yamaguchi, *Applied Physics Express*, 2009, **2**, 062203.

68. G. Kapil, S. S. Pandey, Y. Ogomi, T. Ma and S. Hayase, *Organic Electronics*, 2014, **15**, 3399.

69. H. S. Jung and J.-K. Lee, *Journal of Physical Chemistry Letters*, 2013, **4**, 1682.

70. A. Islam, H. Sugihara and H. Arakawa, *Journal of Phochemistry and Photobiology A*, 2003, **158**, 131.

71. G. Oskam, B. V. Bergeron, G. J. Meyer, and P. C. Searson, *Journal of Physical Chemistry B*, 2001, **105**, 6867.

72. T. Daeneke, A. J. Mozer, Y. Uemura, S. Makuta, M. Fekete, Y. Tachibana, N. Koumura, U. Bach and L. Spiccia, *Journal of American Chemical Society*, 2012, **134**, 16925.

73. A. Yella, H.-W. Lee, H. N. Tsao, C. Yi, A. K. Chandiran, M. K. Zakeeruddin, and M. Gratzel, *Science*, 2011, **334**, 629.

74. J. He, H. Lindstrom, A. Hagfeldt and S.-E. Lindquist, *Solar Energy Materials and Solar Cells*, 2000, **62**, 265.

75. M. Durr, A. Bamedi, A. Yasuda and G. Nelles, *Applied Physics Letters*, 2004, **84**, 17.

76. T. Kinoshita, J. T. Dy, S. Uchida, T. Kubo and H. Segawa, *Nature Photonics*, 2013, **7**, 535.

77. M. Yanagida, N. O.-K.Omatsuzaki, M. Kurashige, K. Sayama & Hideki Sugihara, *Solar Energy Materials & Solar Cells*, 2010, **94**, 297.

78. T. Yamaguchi, Y. Uchida, S. Agatsuma and H. Arakawa, *Solar Energy Materials & Solar Cells*, 2009, **93**, 733.

79. W.-S. Jeong, J.-W Lee, S. Jung, J. H. Yun and N.-G Park, *Solar Energy Materials & Solar Cells*, 2011, **95**, 3419.

80. S. Ito, I. M. Dharmadasa, G. J. Tolan, J. S. Roberts, G. Hills, H. Miura, J.-H. Yum, P. Pechy, P. Liska, P. Comte and M. Gratzel, *Solar Energy*, 2011, **85**, 1220.

81. A. Nattestad, A.J. Mozer, M.K.R. Fischer, Y.-B. Cheng, A. Mishra, P. Bauerle and U. Bach, *Nature materials*, 2010, **9**, 31.

82. H. Choi, T. Hwang, S. Lee, S. Nam, J. Kang, B. Lee and B. Park, *Journal of Power Sources*, 2015, 274, 937.

83. H. Seo, S. Hashimoto, D. Ichida, N. Itagaki, K. Koga and M. Shiratani, *Electrochimica Acta*, 2015, doi: 10.1016/j.electacta.2015.04.105.

84. M. Murayama and T. Mori, *Thin Solid Films*, 2008, **516**, 2716.

85. M. Murayama and T. Mori, *Journal of Physics D: Applied Physics*, 2007, 40, 1664.

86. K. Uzaki, S. S. Pandey and S. Hayase, *Journal of Photochemistry and Photobiology A: Chemistry*, 2010, **216**, 104.

87. K. Uzaki, S. S. Pandey, Y. ogomi and S. Hayase, *Japanese Journal of Applied Physics*, 2010, **49**, 082301.

88. J. Usagawa, S. S. Pandey, S. Hayase, M. Kono, and Y. Yamaguchi, *Applied Physics Express*, 2009, 062203.

89. J. Usagawa, M. Kaya, Y. Ogomi, S.S. Pandey, and S. Hayase, *Journal of Photonics Energy*, 2011, **1**, 011110.

90. A. K. Baranwal, T. Shiki, Y. Ogomi, S. S. Pandey, T. Ma and S. Hayase, *RSC Advances*, 2014, **4**, 47735.

91. S.P. Bremner,M. Y. Levy, C. B. Honsberg, *Progress in Photovoltaics: Research & Applications*, 2008, **16**, 225.

Chapter 2

Experimental section for optical and photovoltaic property

Solar cell innovation is being utilized as a part of private, business and military applications and are produced in an extensive variety of levels with different transformation efficiencies. It is critical to acquaint with the parameters and characterization technique accessible for solar cell upon irradiance of photon energy.

2.1 Photovoltaic device characterizations

2.1.1 I-V characteristics

The current-voltage (I-V) curve of DSSCs describe its energy conversion potential at the existing situation of irradiance and temperature. Specifically, the I-V curve represents the sequence of current and voltage at which the DSSC could be operated, while maintaining the irradiance and cell temperature constant. Figure 1 displays a typical I-V curve and the power-voltage (P-V) curve that is computed from it, maintaining key points on these curves. The width span of the I-V curve (Fig. 1) ranges from the short circuit current (Jsc) at zero volts, to zero circuit current at the open circuit voltage (Voc). At the decline of the I-V curve is the maximum power point (Pmax with Imp,Vmp), the point at which the DSSC generates maximum electrical power. It also demonstrates that at voltages well below Vmp, the movement of solar-generated electrical charge to the external circuit is relatively independent of output voltage. Near the decline of the curve, this behavior of I-V curve starts to change. With the further increase in voltage, an increasing amount of the charges recombine within the DSSC itself rather than flowing out through the load. At Voc, all of these charges recombine internally. The maximum power point, (I,V) point at which the product of current and voltage reaches its maximum value is located at the decline of the I-V curve.

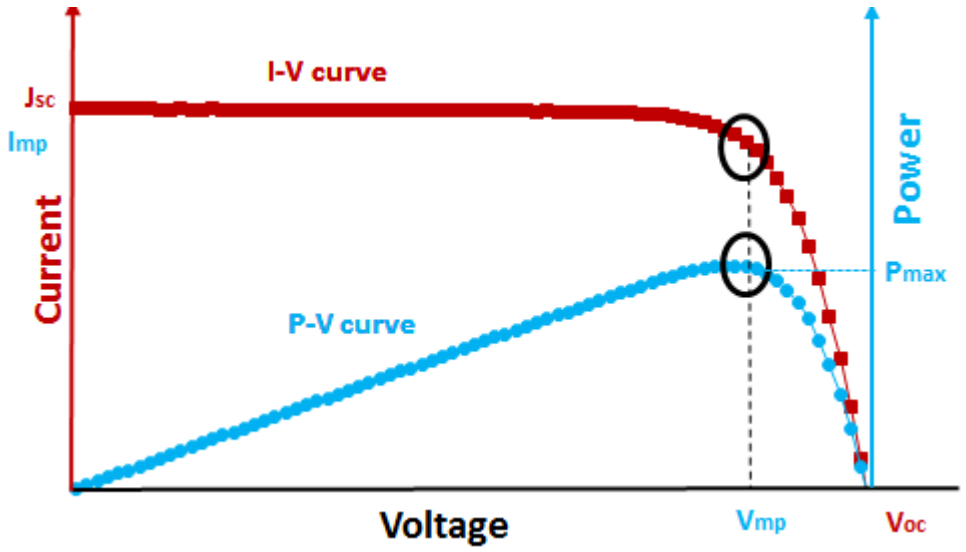

Figure 1. The I-V characteristics and P-V characteristics of a DSSC showing the Pmax (maximum Power output), Imp (maximum power output current), Vmp(maximum power output voltage).

The pattern of I-V characteristics of DSSCs can be usually well reproduced by the simple diode equivalence circuit model of Fig. 2. corresponding to the following I-V Equation [1]

$$i_{CELL} = i_{ph} - i_o\left(e^{\frac{-q_e(V_{CELL}+i_{CELL}R_S)}{mk_BT}} - 1\right) + \frac{V_{CELL} + I_{CELL}R_S}{R_{sh}} \qquad (1)$$

Here i_{ph} is the photocurrent density modelled as a current source and i_o is the dark current of diode, q_e is electronic charge, R_S is series resistance of cell, R_{sh} is shunt resistance of cell, m is diode ideality factor.

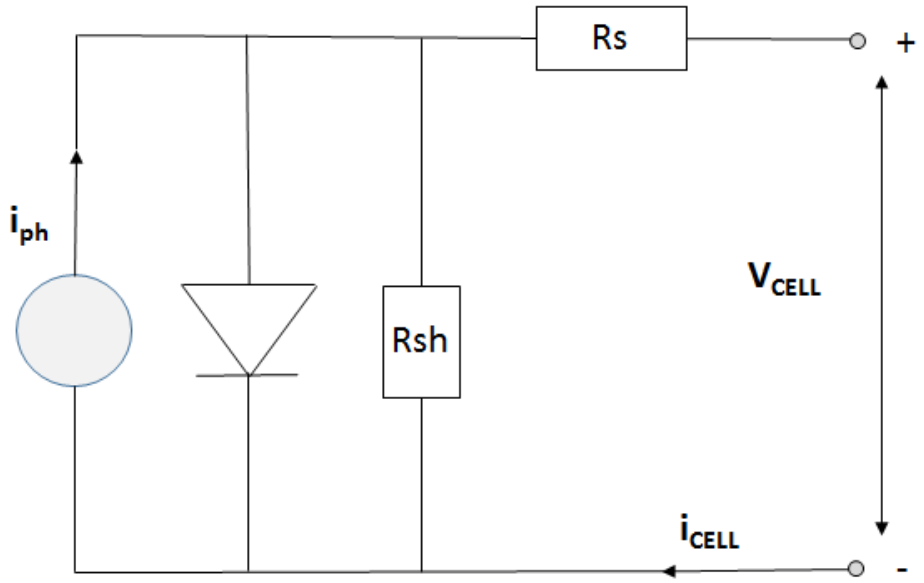

Figure 2. Basic diode equivalent circuit model of a solar cell.

2.1.2 Dark current:

This is the current flowing in the solar cell or in DSSC under the dark or no illumination condition (Fig. 3). Dark current provides the quantitative information about the recombinations processes occuring inside the cell interfaces [2]. In dye sensitized electrochemical cell (DSSCs) the dark current arises from the recombination of conduction band electron to redox shuttle (Equation 2) [3]. The recombinations occur despite the fact that dye monolayer is able to cover the mesoporous layer. The electrolyte nanoparticles are able to reach the empty spaces of mesoporous layer and the recombinations take place. Many additives have been used in electrolyte to cover the empty state to suppress the rate of reduction, which ultimately enhances the photovoltaic performances.

$$I_3^- + 2e_{cb}^-(T_iO_2) \rightarrow 3I^- \qquad (2)$$

Under the absence of illumination the solar cell I-V behaviour is similar to diode curve and is given by following Equation 3 [4].

$$I_{dark}(V) = I_o\left(e\left(\frac{qV}{nkT}\right) - 1\right) \qquad (3)$$

Here I_o is constant associated with reverse saturation current, n is ideality factor and defines the quality of diode, k is Boltzmann constant, T is temperature in kelvin.

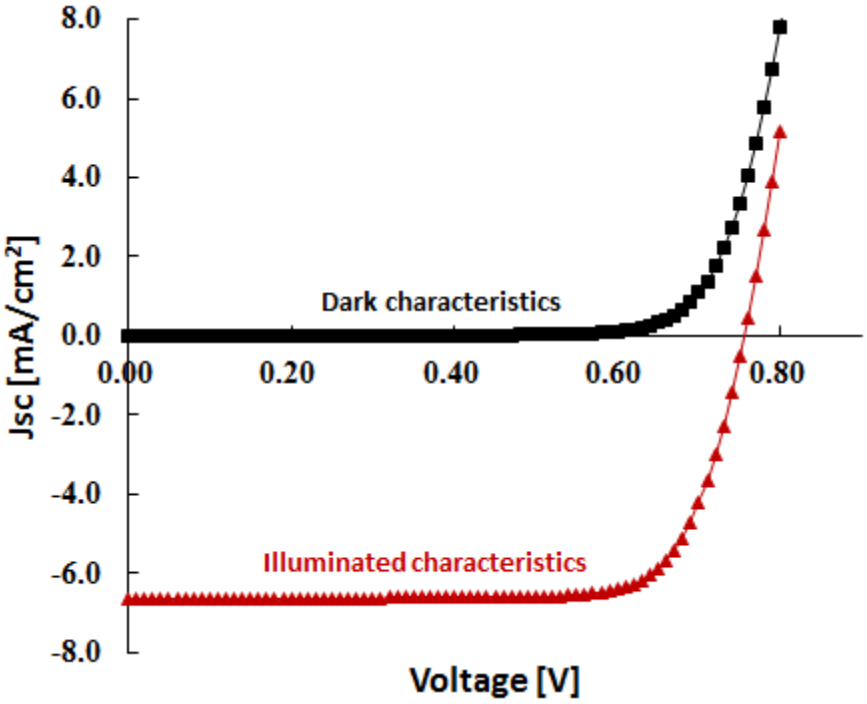

Figure 3. I-V characteristics under dark condition and under AM1.5 illumination condition.

2.1.3 Short circuit current:

The short circuit current (Jsc) is the maximum possible current density that can flow within the solar cell under short circuit condition. It is defined by the following Equation [5]

$$J_{sc} = \int_{\lambda_0}^{\lambda_{onset}} IPCE(\lambda) e \phi_{ph}(\lambda) d\lambda \qquad (4)$$

Here λ_0 is starting wavelength for solar spectrum harvesting, λ_{onset} is absorption onset of dye absorption wavelength, $IPCE(\lambda)$ is incident light to converted electron within specified wavelength region, $\phi_{ph}(\lambda)$ flux under 1.5AM and e is electronic charge.

The J_{sc} is highly dependent towards the TiO_2 photo anode active layer thickness. The active layer thickness is important for charge injection from excited dye molecule owing to its increased area, on the contrary they promote the charge recombination. The increase in J_{sc} can be achieved up to

certain optimum thickness, after that charge recombination will dominate to lower the J_{sc} [6]. Temperature has known effect on modifying the photovoltaic response of DSSC due to its effect on increased diffusion constant [7]. The increased diffusion constant induces the charge recombination and at the aftermath of these two events the overall J_{sc} decreases with rise in temperature [8-10]. The intense light increases the rate of charge generation and facilitates the increased J_{sc} with increase in intensity [11]. Figure 4 is exhibiting the solar photon flux ($m^{-2}s^{-1}nm^{-1}$) and calculated photocurrent with Equation 4, while assuming 100% IPCE and considering the UV region to band onset of sensitizer. The Jsc calculated was 27mA/cm^2 for IPCE onset of 800nm and 38mA/cm^2 for onset IPCE of 1000nm.

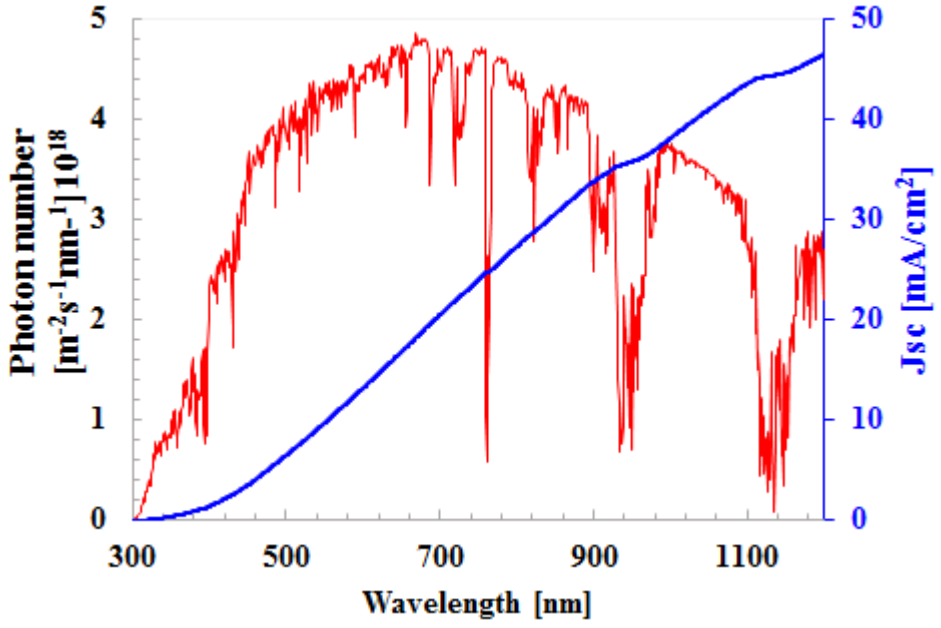

Figure 4. Observation of the calculated potocurrent from Equation (4), integrated from 280nm to corresponding wavelength with an assumed IPCE of 100% along with calculated Photon number (ASTM G173-03 Reference Spectra Derived from SMARTS v. 2.9.2 were downloaded from http://rredc.nrel.gov/solar/spectra/am1.5/).

2.1.4 Fill factor:

The Fill Factor abbrebiated as FF exhibits the squareness of the I-V characteristics of the solar cell and it predicts the easiness with which electron can be extracted. It is defined as the ratio of

maximum power generated by solar cell (Pmp=Imp*Vmp) to product of Jsc and Voc (Fig. 5). Its value lies between 0 and 1 and is measure of increase in recombination (decrease in photocurrent) with increasing photovoltage. Mathematically FF is defined by Equation 5.

$$FF = \frac{I_{mp}V_{mp}}{J_{sc}V_{oc}} \quad (5)$$

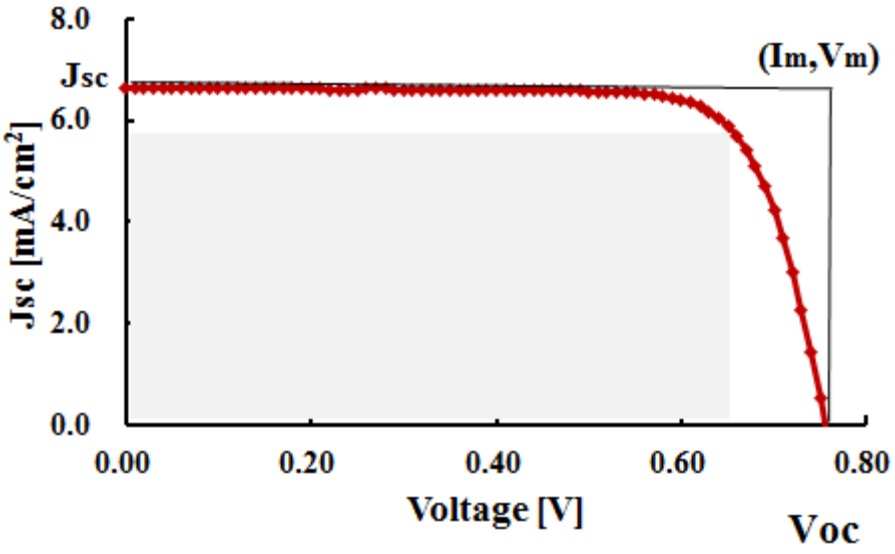

Figure 5. I-V curve showing the factors responsible for FF determination.

Solar cells with high FF exhibit lower equivalent series resiatance and higher equivalent shunt resistance. The higher thicker active layer are prone to recobinations and facilitate higher series resistance and poor FF [12]. The effect of light intensity and temperature on FF is predicted based upon cumulative behaviour of Jsc and Voc [11].

2.1.5 Open circuit voltage:

The Open circuit voltage is the maximum voltage that a solar cell can deliver under no load condition. It is the voltage at which external load does not flow any current. It signifies the forward voltage corresponding to which photo current are being compensated by dark current. In general the open circuit voltage is given by the Equation [5]

$$V_{oc} = \frac{1240}{\lambda_{onset}[nm]} - V_L(Volts) \quad (6)$$

Here λ_{onset} is the absorption onset and V_L is the internal loss in voltage

DSSCs are excitonic solar cell and their Voc can be determined by the difference between the fermi level in semiconductor nanoparticles and electrolyte redox shuttle potential and are schematically represented in Fig. 6.

$$V_{oc} = \left(\frac{kT}{e}\right)\ln\left(\frac{I_{inj}}{n_{cb}k_{et}[I_3^-]}\right) \quad (7)$$

I_{inj} is the flux of charge resulting from sensitized injection, $k_{et}[I_3^-]$ is the rate constant of dye reduction [3]. Concentration of electrons (n_{cb}) at the TiO_2 surface, k is Boltzmann constant, T is the operating temperature (kelvin), e is electronic charge.

It has been shown that V_{oc} has found dependency on light intensity as $\left(1.7\frac{kT}{q}\right)$ and here T is absolute temperature [7]. However it have shown the tendency of decrease with increase in temperature and film thickness. The effect of temperature has two consequences going on. Firstly with the effect of temperature, diffusion of charge will increase rapidly than charge mobility. Thus at the open circuit voltage and to maintain the charge balance the more voltage will be needed to counterbalance the temperature effect [7,11,12]. In contrary during other phenomenon, assuming the charge generation rate constant with temperature rise, charge recombination rate will increase. To achieve the steady state, charge density within device need to be lowering down and causing lowering in V_{oc}. This second phenomenon is supposed to be dominant and lowering is observed [7]. The increased film thickness are more prone to recombination and facilitating poor open circuit voltage. In other way the thicker film will promote the preabsorption and lowering the average charge carrier density and thus the open circuit voltage [13,14].

The light intensity effect can be attributed as with intense light, charge generation rate increases and results in increased chemical potential within the device, making the high open circuit voltage. On the other way reduced charge life time obstruct the chemical potential. First phenomenon is quiet dominant and making the effective in increasing the open circuit voltage [3,7,11].

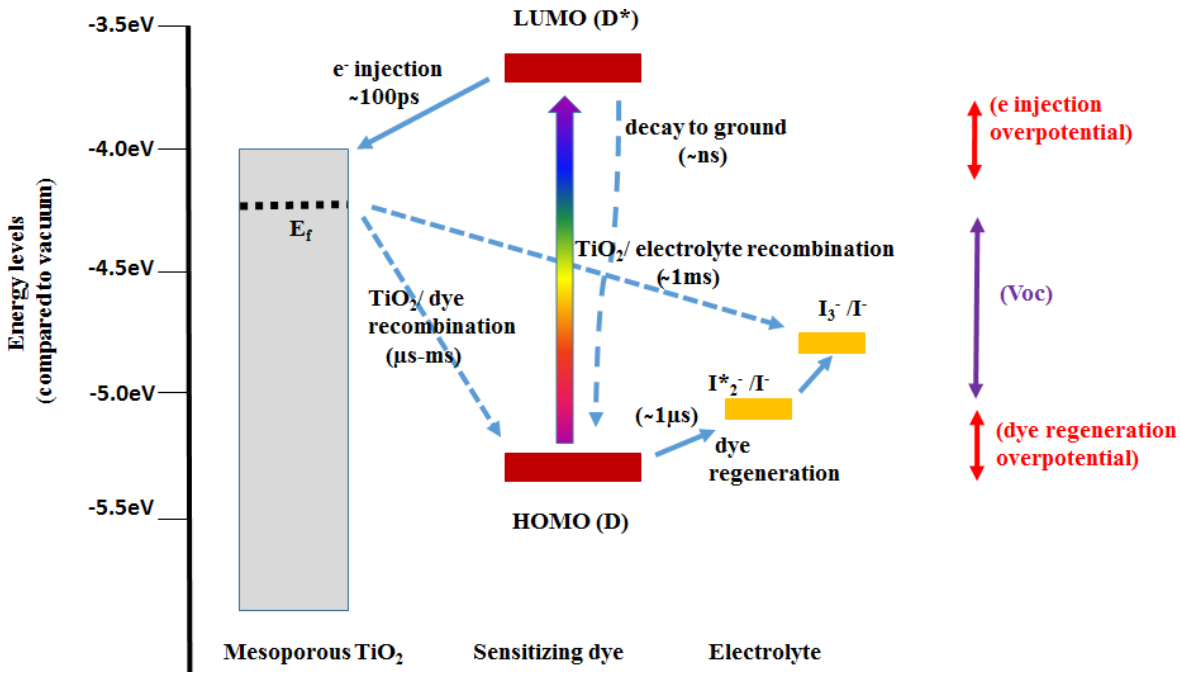

Figure 6. Voc determination and recombinations processes occurring in a DSSC (reproduced from previous chapter).

2.1.6 Incident photon to converted electron (IPCE):

The IPCE of a DSSC corresponds to the ratio of number of electrons measured as photocurrent in external load to the monochromatic photon flux that drives the cell. This is determined by three factors η_{LH} is the light harvesting capability from sun, η_{INJ} is the electron injection efficiency at electrolyte-mesoporous interface, $\eta_{COL}(\lambda)$ is the electron collection efficiency and all these factors are dependent on wavelength (Fig. 7) [15].

$$\lambda_{IPCE}(\lambda) = \eta_{LH}(\lambda)\eta_{INJ}(\lambda)\eta_{COL}(\lambda) \qquad (8)$$

It can be calculated by the recording of steady state i_{SC} produced by a calibrated and low intensity monochromatic photon flux incident on cell by the scanning of the particular wavelength range of light with a monochromator. Traditionally DSSCs IPCE usually show the nonlinear behavior with the light intensity due to mass transport limitation of electrolyte and dependency of diffusion length on electron concentration [15-18].

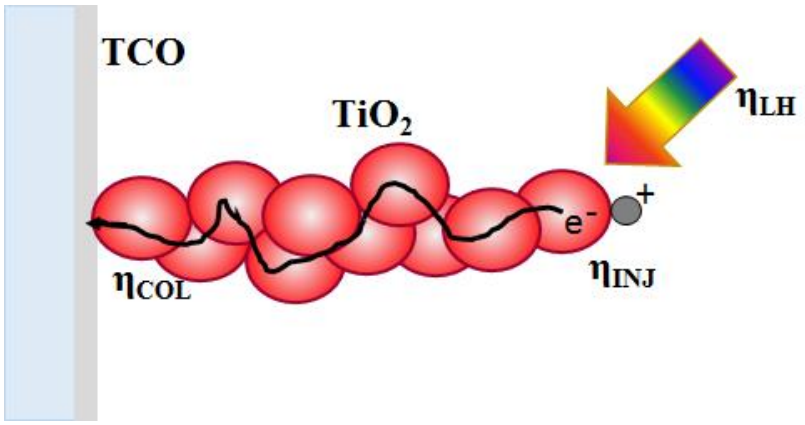

Figure 7. Schematic representation of the factors responsible for the determination of photocurrent in DSSCs.

The typical IPCE of a DSSC utilizing visible region harvesting dye has been exhibited in the Fig. 8 with blue line. The IPCE is superimposed over the c-Si photoharvesting spectra and is broadened at the wavelength onset of 700nm. The onward wavelength region are unharvested and have potential for IPCE broadening to achieve the high efficient DSSCs.

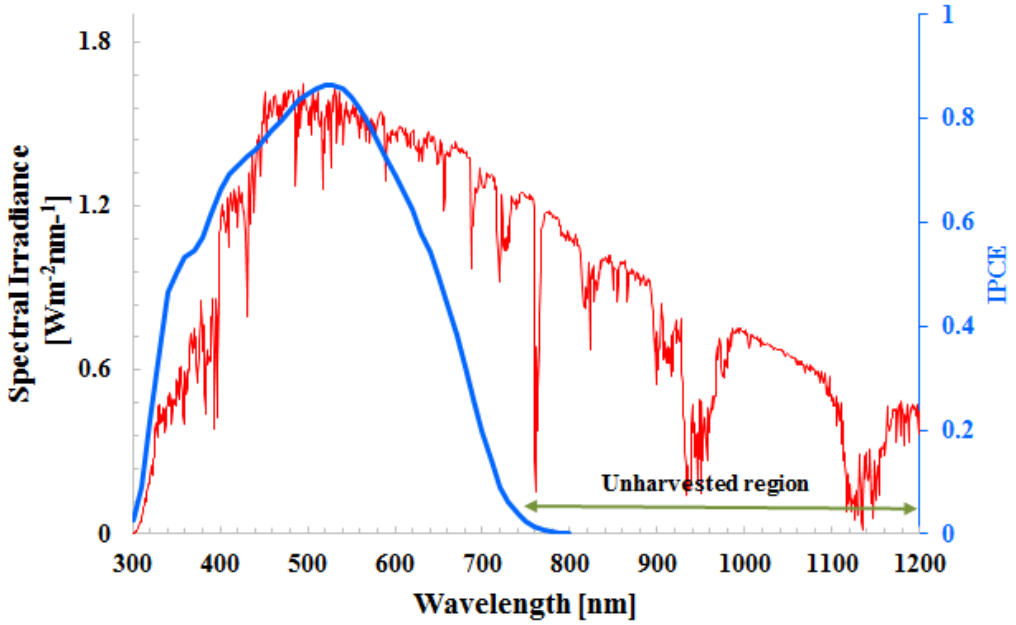

Figure 8. IPCE spectra of a typical visible region harvesting DSSC superimposed on Si solar cell IPCE showing the unharvested spectra.

The Fig. 8 exhibits that the unharvested solar spectra of NIR region is essential to achieve the high performance DSSCs. As explained in the previous chapter, the different DSSCs of complementary harvesting spectra collaborating in tandem architecture can be employed to achieve high performance.

2.2 Air mass:

The distance travelled by the sun rays affects the intensity availability at the solar panel and Air Mass is the measure of the how long path has been taken by sun light through atmosphere. The solar ray has to travel through the atmosphere consisting of O_2, H_2O, CO_2 and the AM signifies the reduction in power of light. It is defined as the path taken by the solar light in atmosphere normalized to the possible shortest path of overhead sun.

Mathematically it can be written as

$$AM = \frac{1}{Cos\theta} \tag{9}$$

The standard AM 1.5 spectrum is defined at an incidence angle of 48.2˚ from the zenith and is shown in the Fig. 9.

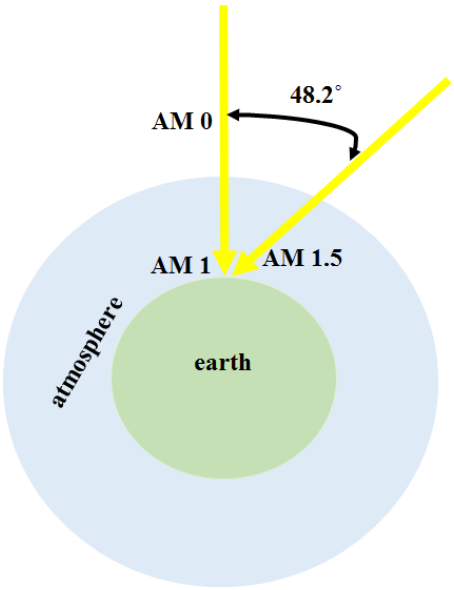

Figure 9. Light incident on earth surface and representation of Air Mass.

The Standard Test Conditions (STC) has been used for the photovoltaic performance evaluation of the solar cells.

These conditions are universally adopted and are followed as per,

- Cell temperature should be maintained at 25˚C for measurement.
- Spectral irradiation is maintained at 100 mW/cm^2 .
- Spectral energy distribution is maintained according to AM 1.5 condition.

Figure 10. Solar simulator used in this thesis for I-V and IPCE measurement.

2.3 Solar simulator and spectroradiometer:

Tandem DSSCs along with series stacked top cells and bottom cells photovoltaic performances were measured with solar simulator (CEP-2000 Bunko Keiki Co. Ltd, Japan) equipped with a xenon lamp (Bunko Keiki BSO-X150LC) for the light illumination (Fig. 10). The spectrum of the

solar simulator and its power were adjusted to be 100 mW/cm^2 at AM 1.5 using a spectroradiometer (LS-100, Eiko Seiki, Japan). Standard amorphous silicon photodetector (Bunkokeiki BS-520 S/N 353) with similar light sensitivity of the DSSCs was used to confirm and correct the power of irradiated light of the solar simulator. Photovoltaic parameters were measured with 0.2025cm^2 mask on TiO_2 coated substrate to avoid the exaggerated performance induced by reflected back light. Photocurrent action spectra of the devices were also measured with constant photon flux of (1X 10^{16}) photons/cm^2 at each wavelength in DC mode employing a photo-action spectrum measurement system connected to the solar simulator (CEP-2000, Bunkokeiki, Japan).

2.4 UV-vis spectroscopy:

UV-vis spectrometry instrument is used to investigate the optical properties like absorption, reflection and transmission properties of different materials either of organic molecules or transition materials. It utilizes the ultraviolet light (200-400 nm) and visible light (400-760 nm) for the above analysis. The deuterium light source are used to enlighten the UV region and tungsten lamp for part of visible and the whole of visible region. The visible region absorbance or reflectance spectra directly interpreted the distinguished colour of the involved chemicals. The UV region absorbance is measured from the transition of electron from ground state to excited state upon irradiance of light energy. Schematic representation and block diagram of the instruments are represented by Fig. 11 and Fig. 12 respectively.

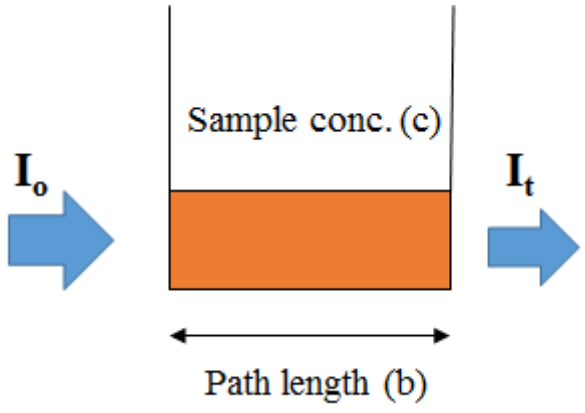

Figure 11. Schematic representation of the UV-vis process.

Using the UV-vis spectroscopy it is possible to calculate the transmittance, absorption and the concentration of the desired molecules.

Transmittance is defined as the ratio of transmitted intensity to the input light intensity. Reflectance can be defined as the logarithm of the transmittance.

Transmittance $=I_t/I_o$, Absorbance (A) = log $[1/(I_t/I_o)]$, According to Lambert Beer`s law,

Absorbance (A) = absorption coefficient (α)*path length (b)*sample concentration (c)

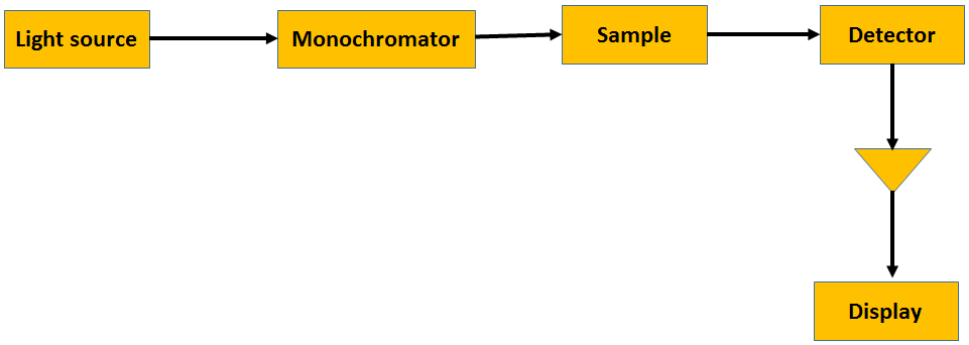

Figure 12. Block diagram of the UV-vis instrument.

2.5 Transmission spectrum:

Transparent conductive oxide (TCO) layers are integral part of fabrication of DSSCs. The coexistence of electrical conductivity and optical transparency are the requisite phenomenon of these materials. The common TCO plates most utilized now a days are F-SnO_2, Sn-In_2O_3, Sb-SnO_2. The electrical conductivity of these thin films are due to oxygen vacancies or by external doping. The conductivity of the thin film depends on the charge carrier concentration and is given by the following Equation.

$$\sigma = \mu ne \qquad (10)$$

Here μ is electronic charge mobility, n is electronic charge density and e is electronic charge.

The electronic mobility is given by $\mu = \frac{e\tau}{m^*}$ (11)

Here τ is mean time between the collisions, m^* is the effective electron mass. Equation 10 and 11 concludes the negatively correlation between the electronic charge density and mobility. On the other hand this interprets the high charge carrier density of TCO layers, reduces the carrier mobility and the conductivity does not increase after a certain extent and is responsible for photon transmission loss (Fig. 13).

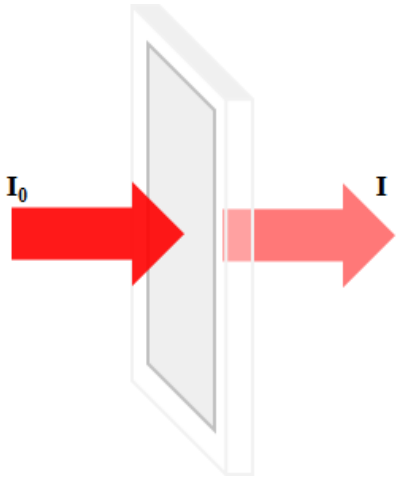

Figure 13. Schematic showing the light transmission loss while passing through a TCO layer.

TCO thin film are wide band gap semiconducting oxide and should have low extinction coefficient. Optical properties of TCO are dependent towards refractive index (n), extinction coefficient (k), band gap (Eg), and the geometry of material involved. Geometry includes the external parameters like film thickness, uniformity and the surface roughness. Rest of the optical parameters are intrinsic in nature and are materials properties. TCO layer optical properties are also dependent towards the optical properties of substrate upon which the TCO layer is coated. Sheet resistance of a conductive thin film is given by

$$R_s = \frac{1}{\sigma t} \quad (12)$$

Absorbance $$A \cong 1 - \exp^{\frac{\alpha}{\sigma R}}$$ (13)

Here R_s is sheet resistance, σ is conductivity, t is thickness of film, A is absorption in the TCO film, R is reflection. These two Equations stated that by lowering the thickness of the TCO film, transmission increases but sheet resistance increases.

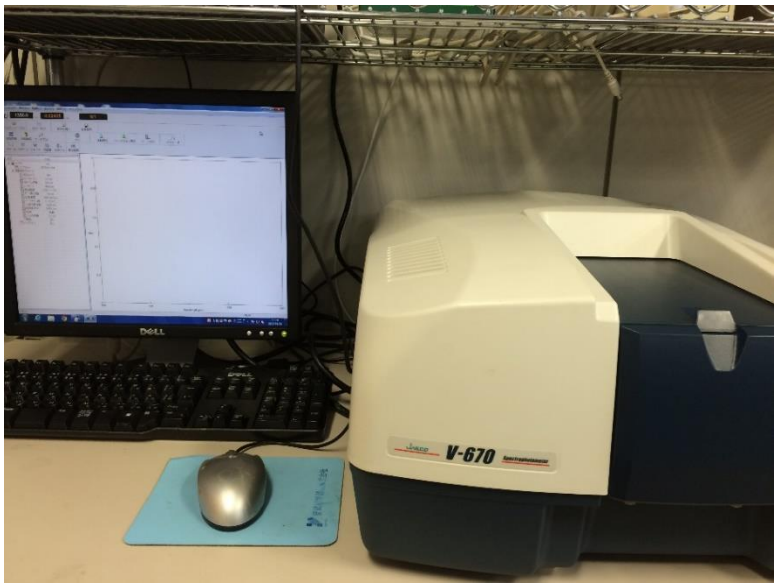

Figure 14. Instrument used in this thesis to carry out the UV-vis and transmission spectra measurement.

2.6 Thickness measurement:

The Dektak 6M Stylus profiler from Veeco was used to measure the thickness profile of mesoporous TiO_2 photoanode employed on FTO glass. It provides the measurements by placing the sample under a diamond-tipped stylus. The diamond stylus is mechanically associated with the core of a linear variable differential (LVD) transformer. The stylus tip is located across the sample as per the user programmed various scan length, time, speed and stylus force. The surface variation of film is covered by stylus motion and the vertically converted motion varies the core position of LVD transformer generating the corresponding electrical signal. The LVD transformer generates an AC reference signal proportional to the stylus positional variation and high precision A/D

converter converts it to digital form. The computer memory can store the data memory for further display and measurement display.

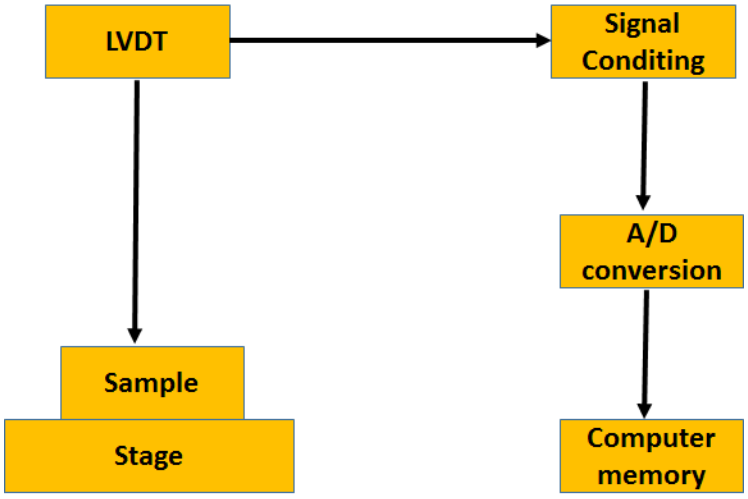

Figure 15. Block diagram of DEKTAK 6M stylus profiler.

The step profilometry can perform the secondary functions like surface roughness, irregularities in the film surface and at the same time maximum, minimum and average heights of the peaks and troughs can also be recorded.

2.7 Sputtering instrument:

Sputtering process is a physical vapor deposition phenomenon to deposit nanoparticles thin films of various materials like dielectric film SiO_2, ZrO_2, TiO_2, transparent films like ITO, ZnO, metal films Au, Ag, Cu, Si, Ti, Sn, Cr, Al, and Ni over the substrate surface. In working, high energetic ion beams are utilized and after collision with each other they produce an elastic transfer of momentum and displace the atoms from the surface of target. The released secondary electron system from the target are responsible to maintain the weakly charged gas particle system called plasma. Figure 16 describes the basic sputtering system and sputtering process. The free electrons travel to the neutral gas atoms to drive the outer shell electrons of the gas atoms by creating positively charged particles (more in number) and negatively charged electrons. The neutral gas

achieves positively charged ion (e.g. Ar^+) and accelerates towards the cathode liberating more free electrons by transfer of energy. The extra electrons generated releases the ions and again plasma formation takes place. The free electrons can combine to the positive charged ions form the neutral gas atoms again.

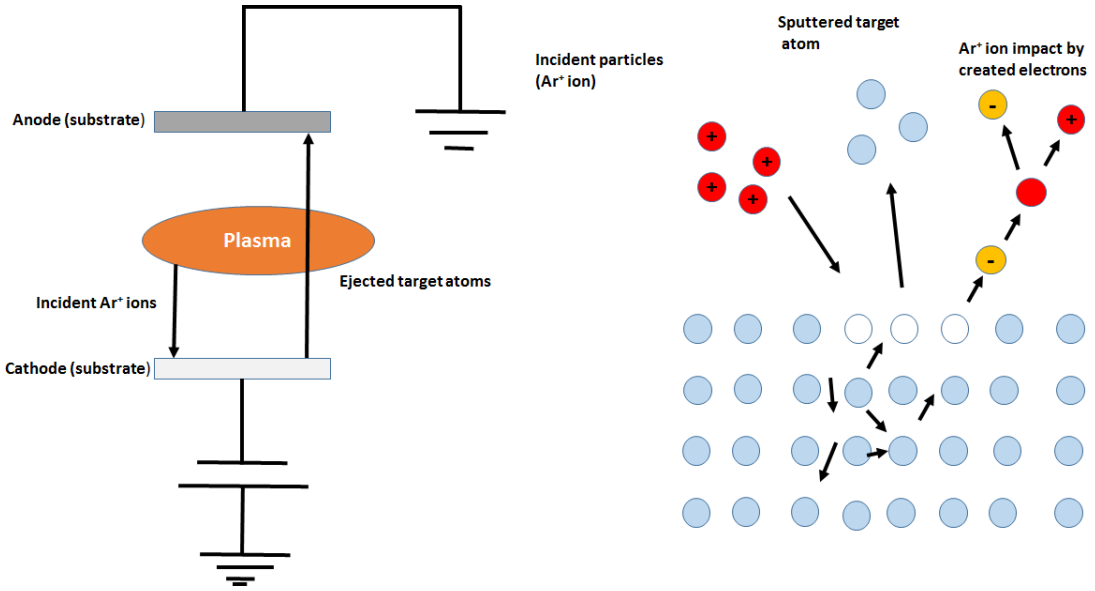

Figure 16. (a) Basic sputtering system and (b) sputtering mechanism.

In magnetron dc sputtering, free electrons are confined above the target surface by applied magnetic field at the back of the cathode. Under effect of magnetic field, these electrons increases the possibility of ionizing the gas molecules by many orders. In our tandem DSSCs fabrication process, we sputtered a thin film of Ti (240 nm) from both side on a metal mesh by employing a sputtering apparatus (CFS-4EP-LL, Shibaura Mechatronics, Japan) as shown in the Fig. 17. The counter electrode utilized in thesis work have the sputtered Pt either 1 nm (intermediate layer) or 60 nm thicker (bottom cell counter electrode) for electrolyte catalytic activity.

Figure 17. Apparatus employed to sputter the Ti nanoparticles on SUS-mesh and Pt nanoparticles on FTO glass.

References:

1. J. Halme, P. Vahermaa; K. Miettunen and P. Lund, *Advanced Energy Materials*, 2010, **22**, E210-234.
2. A. L. Fahrenbruch, R.H. Bube; Fundamentals of solar cells. Photovoltaic solar energy conversion; Academic Press: New York (1983).
3. M. K. Nazeeruddin, A. Kay, I. Rodicio, R. H.-Baker, E. Muller, P. Liska, N. Vlachopoulos and M. Gratzel, *Journal of American Chemical Society*, 1993, **115**, 6382.
4. B. Qi and J. Wang, *Physical Chemistry Chemical Physics*, 2013, **15**, 8972.
5. J. Sobus and M. Ziotek, *Physical Chemistry Chemical Physics*, 2014, **16**, 14116.
6. M. K. Nazeeruddin, R. H.-Baker, P. Lisca and M. Gratzel, *Journal of physical Chemistry B*, 2003, **107**, 8981.
7. H. J. Snaith, L. S.-Mende, M. Gratzel and M. Chiesa, *Physical Review B*, 2006, **74**, 045306.
8. M. Toivola, L. Peltokorpi, J. Halme and P. Lund, *Solar Energy Materials and Solar Cells*, 2007, **91**, 1733.
9. L. Andrade, S. M. Zakeeruddin, M. K. Nazeeruddin, H. A.-Ribeiro, A. Mendes and M. Gratzel, *Physical Chemistry Chemical Physics*, 2009, **10**, 1117.
10. K. Ocakoglu, F. Yakuphanoglu, J. R. Durrant and S. Icli, *Solar Energy Materials and Solar Cells*, 2008, **92**, 1047.
11. I. G.-Valls, Y. Yu, B. Ballesteros, J. Oro and M. l.-Cantu, *Journal of Power Sources*, 2011, **196**, 6609.
12. A. Mathew, G. M. Rao and N. Munichandraiah, *Materials Chemistry and Physics*, 2011, **127**, 95.
13. M. G. Kang, K. S. Ryu, S. H. Chang, N. G. Park, J. S. Hong and K.-J. Kim, *Bulletin of Korean Chemical Society*, 2004, **25**, 5.
14. S. Zhang, X. Yang, Y. Numata and L. Han, *Energy & Environmental Science*, 2013, **6**, 1443.
15. J. Halme, G. Boschloo, A. Hagfeldt and P. Lund, *Journal of Physical Chememistry C*, 2008, **112**, 5623.
16. P. M. Sommeling, H. C. Rieffe, J. A. M. V. Roosmalen, A. Schonecker, J. M. Kroon, J. A. Winke and A. Hinsch, *Solar Energy Materials and Solar Cells*, 2000, **62**, 399.

17. A. C. Fisher, L. M. Peter, E. A. Ponomarev, A. B. Walker and K. G. U. Wijayantha, *Journal of Physical Chemistry B*, 2000, **104**, 949.

18. T. Trupke, P. Wrfel and I. Uhlendorf, *Journal of Physical Chemistry B*, 2000, **104**, 11484.

Chapter 3

Fabrication and characterization of TCO-less Tandem DSSC

3.1 Introduction:

Dye Sensitized Solar Cells (DSSCs) are one of most promising photovoltaic devices owing to ecological and low cost fabrication process [1-4]. Among 3rd generation solar cells and with comparison to organic solar cell, DSSCs are high in demand due to absence of vacuum process and better performance at large scale area [5,6]. Recently Kakiyage and Hanaya et al have achieved a mile stone of 14.3% efficient DSSC [7]. The demand of energy with time and technology improvement further promotes the need of scale up in DSSCs efficiency. High performance sensitized solar cell is possible by suitable modification of constituents of mesoporous layer, sensitizer involved or the blend of these nanomaterials incorporating at novel device level. Single sensitizer based DSSCs have shown limited absorption spectra and enhanced light harvesting from visible to near infrared (NIR) region has been reported by panchromatic usage of sensitizer. Mixing different sensitizers having different photo absorption regions seems to be promising however sensitizers employed of this arrangement possess prone to interaction with each other and photoconversion efficiency does not seems to be much improved [8-10]. Our group has earlier reported the bilayer sensitizer stained TiO_2 working electrode DSSC and the limited site availability of photoanode imposed hindrance towards considerable photovoltaic enhancement [11,12,13]. Another prominent way to enhance photo absorption region at device architecture level is to employ tandem structure, where two photo cells are connected in series or in parallel [14-18]. In tandem DSSCs (T-DSSCs), a top cell utilizes shorter wavelength region and a bottom cell harvests the longer wavelength region photon. In Parallel tandem cell arrangement, open circuit voltage (Voc) matching of subcells is ideally needed and sum of short circuit current (Jsc) (top cell and bottom cell) is obtained [14,19]. In series tandem cell, by matching the photocurrent density of top and bottom cells, the sum of open circuit voltage (Voc_{top} + Voc_{bottom}) of the top (Voc_{top}) and that of bottom cells (Voc_{bottom}) are ideally obtained. Many T-DSSCs have been reported [19-20] so far, however, almost all T-DSSCs have mechanically stacked structures. In these cells, light reaching the bottom electrode has to be pass through at least three transparent conductive oxide layers. These superfluous intermediate conductive glasses are responsible

towards obstacle in light transmission owing to inherent charge carrier concentration available and photon losses occurs.

T-DSSCs with TCO-glass/porous titania/dye1/electrolyte/dye2/porous NiO/TCO-glass have been reported, where photons reaching to the bottom electrode can pass through only one TCO-glass substrate [21-22]. This provides simple T-DSSC structure with NiO photocathode and efficient photon intensity at bottom cell is achieved, however, additional Voc is limited to about 0.1 V which is expected by the energy level difference between I_3^-/I^- redox potential and NiO valence band. M. Murayama et al have reported tandem architecture with Pt mesh sheet as intermediate layer [23]. However owing to Pt sheet, this structure does not seems to be cost effective and attractive towards industrialization purposes. Moreover the obtained efficiency was deeply affected by its optical transmittance. Y.Y. Yang et al have recently published tandem structure with Cu_2S intermediate counter electrode and quantum dot sensitized solar cell as top and bottom electrodes. However the obtained efficiency was less than 4% [24]. A quiet favourable and economical approach towards the fabrication of transparent conductive oxide less DSSCs with back contact electrode structure (TCO-less DSSC) has been reported [25-26]. The TCO-less DSSC is composed of glass substrate/TiO_2-dye layer/porous metal layer/electrolyte/counter electrode. The advantage of the TCO-less DSSC is the efficient light harvesting properties because light can be harvested directly without passing through TCO-layers. It has been reported that the TCO glass consist of around 20% cost burden of DSSCs fabrication [27] and the TCO-less back contact architecture with minimal conductive glass make it possible towards more economical realization. On the other hand it has been reported that the TCO-less back contact DSSCs have almost the same performance as that of TCO based DSSCs [25]. By using this TCO-less structure in the bottom electrode, the number of TCO layers can be reduced and light harvesting properties by the bottom electrode can be improved. TCO-less structure has shown a very attractive approach towards futuristic and emerging sensitized solar cell and has found application in different novel architectures like fiber type TCO-less cylindrical tandem DSSCs as reported previously [28].

Our group have also reported flat T-DSSCs where photons can pass through only one TCO substrate before reaching the bottom electrode by using the back contact structure. The flat T-DSSCs cell consists of TCO glass/TiO_2-dye layer (top electrode)/electrolyte/transparent Pt/compact TiO_2 /porous TiO_2 layer-dye (bottom electrode)/electrolyte/counter electrode structure. Though the structure was capable to

harvest enhanced light at bottom cell consisting of less TCO layers, the authors were able to observe actually a little higher Voc than that of the corresponding single cell. However, the Voc increase was limited because of electrolyte diffusions between top and bottom electrodes through pin holes of compact layer fabricated in the bottom electrode [29].

Here in this chapter we report series stacked DSSCs i.e. T-DSSCs architecture where bottom cell electrode structure has been fabricated using either one FTO glass or with completely metal structured (no FTO glass). The resulting cost effective T-DSSCs with efficient photon flux at bottom cell are able to utilize only two TCO glass instead of four, making it favourable choice towards futuristic tandem solar cell. The novel TCO-less T-DSSCs structures are capable to suppress absorption loss of infrared illumination (IR) by utilizing semi-transparent Pt sputtered FTO glass as an intermediate layer between top and bottom cell.

3.2 Experimental details:

3.2.1 Materials

All materials utilized in the present report are commercially available and were used without any further purification. Nanoporous highly transparent TiO_2 paste HT/SP (Solaronix, SA) and semi-transparent TiO_2 paste D/SP (Solaronix, SA) were utilized for the fabrication of top and bottom photoanodes respectively. To fabricate the tandem DSSCs by mechanically stacking top and bottom cells, corresponding mesoporous photoanodes were sensitized with indoline dye D-131 (Mitsubishi Paper Mills, Japan) and ruthenium dye cis-bis-(isothiocyanato)bis(2,2'-bypyridyl-4,4'-dicarboxy-lato)ruthenium(II)bis-tetrabutyl ammonium (N-719, Solaronix SA), respectively. The selection of these two dyes were performed for the sensitization of top and bottom electrodes owing to their complementary light absorption properties, an important requirement of sensitizer for tandem formation. The chemical structures of the dyes utilized in top cell (D131) and bottom cell (N719) along with their electronic absorption spectra (in solution form) are shown in the Fig. 1. Photoanode of TCO-less DSSC as bottom electrode was fabricated using mesoporous TiO_2 on flexible stainless steel mesh (SUS-730, Asada mesh Co. Ltd., Japan) having wire diameter of 13 μm with the spacing between the wire of 16 μm. In order

to avoid the contact between photoanode and counter electrode of top cell DSSC, a hot melt polymer film Himilan (Mitsui-DuPont Polychemicals Japan) of 30 µm thickness was used as spacer. The electrolytes and solvents utilized in this thesis were of reagent grade and used without any further purifications. The thickness of the nanoporous TiO_2 layer coated on the Fluorine doped Tin oxide glass (FTO glass) was measured using DEKTAK 6M (STYLUS PROFILER).

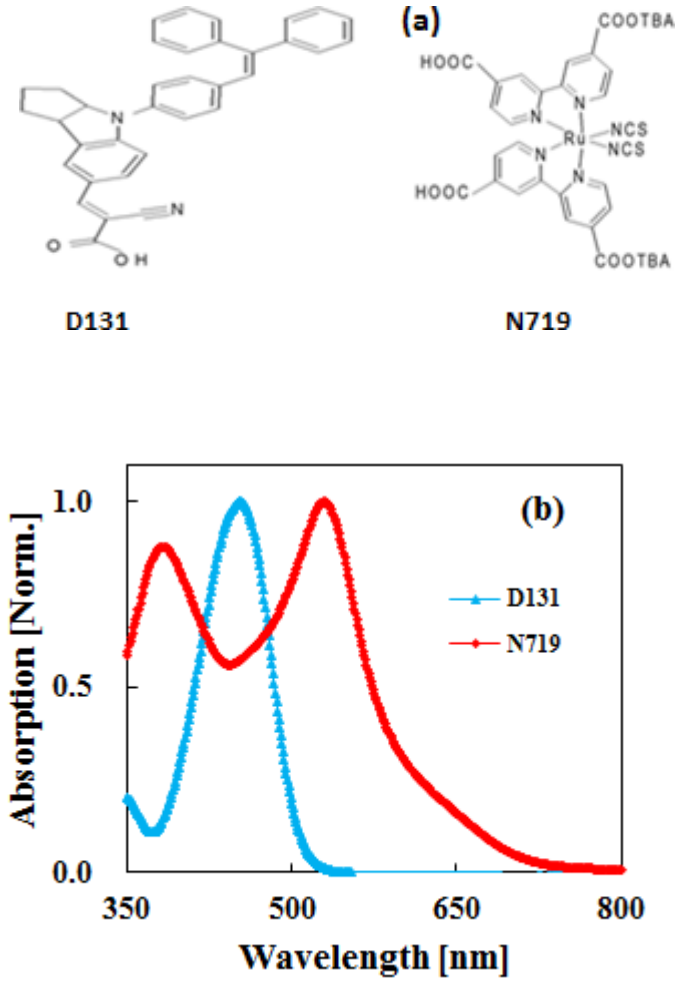

Figure 1. (a) Chemical structures and (b) electronic absorption spectra (ethanol solution) of the dye sensitizer, Ref [30].

3.2.2 Cell fabrication

3.2.2.1 TCO tandem DSSCs

TCO based tandem DSSCs consisting four TCO plates were prepared in the device configuration FTO glass/TiO_2-DyeA/electrolyte/semi-transparent Pt-FTO glass/ FTO glass /TiO_2/ DyeB/ electrolyte/ Pt-FTO glass which is schematically shown in the Fig. 2. Fluorine doped tin oxide (FTO) glasses were cleaned with detergent water, distilled water, acetone, IPA and distilled water respectively prior to use. After cleaning the glasses were subjected by N2 gas flow to make it dry and further operated with UV-ozone treatment in order to make surface hydrophilic and free of organic impurities.

Top cell fabrication:

Mesoporous TiO_2 layer for the top electrode was prepared by screen printing TiO_2 HT/SP paste followed by baking at 450˚C for 30 minute. This printed TiO_2 on FTO glass was immersed in 0.5 mM D-131 (acetonitrile: t-butyl alcohol (1:1 v/v)) for 4 hrs at room temperature for the dye adsorption. The counter electrode of the top cell should allow the maximum photon to reach the bottom cell and semi-transparent catalytic Pt layer of 1nm was deposited on a FTO glass by sputtering apparatus (CFS-4EP-LL, Shibaura Mechatronics, Japan). To make the top cell, D131 sensitized FTO based photoanode was assembled with semi-transparent Pt-coated FTO glass and Himilan film spacer followed by electrolyte insertion. After that the cell was sealed properly with epoxy resin.

As the bottom cell is able to receive only the remaining photons unabsorbed and passing through the top cell, it is important to optimize the thickness of nanoporous TiO_2 layer used for the sensitization of D131 dye of the cells. In this context, the possible variation of TiO_2 thickness has been made. The transmission of the light through the D131 stained varying thickness of TiO_2 nanoporous layer and falling on to the bottom cell was measured and is shown in Fig. 3. It can be clearly seen that with increasing thickness of the TiO_2 layer there is decrease in the transmittance of light, indicating maximum light transmission of around 70 % for the thickness of 1 μm.

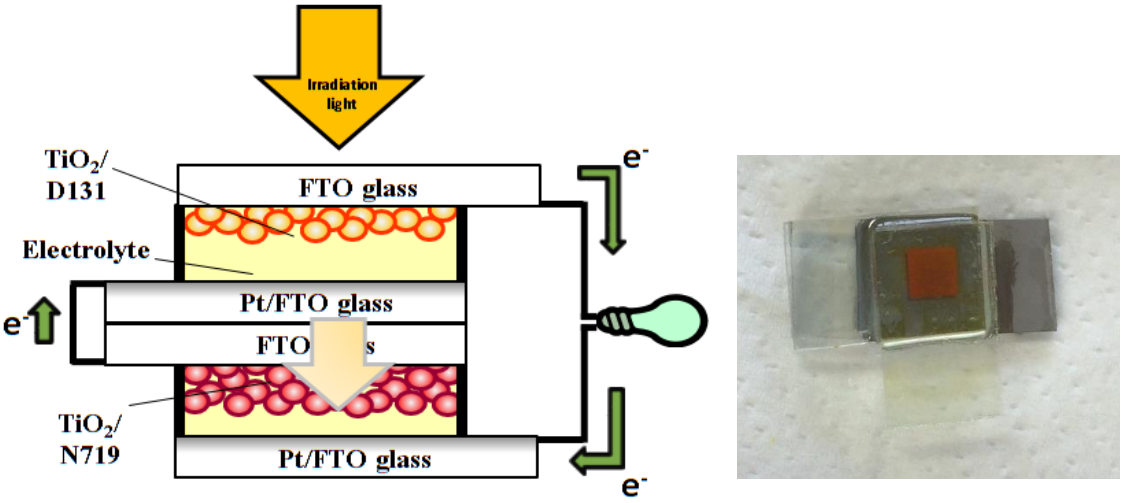

Figure 2. Schematic representation of TCO based Tandem DSSC having top cell thickness 1µm while bottom cell thickness 16µm, Ref [30].

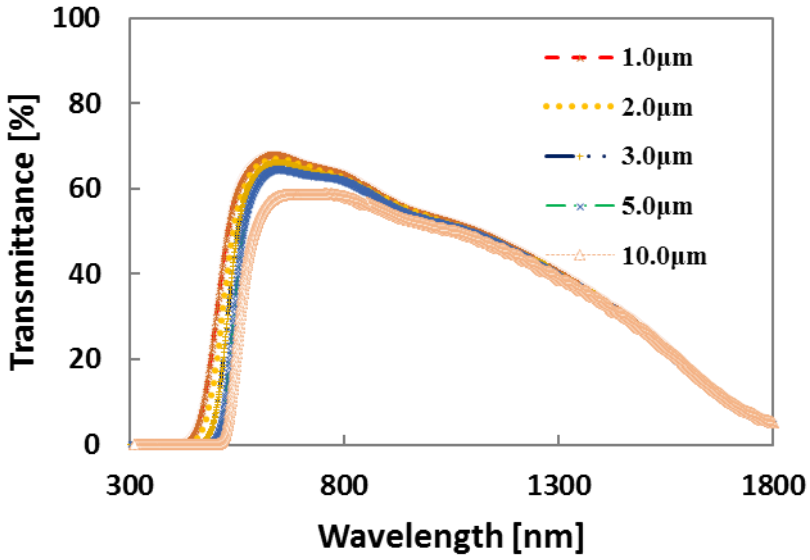

Figure 3. Change in the light transmission as a function of thickness of nanoporous TiO_2 layer of the top cell, Ref [30].

Bottom cell fabrication:

Nanoporous TiO_2 layer of the bottom electrode was prepared by screen printing TiO_2 D/SP paste followed by baking at 450˚C for 30 minute. The screen printed sample was immersed in 0.3 mM solution of N719 dye in acetonitrile: t-butyl alcohol (1:1 v/v) for 48 hours at room temperature. The bottom cell was assembled by similar process as of the top cell, except by employing counter electrode having 60nm thick Pt nanoparticle on FTO glass.

The TCO tandem DSSCs were then fabricated by mechanically stacking the top cell and the bottom cell in such a way that both are series connected (Fig. 2). Electrolyte used for top cell as well as bottom cell consisted of I_2 (50 mM), LiI (500 mM), 4-tert butyl Pyridine (580 mM) and 1-Ethyl 3-methylimidazoliumiodide (600 mM) in dehydrated acetonitrile.

In order to reduce one of costly materials TCO component in the tandem DSSCs, effort were made to remove the counter electrode of bottom cell. For this purpose the FTO glass was substituted by flexible titanium (Ti) foil. The architecture is shown in Fig. 4.

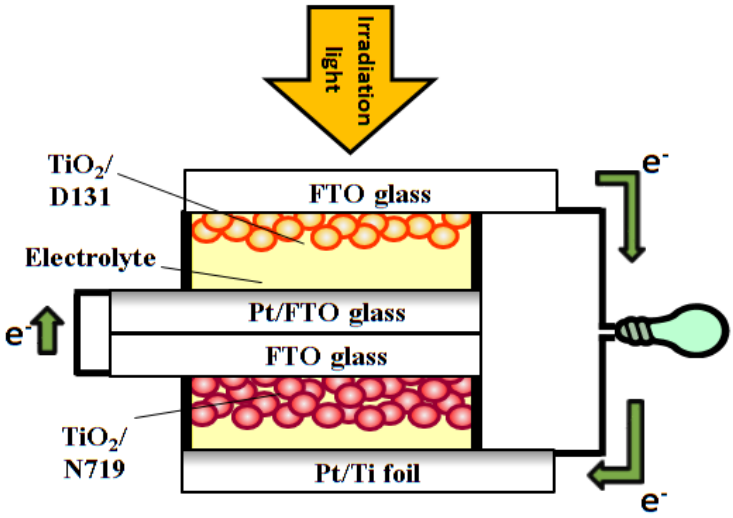

Figure 4. Schematic representation of TCO based tandem DSSCs with 60nm thick Pt sputtered Ti foil as bottom cell counter electrode.

3.2.2.2 TCO-less tandem DSSCs

TCO-less bottom cell fabrication:

In this device architecture, one of FTO glass of bottom electrode of TCO tandem DSSC was replaced by flexible metal mesh based TCO-less photoanode. This reduces one of the four TCO plates commonly used in standard mechanically stacked TCO tandem DSSCs. TCO-less tandem DSSC fabricated in this work consists of FTO glass/TiO_2-D131/electrolyte/semi-transparent Pt-FTO glass/ N719-TiO_2/metal mesh/electrolyte/Pt-FTO glass as schematically shown in the Fig. 5. Flexible and porous metal mesh used to fabricate the TCO-less photoanode not only serves the purpose of holding the nanoporous TiO_2 layer but functions as back contact current collecting grid also. TCO based top cell sensitized with D-131 dye was prepared in the similar manner as discussed in the section.

To prepare the TCO-less bottom cell photoanode, a porous TiO_2 paste (D/SP) was screen printed on Ti (240 nm) sputtered stainless steel mesh (SUS-730) followed by baking at 450˚C for 30 min. The sputtering of Ti nanoparticle layer on SUS mesh has the effect in blocking the electron back recombination by electrolyte [26]. This porous mesh coated with nanoporous TiO_2 was immersed in N719 dye solution for 48 hrs for dye adsorption. After dye absorption, samples were washed with similar solvent in order to remove residual un-adsorbed dyes. Bottom cell was prepared by assembling TiO_2 coated Ti/SUS mesh stained by N719 dye and Pt sputtered FTO glass. In order to avoid short circuit and to fill the space with electrolyte, porous polytetrafluoroethylene (PTFE) film having thickness of 35µm (H010A293D), 0.1µm pore size, ADVANTEC) was placed in between mesh and Pt/FTO glass counter electrode. After insertion of electrolyte, both of the bottom and top cells were finally sealed with the epoxy resin. TCO-less tandem DSSC was then finally fabricated by mechanically stacking the TCO-based top cell sensitized with D131 dye and TCO-less bottom cell sensitized with N719 dye.

3.2.2.3 TCO-less tandem DSSCs consisting two FTO plates

The new tandem device architecture have been proposed by avoiding the FTO glass of the TCO tandem DSSC bottom cell by implementing a new TCO-less device architecture. Towards this approach, nanoparticle Pt coated FTO counter electrode of bottom cell of TCO-tandem DSSC (Fig. 2) was replaced by nanoparticle Pt coated flexible titanium (Ti) metal foil. Ti metal foil are

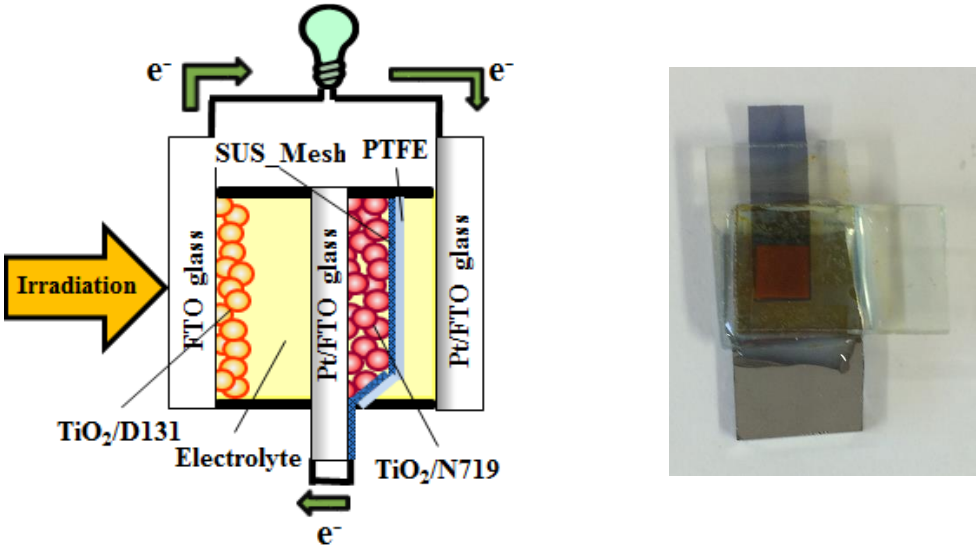

Figure 5. Schematic structure of TCO-less tandem DSSC with three FTO glass as transparent conducting substrate having 1µm thickness top cell and 16µm thickness bottom cell, Ref [30].

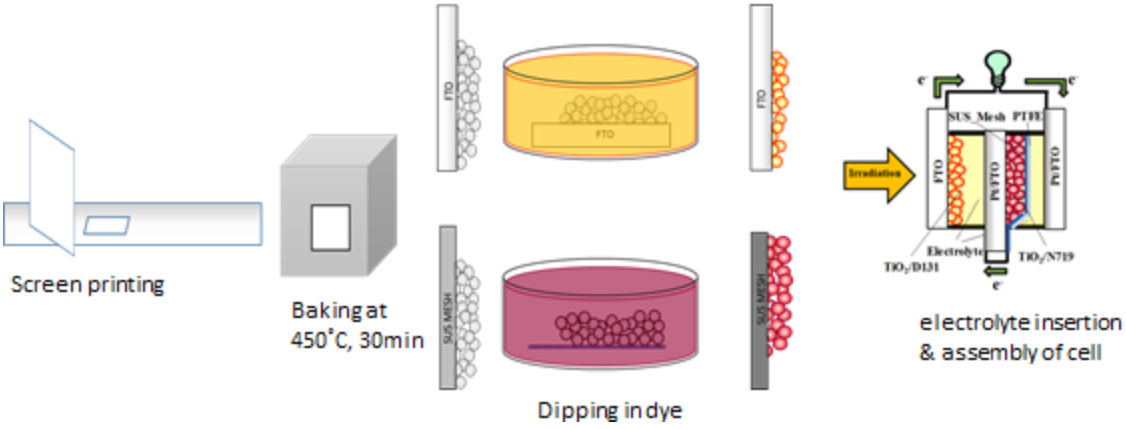

Figure 6. Schematic of the general process of TCO-less Tandem DSSC fabrication process.

well known flexible metal with high temperature sinterability, better conductivity and are economical than FTO glass. These properties of Ti foil places it an alternative of FTO glass with nontransparent application leading light weight DSSCs fabrication. TCO-less tandem DSSCs consisting of no TCO glass in bottom cell were fabricated in the device architecture FTO glass/TiO_2-D131/ electrolyte/semi-transparent Pt-FTO glass/ N719-TiO_2-metal-

mesh/electrolyte/Pt-Ti Foil as shown in Fig. 7. The basic fabrication process for individual TCO based top cell sensitized with D131 and completely TCO free N719 sensitized bottom electrode was similar to that discussed earlier. The only difference in TCO-less bottom electrode fabrication lies in the removal of Pt-coated FTO glass as counter electrode by Pt sputtered Ti-foil as the counter electrode. Thickness of the sputtered catalytic Pt layer on the Ti-foil was maintained at 60 nm.

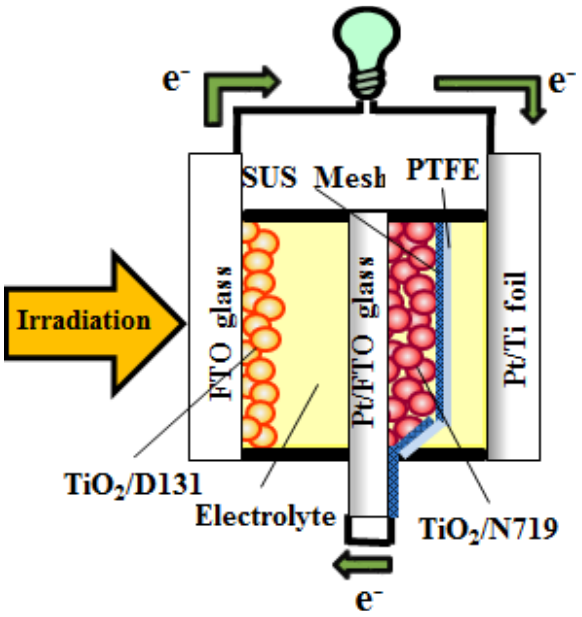

Figure 7. Schematic structure of TCO-less tandem DSSC with only two FTO glass as transparent conducting substrate. The thickness of top cell is 1µm and bottom cell has thickness 16µm, Ref [30].

3.3 Results and discussion

3.3.1 Optimization of top cell Jsc in TCO tandem DSSCs

In series connected cells of T-DSSCs, top cell performance in terms of its optimum thickness, light transmission through the top cell along with the complementary light absorption and photon harvesting with respect to the bottom cell play a crucial role. In previous section we have shown the effect of top cell TiO_2 thickness towards optical transparency. In the series connected cells of T-DSSCs, overall efficiency is mainly controlled by the cell with the lower Jsc,

while large mismatch in bottom cell and top cell Jsc results in poor fill factor (FF) ultimately leads to the poor performance. The effects of top cell photo anode thickness on Jsc and fill factor for fabricated tandem solar cell has been summarized in Fig. 8. On the other hand Fig. 9 exhibits the photovoltaic characteristics of TCO-based single cell and T-DSSCs fabricated using D131 sensitized top cell of 3µm and N719 sensitized bottom cell as per the TCO tandem DSSC device architecture (shown in Fig. 2). It can be seen from this Fig. 8 that Voc of the T- DSSC is the sum of the Voc of top and bottom cells which is a typical characteristics of the series connected T-DSSCs. Table 1 shows that, T-DSSC only shows a little increase in the external power conversion efficiency (4.3 %) as compared to best single cell (3.8 %, top cell). In spite of the summation of the Voc in T-DSSC, the very low FF owing to highly mismatched Jsc of the top and bottom cells could be responsible for the only slight enhancement of the photoconversion efficiency.

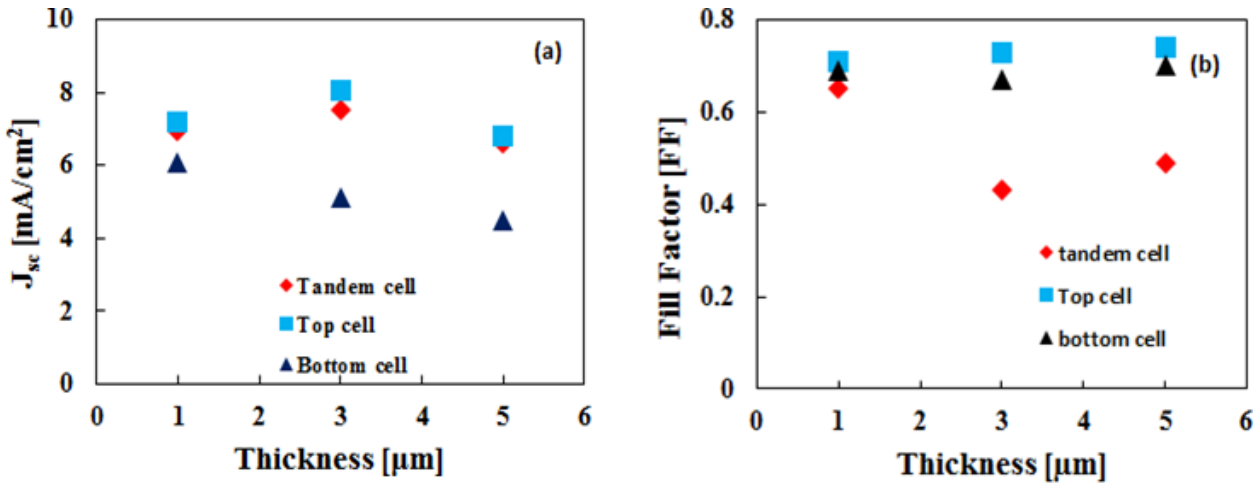

Figure 8. The effect of top cell mesoporous layer thickness effect on TCO Tandem DSSC (a) short circuit current density (Jsc) (b) Fill factor (FF).

3.3.2 TCO tandem DSSCs performance

Based on the observation of decrease in the light intensity transmitting through the dye D131 sensitized top cell, effect of the thickness of nanoporous TiO_2 layer on the photovoltaic performance of TCO tandem DSSCs (Fig. 2) was investigated and these results are shown in Fig 10. With the increase in thickness of top cell mesoporous layer, the photon flux harvesting of top

Table 1. Photovoltaic parameters for single cell and T-DSSC in TCO-tandem DSSC (Fig. 2) configuration of TCO tandem DSSCs with 3µm thick top cell photoanode and 16 µm thick bottom cell photoanode.

	J_{sc}(mA/cm^2)	V_{oc}(V)	*FF*	η(%)
Tandem Cell	7.50	1.34	0.43	4.32
Top Cell	8.06	0.71	0.67	3.84
Bottom Cell	5.13	0.64	0.73	2.04

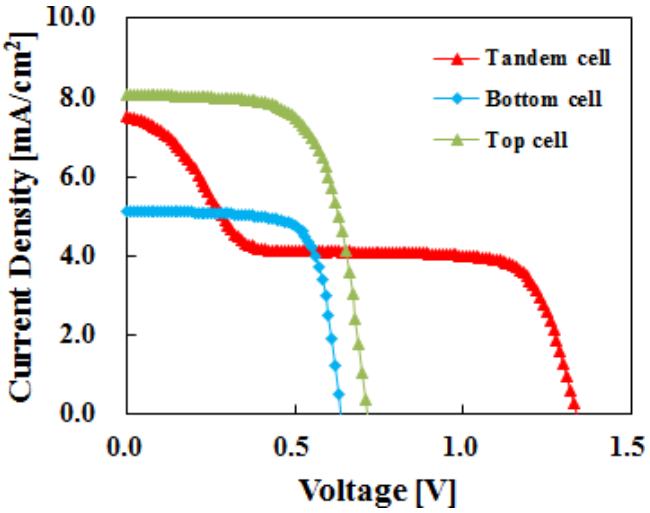

Figure 9. I-V curves for D131 sensitized top cell and N719 sensitized bottom cell along with TCO Tandem DSSC (Fig. 2) after the simulated solar irradiation. Thickness of the top cell nanoporous TiO_2 layer was 3 µm and bottom cell TiO_2 thickness was maintained at 16 µm, Ref [30].

cell increases. At the same time this enhanced photo harvesting by top cell reduces the intensity of the photon reaching the bottom cell and the adverse effects on the performance of bottom cell has been observed. In all cases Voc in T-DSSCs was always the sum of the Voc of respective top and bottom cells but FF was found to decrease drastically when the thickness of the top cell TiO_2 layer

increased over 1 µm ultimately, leading to hampered overall photoconversion efficiency of the TCO Tandem DSSC (shown in Fig. 2).

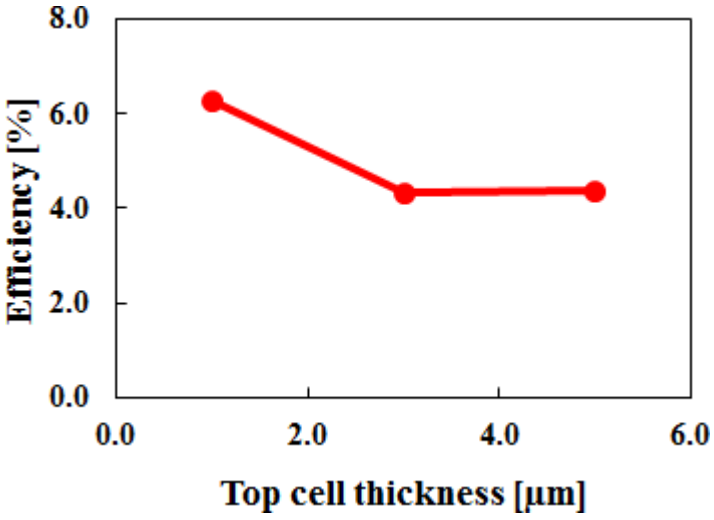

Figure 10. Effect of thickness of nanoporous TiO_2 sensitized with D131 in top cell on the photoconversion efficiency of TCO-based T-DSSCs, Ref [30].

Best photovoltaic performance (6.28%) and photon harvesting behaviour of the TCO tandem DSSC (architecture of Fig. 2) were, therefore, obtained with top cell sensitized D131 having 1µm thick nanoporous TiO_2. The IV characteristics and the IPCE spectra are shown in Fig. 11 along with the photovoltaic parameters are shown in the Table 2. It clearly indicates that relatively better match Jsc of the top cell (7.17 mA/cm^2) and bottom cell (6.07 mA/cm^2) results in the observation of better FF of 0.65 ultimately leading to the much improved photoconversion efficiency as compared to their individual top and bottom cell counterparts.

The TCO tandem DSSCs with Ti foil bottom cell counter electrode (Fig. 4) photovoltaic performance has been shown in Fig. 12 and in Table 3. The fabricated tandem cell shows better efficiency (6.64%) than previous TCO tandem architecture and it can be ascribed to enhanced catalytic activity of bottom cell counter electrode.

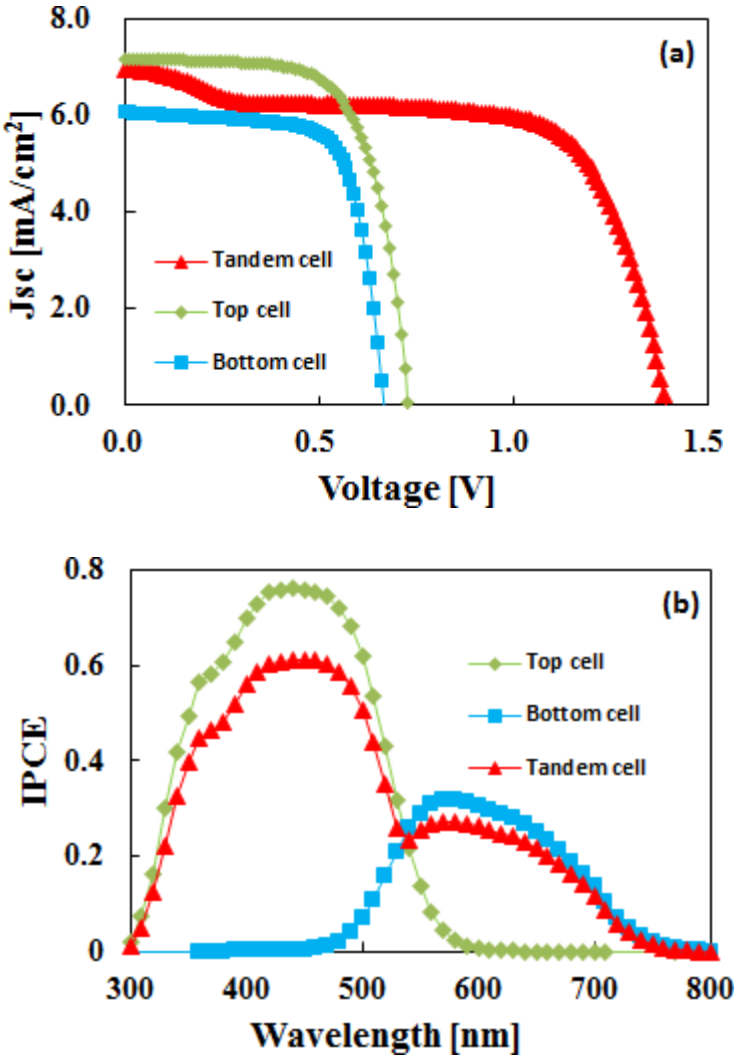

Figure 11. I-V curves (a) and photocurrent action spectra (b) for D131 sensitized top cell and N719 sensitized bottom cells along with TCO tandem DSSC (Fig. 2), Ref [30].

Table 2. Photovoltaic parameters for TCO based single top and bottom cells along with TCO tandem DSSC (Fig. 2) having TiO_2 layer thickness (1 µm) in the top cell.

	J_{sc} (mA/cm^2)	V_{oc} (V)	*FF*	Efficiency (%)
Tandem Cell	6.96	1.40	0.65	6.28
Top Cell	7.17	0.73	0.67	3.53
Bottom Cell	6.07	0.67	0.71	2.89

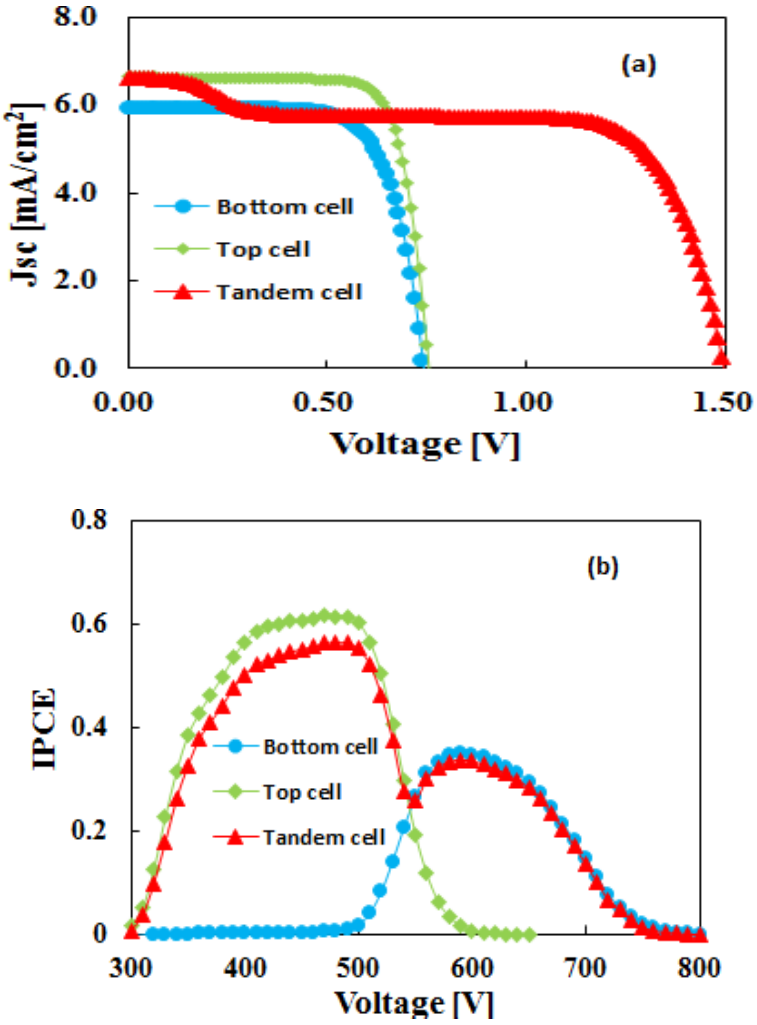

Figure 12. I-V curves (a) and photocurrent action spectra (b) for D131 sensitized top cell and N719 sensitized bottom cells of TCO tandem DSSC (Fig. 4) architecture with Ti foil counter electrode.

3.3.3 Working principle of TCO-less tandem DSSCs with three TCO substrates

In the present work, T-DSSC is fabricated by mechanically stacking two DSSCs (Top and bottom cells) connected in the series with an attempt to remove one of the TCO component from the bottom cells implementing the protected metal mesh based TCO-less DSSC architecture reported by our group previously [26]. Figure 13 depicts the schematic representation and electron flow in

Table 3. Photovoltaic parameters for TCO based single top and bottom cells with Ti foil as counter electrode in TCO tandem DSSC (Fig. 4) having TiO_2 layer thickness (1 μm) in the top cell.

	J_{sc} (mA/cm^2)	V_{oc} (V)	*FF*	Efficiency (%)
Tandem Cell	6.61	1.50	0.67	6.64
Top Cell	6.64	0.76	0.78	3.89
Bottom Cell	5.93	0.74	0.72	3.16

series connected TCO-less T-DSSCs consisting with TCO-based top cell sensitized with D131 and TCO-less bottom cells sensitized with Ruthenium dye N719. Irradiation of light flux was introduced directly on top cell passing through the two FTO layers and mesoporous TiO_2/dye layer top cell reaching to the TCO-less bottom cell. Illumination with light having energy greater or equal to band gap of top cell dye (D131) is capable to excite the electrons from $(HOMO)_{top\ cell}$ to $(LUMO)_{top\ cell}$. Simultaneously, bottom cell stained with dye N719 also absorbs the remaining light flux passed out from the top cell. The complementary electronic absorption spectra of dyes D131 and N719 (Fig. 1) indicates that photon beyond 500 nm which were unable to be absorbed by the top cell are now available for the bottom cell. Remaining reduced intensity light available at bottom cell and greater or equal to band gap of bottom cell dye (N719) excites electron from $(HOMO)_{bottom\ cell}$ to $(LUMO)_{bottom\ cell}$. Since LUMO of both of dyes utilized in the present case energetically match and higher than conduction band level of mesoporous TiO_2. This energetic matching leads to the facile electron injection and electron collection by mesoporous TiO_2 layer. The bottom cell electron are collected by mesoporous TiO_2 on protected metal mesh (TCO-less bottom cell). Electrons from the top cell photoanode find their path by external load to counter electrode of the bottom cell. At the same time, electrons collected by the TCO-less photoanode of the bottom cell also reaches to counter electrode of the top cell. These collected electrons at counter electrodes of the corresponding top cell and bottom cell reduce the oxidized redox species (electrolytes) and finally lead the dye regeneration.

$$D + h\nu \rightarrow D^{*} \qquad \text{Excitation process}$$

$$D^{*} + TiO_2 \rightarrow e^{-}_{TiO_2} + S^{+} \qquad \text{Injection process}$$

$$e^{-}_{TiO_2} + C.E. \rightarrow TiO_2 + e^{-}(C.E.) \qquad \text{Energy Generation}$$

$$S^{+} + \frac{3}{2} I^{-} \rightarrow S + \frac{1}{2} I_3^{-} \qquad \text{Regeneration of dye}$$

$$\frac{1}{2} I_3^{-} + e^{-}_{C.E.} \rightarrow \frac{3}{2} I^{-} + C.E. \qquad \text{Electron recapture reaction}$$

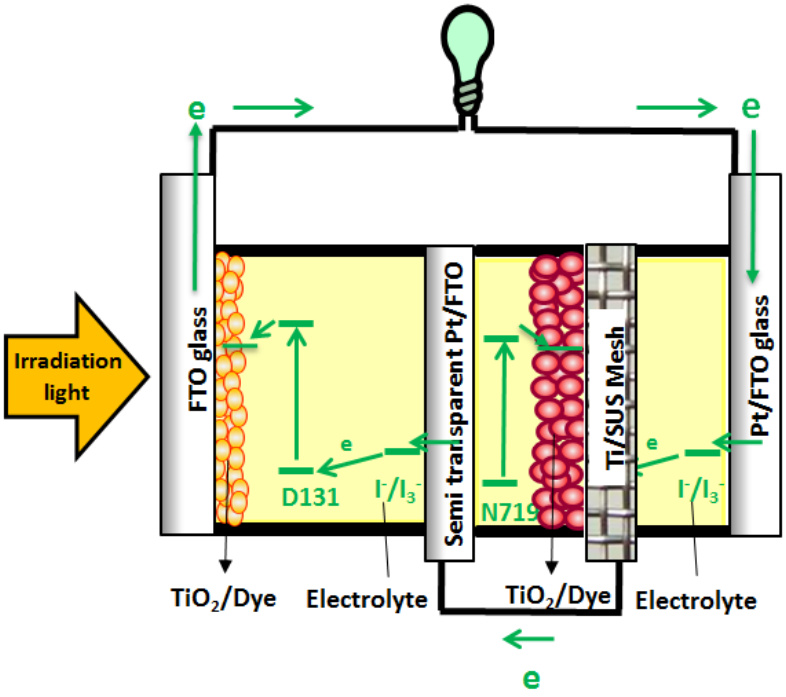

Figure 13. Schematics working principle of TCO-less tandem DSSC, Ref [30].

3.3.4 Optimization of bottom cell Jsc in TCO-less tandem DSSCs

As discussed in the previous section, mechanically stacked TCO tandem DSSCs usually consist of four FTO glasses as TCO substrates. TCO is not only one of the costly components of the DSSCs with but it also affects the transmission of light while passing from top to bottom as shown in Fig. 14. Back contact (BC) TCO-less tandem DSSCs were fabricated and transmission of light at the surface of bottom cell TiO_2 photoanode were measured and compared with TCO Tandem DSSC based bottom cell counterparts. The photon transmission spectra available to bottom cell of different tandem architecture are shown in Fig. 15. It can be clearly seen that only removal of one TCO-layers of the bottom cell by implementing the BC TCO-less device architecture leads to about 20 % enhancement in transmitted light in the wavelength region of 600-1100 nm. These results suggest the usefulness of TCO-less T-DSSC architecture in terms of available light flux to bottom cells especially if these cells are potential near infra-red (NIR) sensitizers.

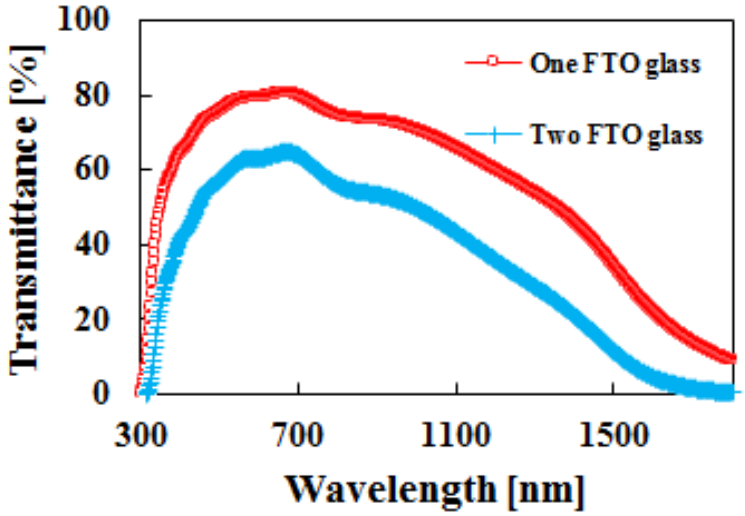

Figure 14. The transmission loss offered by the FTO glass towards photon transmission.

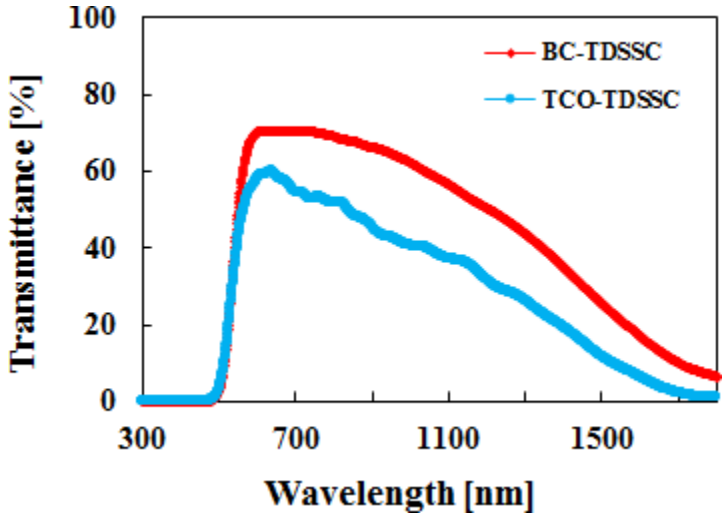

Figure 15. Transmission spectra of T-DSSC for photon passing through three TCO layers (TCO-TDSC of Fig. 2) and only two TCO layers (Back contact T-DSSC shown in Fig. 5), showing availability of photons at respective bottom cell photoanodes, Ref [30].

As discussed earlier in the standard TCO tandem DSSCs, nanoporous TiO_2 with 1 µm thickness attributed the best photovoltaic performance. Optimization of the TiO_2 layer thickness of TCO-less bottom photoanode sensitized with N719 dye was carried out for TCO-less T-DSSC (Fig. 5). Thickness of nanoporous TiO_2 layer coated on the protected metal mesh (bottom TCO-less electrode) was varied and the results is shown in Fig. 16. In all the TCO-less T-DSSCs, Voc about 1.45 V (sum of the Voc of top and bottom cells) was observed, demonstrating the tandem functionality. It is interesting observation from Fig. 16 that an optimum thickness of TiO_2 layer is necessary to harvest the maximum photons reaching the bottom cell. A relatively thinner nanoporous TiO_2 layer leads to inefficient light harvesting while much thicker TiO_2 leads redox ion diffusion limitation leading to reduced performance of the TCO-less bottom cell. In both of the cases mismatch of Jsc of the top and bottom cells leads to reduced FF of T-DSSCs and ultimately results in hampered overall photoconversion efficiency.

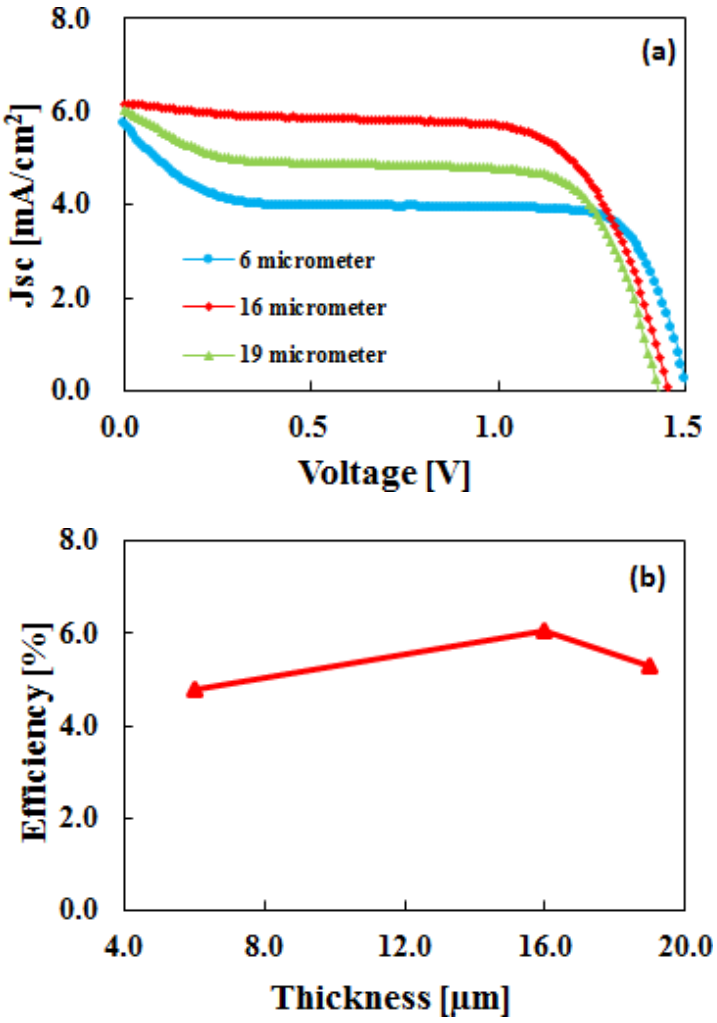

Figure 16. (a) Effect of bottom cell thickness variation on the I-V characteristics on TCO-less T-DSSCs (Fig. 5) and (b) thickness dependence of bottom cell TiO_2 layer on photoconversion efficiency of TCO-less T-DSSCs, Ref [30].

3.3.5 TCO-less tandem DSSCs performance

As revealed from the Fig. 16(b), best photovoltaic performance and photon harvesting of the TCO-less T-DSSC was obtained using 16 µm thick bottom electrode sensitized with N719 in combination with TCO based top cell sensitized with D131 (1 µm TiO_2 layer thickness) and the photovoltaic performance are shown in Fig. 17 and Table 4. Upon simulated solar irradiation, an

external power conversion efficiency of 6.06 % was obtained for this TCO-less T-DSSC (Fig. 5). In addition the Voc of TCO-less T-DSSC (1.45V) is sum of Voc observed for top cell (0.76 V) and bottom cell (0.68V), confirming the successful formation of tandem cell. It is interesting to note that even after removal of one TCO layer, the photoconversion efficiency of TCO-less T-DSSC (containing three TCO layer) is only slightly smaller than that of the conventional TCO Tandem DSSC having four TCO layers) counterpart (6.28 %).

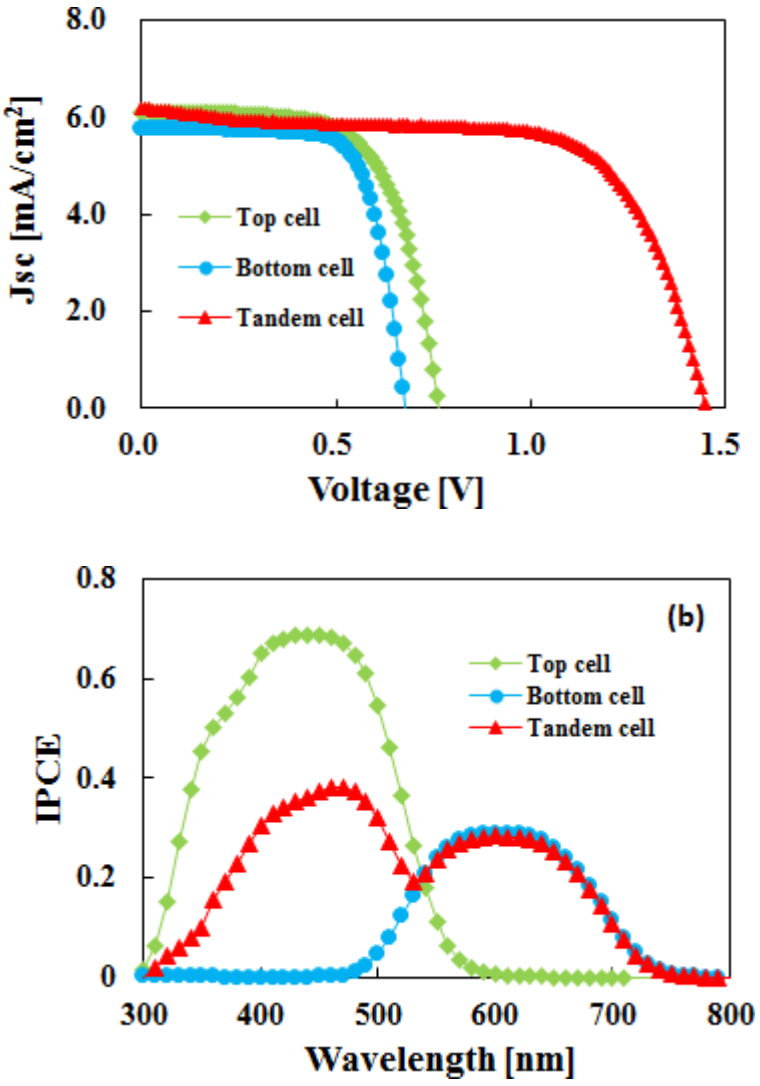

Figure 17. I-V (a) and IPCE (b) characteristics of TCO-less T-DSSC (Fig. 3) after removal of one TCO layer from the bottom cell under simulated solar and monochromatic light illumination, respectively, Ref [30].

Table 4. Photovoltaic parameters of TCO-less T-DSSC (Fig. 3) after simulated solar irradiation.

	J_{sc} (mA/cm^2)	V_{oc} (V)	*FF*	Efficiency (%)
Tandem Cell	6.17	1.45	0.68	6.06
Top Cell	6.12	0.76	0.66	3.06
Bottom Cell	5.79	0.68	0.72	2.83

3.3.6 Performance evaluation of TCO-less tandem DSSCs with two TCO plates:

In order to remove TCO layer completely from the bottom cell, TCO-less T-DSSC was fabricated using back contact TCO-less bottom cell sensitized with dye N719 where Pt coated FTO glass was replaced with the Pt-coated Ti-foil as counter electrode in the device architecture shown in the Fig. 7. The Fabricated TCO-less T-DSSC contains only two TCO layers in the top cell sensitized with D131 having the optimized thickness of nanoporous TiO_2 layer of 1 µm as discussed in the previous section. Figure 18 exhibits the photovoltaic characteristics and photocurrent action spectra for TCO based top cell, completely TCO-less bottom cell along with the series connected TCO-less T-DSSC (Fig. 7) along with the photovoltaic parameters shown in Table 5. This Fig. 18 and Table clearly reveals that completely TCO-less bottom cell sensitized with N719 dye works even better than its TCO based bottom counter parts in terms of all of the device parameters. A very good match of the Jsc for top and bottom cell results in to high FF of 0.69 for the TCO-less T-DSSC (Fig. 7) resulting in to the external power conversion efficiency of 7.10 % which is much better than that of the single cell efficiencies. The observation of the high Jsc and FF for the TCO-less bottom cell (Fig. 7) could be attributed to the more electrocatalytic activity of conductive Ti foil and effective use of incoming photon flux to the bottom cell utilizing the reflected light from the metallic Ti-foil. This was confirmed by the relatively higher IPCE (Fig. 18) of the TCO-less T-DSSC (Fig. 7) when completely TCO free bottom cell was used as compared to TCO-based bottom cell as shown in Fig. 17. At the same, the relatively higher conductivity of the Ti-foil as compared to the FTO glass results in the observation of higher FF.

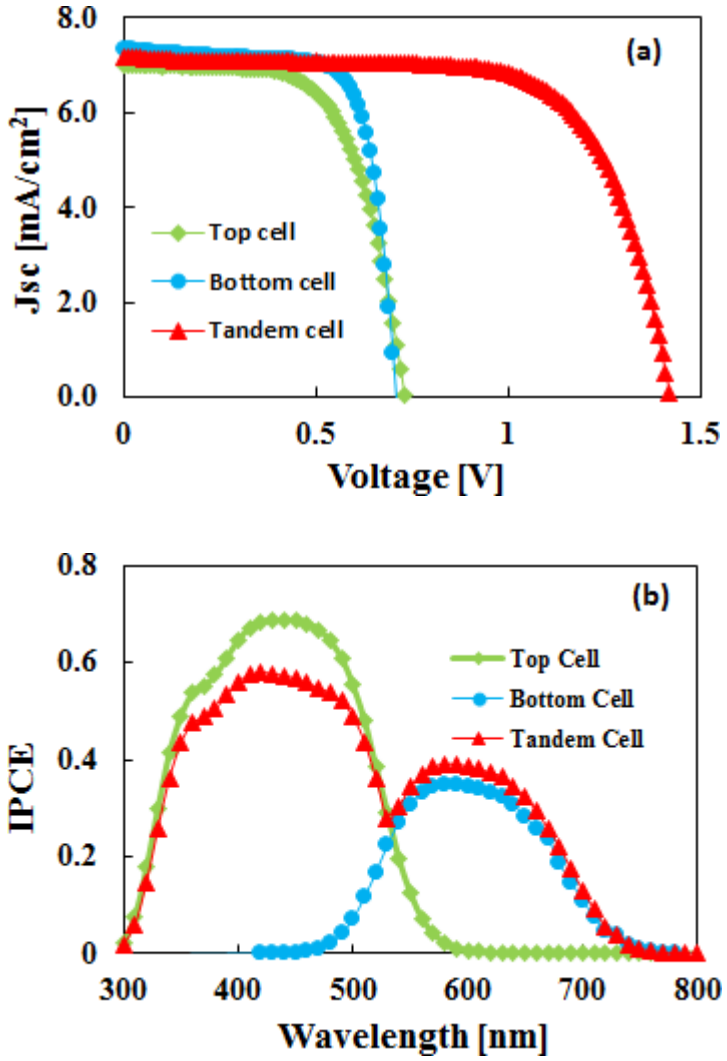

Figure 18. Photovoltaic characteristics (a) and photocurrent action spectra (b) for single cells and TCO-less T-DSSC (Fig. 4) after the complete removal of TCO layer from the bottom cell, Ref [30].

Table 5. Photovoltaic parameters of top cell, TCO-less bottom cell and T-DSSC (Fig. 7) after simulated solar irradiation.

	J_{sc} (mA/cm^2)	V_{oc} (V)	*FF*	Efficiency (%)
Tandem Cell	7.20	1.42	0.69	7.10
Top Cell	7.00	0.73	0.64	3.26
Bottom Cell	7.36	0.71	0.74	3.86

3.4 Conclusion

Mechanically stacked and series connected TCO-less T-DSSCs were attempted in different novel device structures not only to remove the costly TCO components but to enhance efficiency and match the photovoltaic performance with their TCO based T-DSSC counterparts. Optimization in terms of the nanoporous TiO_2 layer utilized for top and bottom cell was carried out to obtain the maximum Jsc for both of the single cells followed by their matching to obtain optimum FF for T-DSSCs. The optimum thickness for the TCO- based top cell sensitized with D131 and TCO-less bottom cell sensitized with N719 dye was found to be 1 µm and 16 µm, respectively. Interestingly, it was found that complete removal of the TCO layer from the bottom cell exhibited the best TCO-less T-DSSC giving Jsc of 7.20 mA/cm^2, Voc of 1.42 V and FF of 0.69 leading to the external power conversion efficiency of 7.10 % under simulated solar irradiation. In spite of removal of two TCO layers in the TCO-less T-DSSC and by containing only two TCO layers, it exhibited superior photovoltaic performance as compared to its TCO based T-DSSC (6.28 %) containing four TCO layers. These results clearly indicate the superiority of our novel TCO-less T-DSSC architecture over TCO based Tandem cells and justify their potentiality towards fabrication of more efficient DSSC by implementing the efficient NIR dyes for bottom TCO-less electrode.

3.5 References:

1 M. Gratzel, *Journal of Photochemistry and Photobiology C, Photochemistry Reviews,* 2003, **4**, 145.

2 W. H. Thomas, A. J. Rebecca, B. F. M. Alex, Van R. Hal and T. H. Joseph, *Energy & Environmental Science,* 2008, **1**, 66.

3 M. Gratzel, *Acc. Chemical Research*, 2009, **42**, 1788.

4 A. Hagfeld, G. Boschloo, L. C. Sun, L. Kloo and H. Pettersson, *Chemical Reviews,* 2010, **110**, 6595.

5 M.A. Green, K. Emery, Y. Hishikawa, W. Warta and E. D. Dunlop, *Progress in Photovoltaics: Research and Applications,* 2015, DOI: 10.1002/pip.2573.

6 H. S. Jung and J.-K. Lee, *The journal of Physical Chemistry Letters*, 2013, **4**, 1682.

7 K. Kakiage, Y. Aoyama, T. Yano, K. Oya, J. Fujisawa and M. Hanaya, *Chemical Communication*, 2015, DOI: 10.1039/C5CC06759F.

8 K. Zhang, C. Qin, X. Yang, A. Islam, S. Zhang, H. Chan and L. Han, *Advanced Energy Materials*, 2014, 1301966.

9 J.-H. Yum, S.-R Jang, P. Walter, T. Geiger, F. Nuesch, s. Kim, J. Ko, M. Gratzel and M.K. Nazeeruddin, *Chemical Communication*, 2007, 4680.

10 J. Chang, C. P. Lee, D. Kumar, P. W. Chen, L. Y. Lin, K. R. J. Thomas and K. C. Ho, *Journal of Power Sources*, 2013, **240**, 779.

11 F. Inakazu, Y. Noma, Y. Ogomi and S. Hayase, *Applied Physics Letters*, 2008, **93**, 093304.

12 Y. Ogomi, S. S. Pandey, S. Kimura and S. Hayase, *Thin Solid Films,* 2010, **519**, 1087.

13 Y. Noma, K. lizuka, Y. Ogomi, S. S. Pandey and S. Hayase, *Japanese Journal of Applied Physics,* 2009, **48**, 020213.

14 W. Kubo, A. Sakamato, T. Kitamura, Y. Wada and S. Yanagida, *Journal of Photochemistry and Photobiology A: Chemistry,* 2004, **164**, 33.

15 M. Durr, A. Bamedi, A. Yasuda and G. Nelles, *Applied Physics Letters*, 2004, **84**, 3397.

16 M. Murayama and T. Mori, *Journal of Physics D: Applied Physics,* 2007, **40**, 1664.

17 W. S. Jeong, J. W. Lee, S. Jung, J. H. Yun and N. G. Park, *Solar Energy Materials & Solar cells* , 2011, **95**, 3419.

18 T. Kinoshita, J. T. Dy, S. Uchida, T. Kubo and H. Segawa, *Nature Photonics*, 2013, **7**, 535.

19 M. Yanagida, N. O. Komatsuzaki, M. Kurashige, K. Sayama and H. Sugihara, *Solar Energy Materials & Solar Cells*, 2010, **94**, 297.

20 T. Yamaguchi, Y. Uchida, S. Agatsuma and H. Arakawa, *Solar Energy Materials & Solar Cells*, 2009, **93**, 733.

21 A. Nattestad, A.J. Mozer, M.K.R. Fischer, Y.-B. Cheng, A. Mishra, P. Bauerle and U. Bach, *Nature Materials*, 2010, **9**, 31.

22 H. Choi, T. Hwang, S. Lee, S. Nam, J. Kang, B. Lee and B. Park, *Journal of Power Sources*, 2015, **274**, 937.

23 M. Murayama and T. Mori, *Thin solid films*, 2008, **516**, 2716.

24 Y-Y Yang, Q-X Zhang, T.-Z Wang, L.-F Zhu, X.-M Huang, Y.-D Zhang, X. Hu, D.-M. Li, Y.-H Luo and Q.-B. Meng, *Electrochimica Acta*, 2013, **88**, 44.

25 Y. Kashiwa, Y. Yoshida and S. Hayase, *Applied Physics Letters,* 2008, **92**, 033308.

26 M. Z. Molla, N. Mizukoshi, H. Furukawa, Y. Ogomi, S. S. Pandey, T. Ma, and S. Hayase, *Progress in Photovoltaics: research and Applications*, 2015, **23**, 1100.

27 J. M. Kroon, N. J. Bakker, H. J. P. Smit, P. Liska, K. R. Thampi, P. Wang, S. M Zakeeruddin, M. Graetzel, A. Hinsch, S. Hore, U. Wurfel, R. Sastrawan, J. R. Durrant, E. Palomares, H. Pettersson, T. Gruszecki, J. Walter, K. Skupien and G. E. Tulooch, *Progress in Photovoltaics*, 2007, **15**,1.

28 J. Usagawa , S. S. Pandey, S. Hayase, M. Kono and Y. Yamaguchi , *Applied Physics Express*, 2009, **2**, 062203.

29 K. Uzaki, S. S. Pandey and S. Hayase, *Journal of Photochemistry and Photobiology A: Chemistry*, 2010, **216**, 104.

30 A. K. Baranwal, T. Shiki, Y. Ogomi, S.S. Pandey, T. Ma and S. Hayase, *RSC Advances*, 2014, **4**, 47735.

.

Chapter 4

TCO-less back contact Tandem DSSCs having extended wavelength photon harvesting

4.1 Introduction:

Stimulated by continuously raising demand of energy and the constraint in fossil fuel resources, the renewable energy resources are pivotal and particularly the solar energy are main source of energy. Among the 3rd generation solar energy resources, dye sensitized solar cells (DSSCs) have attracted attention for cost effective solar energy harvesting aiming towards the realization of low carbon society and diverse response in variable light conditions [1-2]. DSSCs have drawn more attention towards stabilized power output with variation of incident light angle and possess enormous potential in comparison to Si solar cell [3]. On the other hand colorful DSSCs are more appealing and resourceful towards window application. Their performance is highly affected towards the engaged mesoporous layer in collaboration with sensitizer and regenerative agent employed in conjunction with conductive glass. The Photo harvesting capability of DSSCs are inherent from employed sensitizing dyes and the enhanced photovoltaic performance is possible by further exploring the panchromatic photon harvesting from visible to near infra-red (NIR) wavelength region [4,5]. The DSSCs employed of dyes with capability of NIR light absorption have shown lower efficiency. The utilization of these dyes as photosensitizer always have a tradeoff between open circuit voltage and absorption spectra [6]. Panchromatic photon harvesting has been offered by various strategies at sensitizer level. However, these strategies were not as beneficial and have been discussed in the previous chapter.

According to Shockley-Queisser limit of 30% efficiency of single junction device, the power conversion efficiencies of solar cell can be extended beyond this by interconnecting different solar subcells in tandem architecture [7]. Implementation of tandem device architectures provide the capability to make full advantage of not only harvesting photons in wider wavelength region of sunlight effectively but also attainment of higher resultant open circuit voltage (Voc) [8]. The tandem device architecture has been well advocated also in order to extend photoconversion

efficiency by shifting the photon harvesting window up to longer wavelengths in a combination that upper cell have higher bandgap photon window while lower cell have low band gap window. In the construction of mechanically stacked tandem DSSCs incorporating four transparent conductive oxide (TCO) glass plates, the device performance is limited by superfluous intermediate TCO layers towards light intensity available to bottom cells. At the same time they also offer the additional cost burden since in the construction of DSSC, TCO is amongst one of the costly components. Mechanically stacked perovskite – Si or CIGS tandem solar cells has also been reported, but the performances mere affected by intermediate layers, were limited due to photon intensity availability at bottom cell [9, 10]. Therefore, fabrication of tandem cell with suppressed optical transmission loss towards light availability at bottom electrode is still a challenge. To avoid the optical transmission loss with reduction in the fabrication cost, mechanically stacked tandem DSSC utilizing NiO as photo cathode by avoiding intermediate layer have been reported but the efficiency observed was less than 2% [11,12]. Though monolithic tandem solar cell have been known with the drawback of need of extreme engineering of tunnel layer or recombination junction [10,13]. Wenger et al [14] have reported monolithic tandem solar cells using DSSC as top cells and CIGS as bottom cell in order to solve the problems associated with absorption losses in the mechanically stacked series tandem solar cells. Although proof of the concept was demonstrated, electrolyte used in the DSSC top cell lead to the corrosion of CIGS bottom cell leading to the open circuit voltage loss and overall device performance degradation.

In order to improve the photon intensity availability at bottom cells, in previous chapter we have explored the TCO-less tandem DSSC structure utilizing visible region harvesting dyes only as a proof of the concept for the new device architecture [15]. Utilization of TCO-less tandem architecture is a concept and necessary approach towards reduction of fabrication cost. However panchromatic photon harvesting using near infra-red (NIR) light absorption has to be taken for consideration. In this context, mechanically stacked tandem DSSC using four TCO glass plates stained by NIR dyes such as black dye or DX dye were utilized to justify the role of panchromatic photon harvesting in controlling the overall device performance [4,16,17,18]. In this chapter, we would like to propose a new tandem DSSCs device architecture towards combining the back contact TCO-less DSSC as the bottom electrode along with a novel phthalocyanine based NIR dye (PC25) having complementary photon harvesting spectra with visible light absorbing ruthenium dye N719 used in the top cell.

4.2 Experimental details:

4.2.1 Materials: The materials utilized in this work are of reagent grade and used without further processing. The top cell photoanodes, sensitized with Ru based N719 dye (purchased from Solaronix) harvests the narrow wavelength region photon and bottom photoanodes were sensitized with phthalocyanine dye (PC25), having capability to absorb photon wavelength up to 900nm. Electronic structure of both employed dye of top cell and bottom cell are shown in Fig. 2. All the solvents and electrolytes utilized were either dehydrated or anhydrous and used without further grading. FTO glass utilized in the experiment were purchased from Japan sheet glass of 15Ω/□. ITO glass utilized were obtained from GEOMATEC. ITO-PET film having resistivity of 60Ω/□ were purchased from sigma Aldrich.

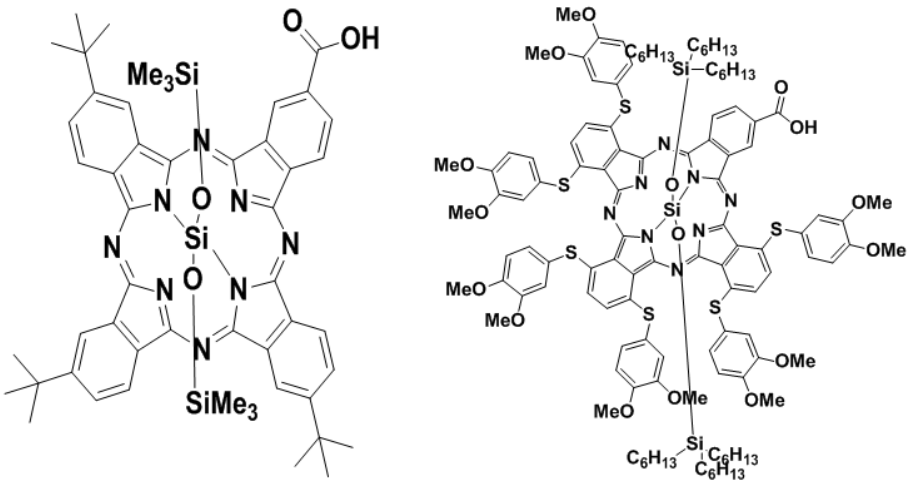

Figure 1. Electronic absorption spectra of Si-Phthalocyanine dye (a) PC16 (b) PC20

Si-Phthalocyanine dye

A way to harvest long wavelength photon are by utilizing Phthalocyanine dyes as harvesting medium and are capable to harvest intensively towards Q band at low intensity and towards Soret

band. They have shown limitation by possessing the solubility and aggregation problem on TiO_2 surface. Other class of Phthalocyanine dye with Si legand has synthesized to cope the above issues. Our lab have synthesized various class of Si-Phthalocyanine sensitizer capable to harvest visible to NIR region in effective way. Figure 1 describes the electronic structure of dye PC16, PC20 and PC25. Their electronic absorption spectra in solution and on TiO_2 has shown by Fig. 4a & 4b.We have optimized these dyes for panchromatic photon harvesting usage. Our approach started from PC16 and is showing the peak absorption at 680nm wavelength. With α substitution in dye PC16, the dye PC25 have shortened the bandgap and shifting of absorption peak towards red region has been obtained. Further perusal of anchoring of C=O group in α substitution position reduces the bandgap making peak spectra shifting towards more red region. Dye PC20 peak lies on 765nm and PC25 peak lies on 790nm wavelength. The broadening of absorption is observed on TiO_2 film and is observed due to aggregation of dye with mesoporous film. Owing to these favorable properties for red region harvesting, we preferred to carry on the PC25 properties to exploit the panchromatic light harvesting.

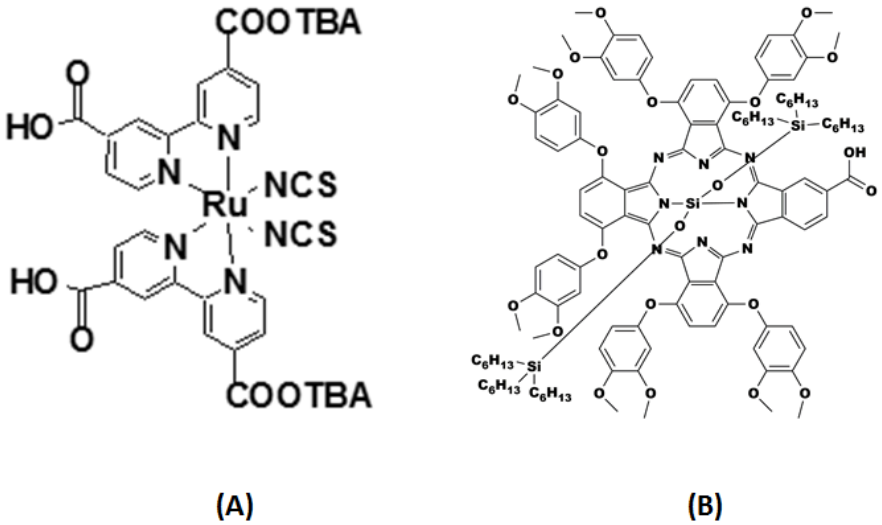

Figure 2. Electronic structure of sensitizers (A) N719 utilized in top cell (B) Phthalocyanine dye PC25 involved in bottom cell sensitization, Ref [15].

Electronic absorption spectra in solution state for sensitizing dyes used in top cell (N719) and bottom cell (PC25) of the tandem DSSC are shown in Fig. 2. It can be clearly seen that they bear completely complimentary light absorption having capability of wide wavelength photon harvesting from visible to NIR region. A dye bath solution of ruthenium dye N719 (0.3 mM in t-Butyl Alcohol: Acetonitrile (volume 1:1)) and PC25 (0.1 mM in THF: Ethanol (volume 1:9)) was utilized for the fabrication of top cells and bottom cells, respectively.

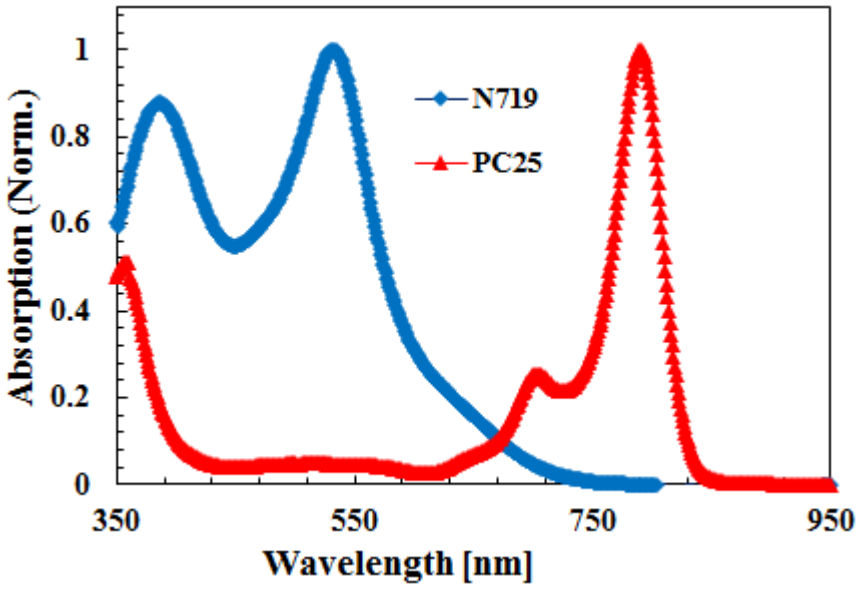

Figure 3. Electronic absorption spectra of sensitizers (A) N719 (B) Phthalocyanine dye PC25 in their respective solvents, Ref [15].

The employed bottom cell dye PC25 was synthesized in our laboratory as per scheme shown in Appendix. The synthesized dye PC25 was confirmed by NMR and mass spectra. Different nature of dyes with different electrolyte compositions were used in the respective top and bottom cells of the tandem DSSCs. Electrolyte utilized for top cell and bottom cell were I_2 (0.05 M), LiI (0.1 M), 4-t-Butylpyridine (0.5M), dimethylpropylimdazolium iodide (DMPII, 0.6 M) and I_2 (0.05M), LiI (1M), DMPII (0.6M) in dehydrated acetonitrile respectively.

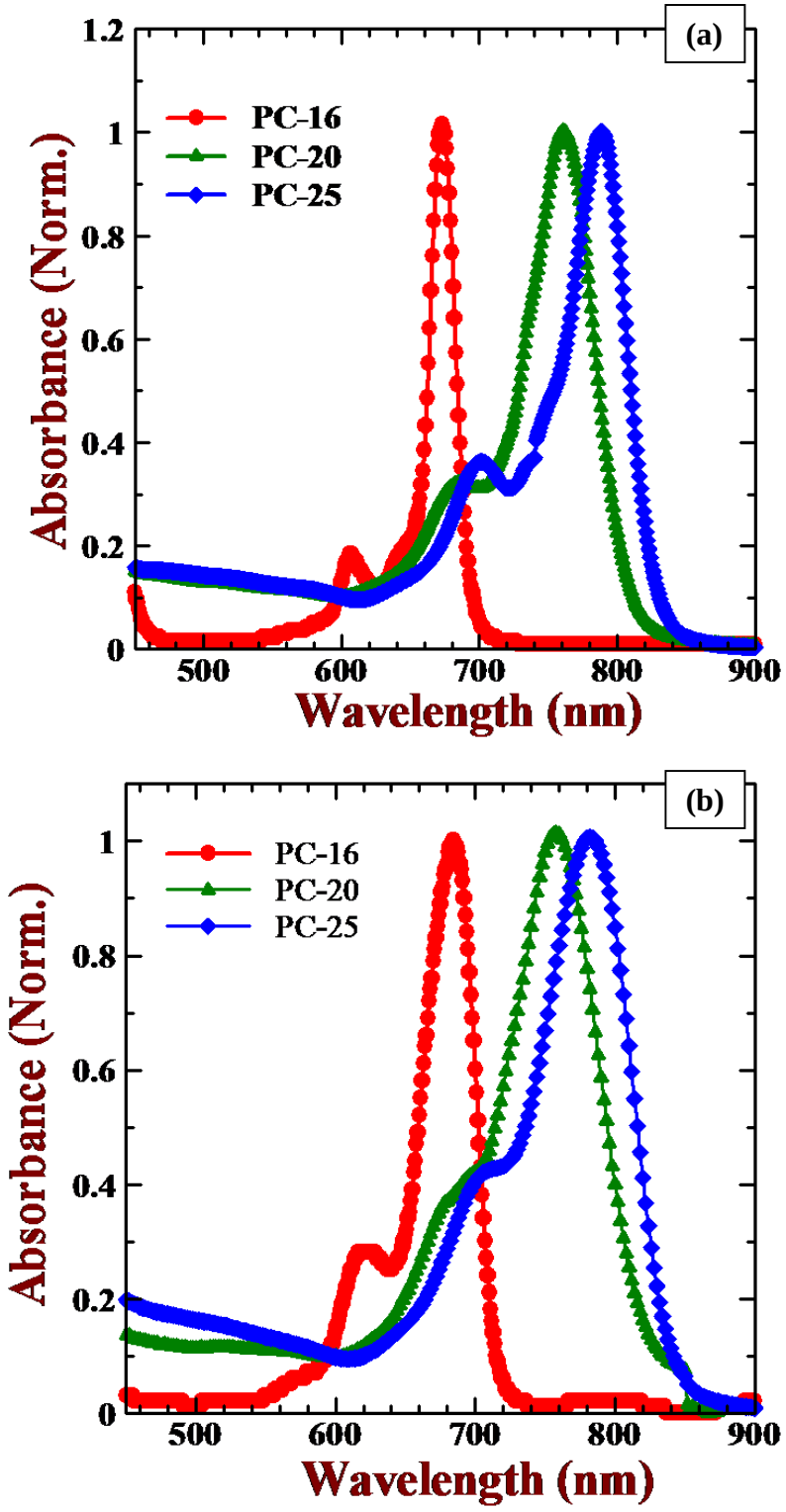

Figure 4. UV-vis spectra of Phthalocyanine dye series PC16, PC20, PC25 (a) in solution in their respective solvent (b) on TiO_2 coated simple glass.

4.2.2 Cell fabrication and measurement:

The tandem DSSCs were fabricated in different architectures and photovoltaic performance were measured at AM 1.5 sun condition under the effect of 100mW/cm^2 light intensity. The fabricated cells were covered with the black metal mask of 0.2025cm^2 area and measurements were performed at 25˚C. I-V characteristics and photo action spectra measurement setup has been elaborated in previous chapter.

4.2.2.1 Conventional TCO tandem DSSCs

The mechanically stacked tandem DSSCs were fabricated because they have attained advantage with their ease of fabrication and integration. The performance realization and matching of individual subcells of mechanically stacked tandem DSSCs have also achieved very relaxed process without any significant constraint. The fabrication process of top cell is similar as of previously explained tandem DSSCs subcells fabrication (chapter 3). The cleaned FTO glasses were put with 40mM aqueous $TiCl_4$ solution (Wako) at 80˚C for 30 minute. The treated glasses were further washed with ethanol and distilled water respectively and further baked at 450˚C for 30 minute to get compact layer of TiO_2 on FTO layer. The formed TiO_2 compact layer is able to strengthen the bonding between screen printed TiO_2 nanoparticles and conductive glass [19,20]. To make the top cell photoanode highly transparent, HT/SP TiO_2 nanoparticles were screen printed on treated FTO plate. The TiO_2 nanoparticles coated substrate were baked at 450˚C for 30 minute. Again the baked substrate were treated with 40 mM $TiCl_4$ solution and were put in hot air at 450˚C for 30 minute. This treatment enhances the surface roughness and the necking of TiO_2 nanoparticles has been increased resulting in enhanced photovoltaic performance [21]. In both treatments the formed rutile TiO_2 layer has lead to the efficiency enhancement due to synergistic effect. The baked substrate were submerged in 0.3 mM N719 dye bath for dye absorption for 24 hours. This photoanode was assembled with 1nm thick Pt sputtered semitransparent FTO glass and electrolyte was inserted and proper sealing were performed. For bottom cell photo anode preparation, the FTO glass was coated with D-37 TiO_2 nanoparticle (Solaronix) and the $TiCl_4$ treatment was performed twice as explained for top cell preparation. The nanoparticle coated plate was immersed in PC25 dye solution for 12 hours and was assembled with 60 nm thick Pt nanoparticle coated FTO glass counter electrode. Electrolyte were inserted and the devices were

sealed properly. The fabricated top cell and bottom cells were placed together in series combination as according to Fig. 5.

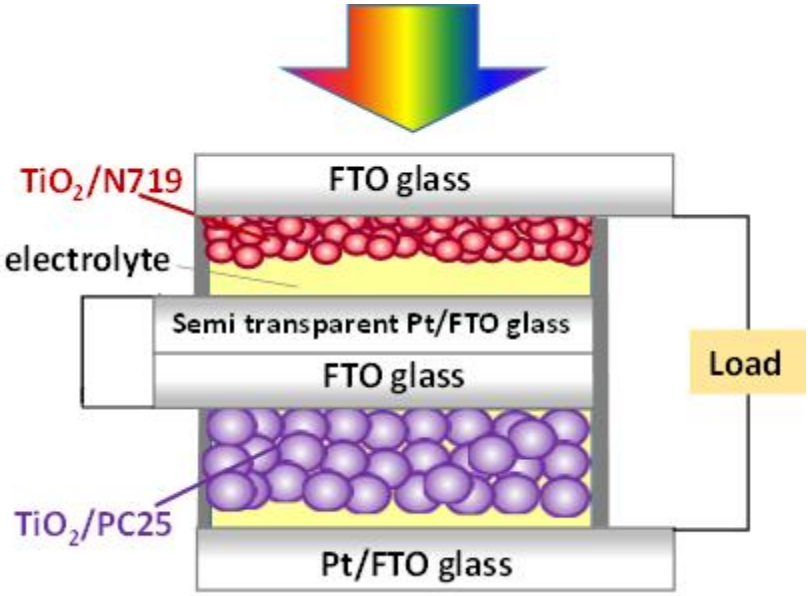

Figure 5. The architecture of conventional TCO Tandem DSSC employing four TCO plates, Ref [15].

As explained in previous chapter the tandem cell utilization is highly dependent towards light intensity availability at bottom cell and top cell photoanode thickness pays a great influence towards the transmission through it. Optimization were performed towards optical and electrical arrangement of tandem cell and the top cell TiO_2 mesoporous layer thickness was maintained to be 3µm. Bottom cell photo anode thickness was varied and optimum photovoltaic parameters were observed at 14µm thicker mesoporous layer.

4.2.2.2 Tandem DSSCs with flexible back contact bottom electrode

The panchromatic photon harvesting with employment of NIR region harvesting dye along with engineering of extent of photon available at bottom cell has been validated by new tandem architecture projected in this chapter. The intermediate layer working as the counter electrode (CE) of the top cell uses semitransparent Pt coated conductive glass offers obstacle towards further light transmission to the bottom cell. It must possess the high light transmission along with the optimum catalytic activity for attaining the enhanced solar energy harvesting. Transparent conductive glass have the imminent property of transmission loss and has been derived from the charge carrier

density available to conductive surface, thickness of conductive layer along with conductive layer-substrate interface property [22,23]. Fluorine doped SnO_2 glass (FTO glass) and Tin doped In_2O_3 glass (ITO glass) are very often used conductive layers in DSSCs. Both conductive glass transmission spectra has been measured and been drawn in Fig. 6. The clear observation from the drawn spectra is the benefit of photon transmission particularly in NIR region of ITO glass for our interest. This provides the way to fabricate more photon efficient bottom electrode and Tin doped Indium Oxide (ITO) coated glass (GEOMATEC) coated with 1 nm thick Pt exhibiting relatively high transparency as compared to FTO glass was employed as intermediate layer (Fig. 7,8 architecture T1, T2 & T3).

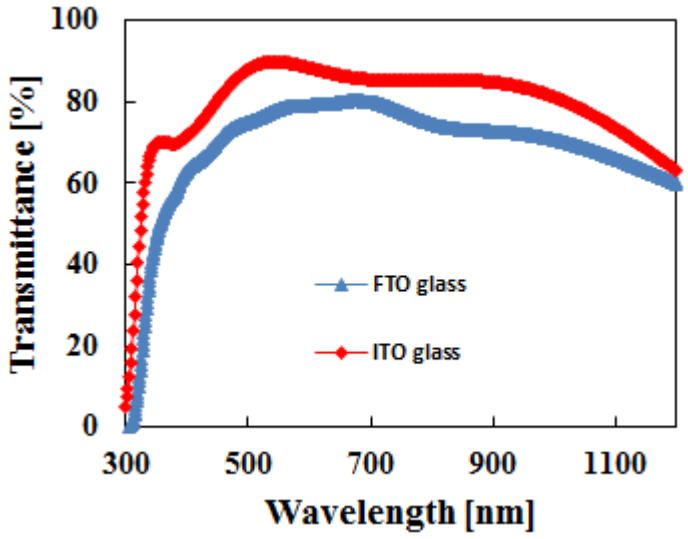

Figure 6. The transmission spectra of utilized ITO glass and FTO glass in this work.

In this novel device architecture, current collecting photo anode of the bottom cell in the conventional mechanically stacked tandem DSSC (Fig. 5) was substituted with TiO_2 coated protected metal mesh as shown in the structure of Fig. 6. This reduces the use of one of the costly TCO component leading reduction of overall manufacturing cost. The bottom cell photo anodes were fabricated as per previously explained TCO-less photo anode except the employed TiO_2 was PST 30NRD having 30 nm particle size. The TiO_2 nanoparticles size has impact on dye adsorption and bulky molecule of dye (here PC25) have better dye adsorption property upon it [24]. The TCO-less photo anode loaded with dye PC25 dye were assembled with 60nm thick Pt coated FTO glass

as counter electrode with PTFE as spacer. After electrolyte insertion the tandem cell were assembled as explained in previous chapter and the fabricated device architecture have been shown in Fig. 7.

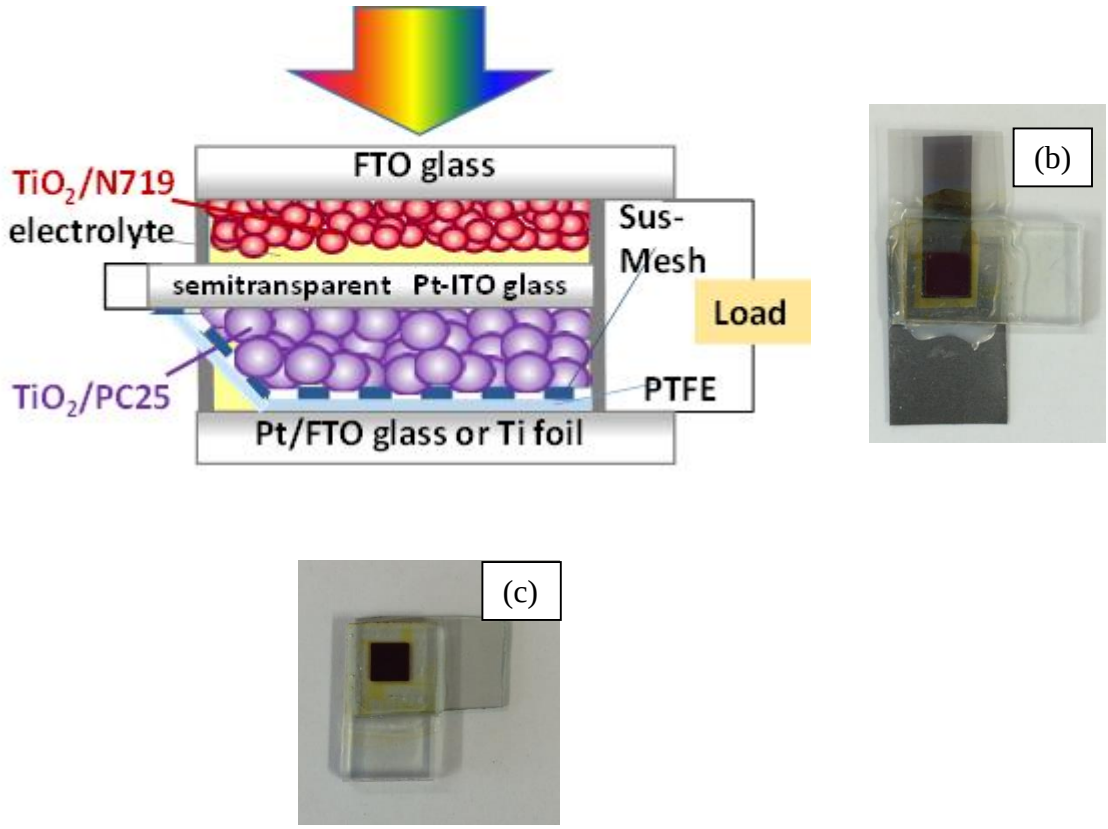

Figure 7. Architecture involved in tandem DSSCs with TCO-less back contact bottom electrode (a) FTO glass as bottom cell counter electrode (T1 architecture) (b) flexible bottom cell with Pt-Ti foil (T2 architecture) (c) Fabricated Top cell with Pt sputtered semitransparent ITO glass as counter electrode Ref [15].

The future led application of flexible DSSCs have drawn a lot of attraction towards metal sheets. They are reported to posses good flexibility, low resistance, high temperature sinterability and are economical also. Ti foil, a less corrosive metal towards iodine electrolyte has found wide application in light weight DSSC fabrication [25,26]. In this work to make the tandem device architecture more economical with enhanced catalytic activity of bottom cell counter electrode, Pt sputtered FTO glass was replaced by Pt sputtered Ti foil (The Nilaco Co., 0.10 mm thick). (structure is shown in Fig. 7)

4.2.2.3 Flexible TCO-less tandem DSSCs employing ITO-PET film

The demand of light weight flexible DSSC is growing very fast with the rise in application of photovoltaic devices. Conductive glasses are known to be brittle in nature and ITO-PET film has the possible exposure towards high flexibility with light weight and mechanical robustness [27]. Apart from the discussed possible reasons behind the transmission obstacle of conductive glass, the conductive layer roughness and substrate thickness also plays a lot. The number of charge carriers available in conductive layer affects the sheet resistivity and inverse relationship to each other. Due to these inherent properties, Flexible ITO-PET film has shown comparable and better transmission property than ITO-glass and particularly in 750 nm onwards of NIR region (Fig. 10). To fabricate the flexible TCO-less tandem DSSC with implication of engineering towards better light transmission of intermediate layers, 1nm thick Pt coated ITO-PET film was explored in this sense. The tandem cell fabrication process was similar to that of explained in previous section. The fabricated flexible tandem cell structure schematic is shown in Fig. 8.

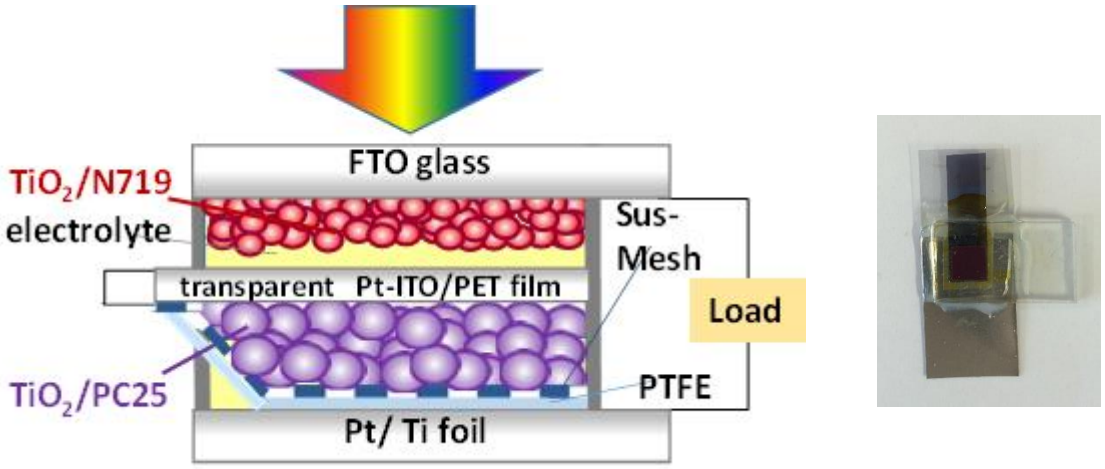

Figure 8. Schematic architecture involved in tandem DSSCs with TCO-less back contact bottom electrode employing flexible bottom cell with ITO/PET film and Pt-Ti foil (T3 architecture) , Ref [15].

4.3 Performance evaluation of various Tandem DSSCs

The DSSCs have got an edge in fabrication of the tandem cell because the short circuit current density (Jsc) of respective subcells can be easily adjusted by modifying the nanoparticle size or its

thickness, nature of sensitizer involved upon it and the electrolyte composition utilized. Another important aspect of tandem DSSC fabrication and performance optimization is optical transmittance available to bottom subcells. In previous chapter we provided the proof of concept towards tandem formation by employing the visible region harvesting dye. In this explained novel TCO-less architecture the photovoltaic performance were optimized by the proper control and adjustment of intensity of incident light on bottom subcell by the orchestrating of intermediate layer. Further high performance tandem cell fabrication is expedited with the advent of time. To achieve the optimum photovoltaic performance by panchromatic photo harvesting, NIR sensitizer Phthalocyanine dye (PC25) with photon harvesting coverage up to 900nm wavelength region has been used. The complementary sensitizers involved for photo harvesting of tandem cell have band gap 2.29ev and 1.48ev for top cell and bottom cell respectively. The respective bandgap energy (shown in Fig. 9) of sensitizers involved also motivate the fabrication of tandem cell with panchromatic photoharvesting.

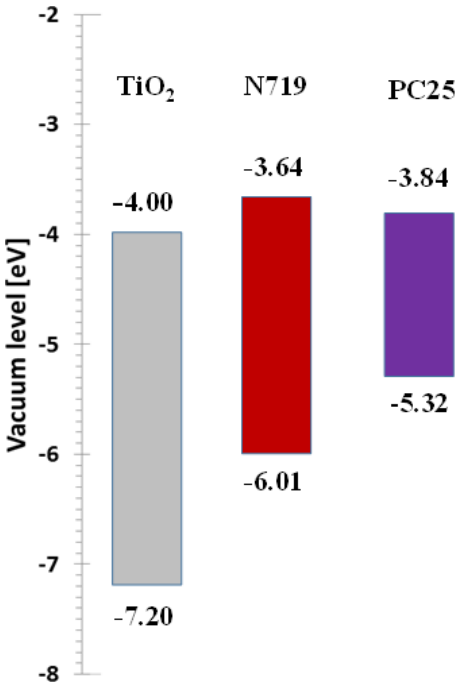

Figure 9. The energy band level of utilized mesoporous TiO_2 and involved sensitizer N719 and PC25 in tandem cell formation.

TCO-tandem DSSCs: Fabrication of conventional tandem DSSC utilizing four TCO plates (TCO tandem DSSC) as reference cell were performed and the performances are shown in Fig. 10. The photovoltaic parameters obtained for the tandem DSSCs along with the respective single cells under simulated solar irradiation (100mW/cm^2) are summarized in Table I. The hampered light transmission from the three top TCO-glasses lead to adjust the Jsc of the top and bottom cells between 8.4-8.7 mA/cm^2 exhibiting the overall tandem DSSC efficiency of 6.9 %. TiO_2 photoanodes thickness of top cell and bottom cell were maintained at 3 µm (HT/SP, Solaronix) and 14 µm (D-37, Solaronix) respectively, by screen printing on FTO glass (15 Ω/□, Japan Sheet Glass).

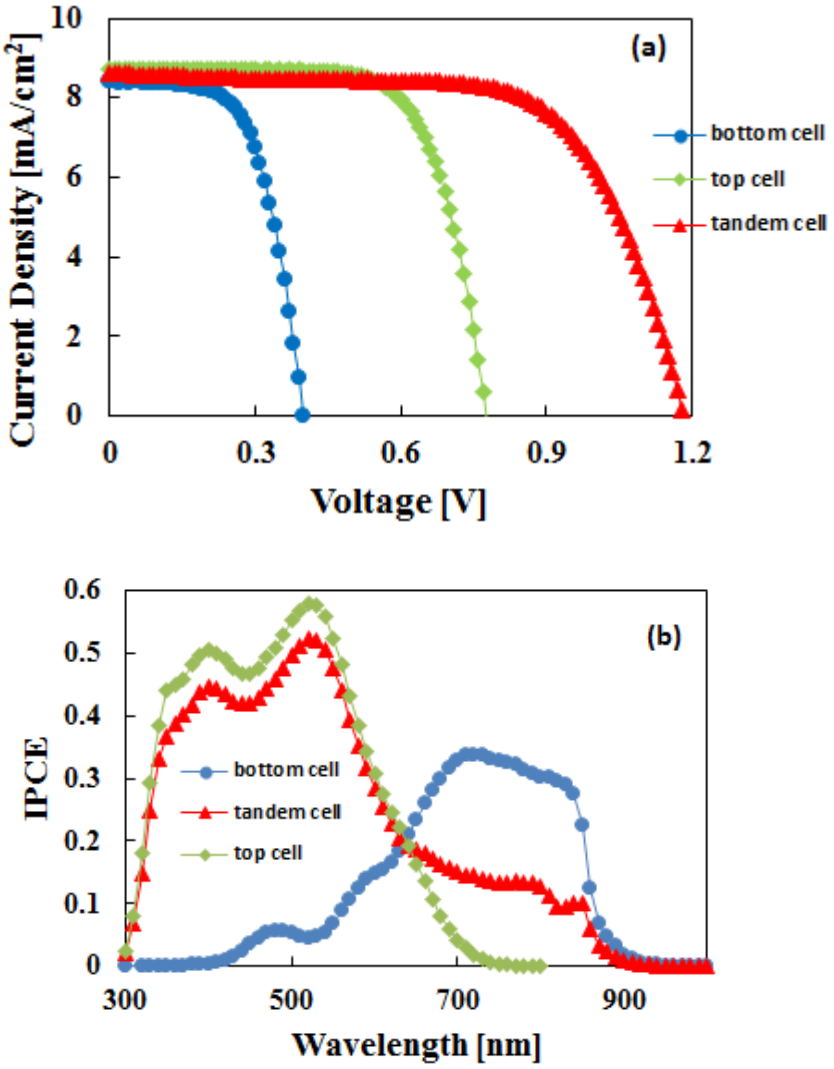

Figure 10. Showing the (a) I-V characteristics under simulated condition (b) photocurrent action spectra of TCO tandem DSSCs employing 4 TCO glass (structure of Fig. 5) ,Ref [15].

Table 1. Photovoltaic parameters of TCO Tandem DSSC under simulated condition

	J_{sc}(mA/cm^2)	V_{oc}(V)	*FF*	η (%)
Tandem Cell	8.61	1.18	0.68	6.88
Top Cell	8.72	0.78	0.70	4.77
Bottom Cell	8.40	0.40	0.61	2.06

To analyze the optical properties of various tandem cell architectures towards the photon availability at the bottom cell photo anode, transmission spectra has been measured and is shown in Fig. 11. The optical advantage of various tandem architecture with intermediate layer arrangement can be observe very clearly. There is enhancement of transmitted light from top cell to bottom cell in different TCO-less tandem architectures. The top cell absorbs and converts photons in visible region with the light absorption peak at 550 nm and remaining light photons are available to be harvested by the bottom cell. It is interesting to see that from wavelength region 700 nm onwards, different tandem architectures (Fig. 7,8) exhibit differential light transmissions as compared to most commonly used four TCO based mechanically stacked tandem cells (Fig. 5). TCO Tandem bearing two intermediate conductive layer unveil greater optical loss and about 50% photon intensity is lost while reaching to bottom cell. By removing the superfluous conductive glass and by utilizing only one TCO plate in intermediate layer the optical advantage has been achieved. The TCO-less tandem DSSCs architecture utilizing ITO-PET film (architecture T3) shows about 30% enhanced light transmission within 700-1100 nm wavelength region. This enhanced light received by the flexible TCO-less bottom cell is expected to enhance the overall efficiency by better Jsc matching of top and bottom cells. The transmission spectra of employed semitransparent intermediate layers in various TCO-less tandem cell (1 nm Pt- ITO glass and 1nm Pt-ITO/PET film) been shown in Fig. 12. Utilized ITO glass has 155nm thick ITO film on 0.7mm thick glass and ITO-PET film has 100nm thick ITO film on 127μm thick PET film. We suppose the thinner layer of ITO film on thinner PET film are responsible towards relatively better transmission property than ITO glass although polymer substrate are supposed to be less smoother than glass.

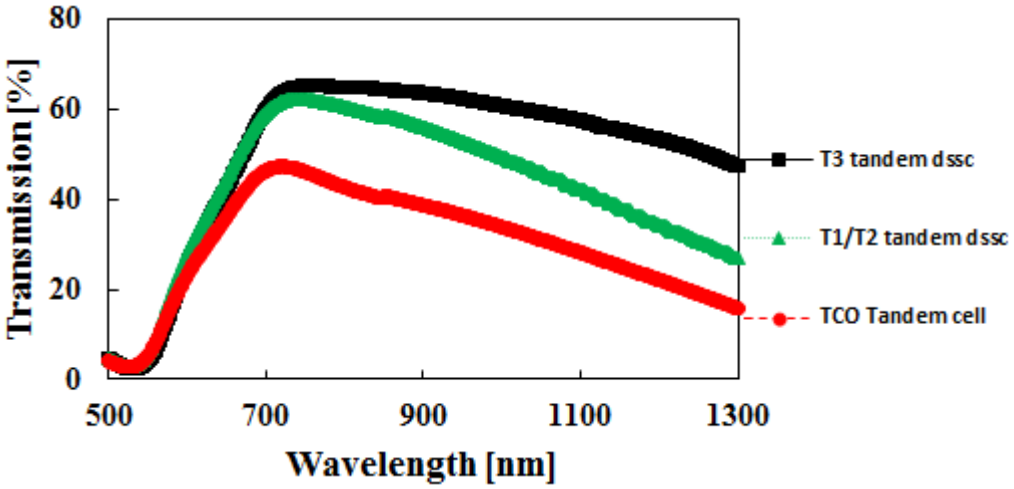

Figure 11. The transmission spectra exhibiting the light intensity availability at bottom cell photo anode of different architecture tandem DSSCs (a) TCO tandem DSSCs: conventional tandem DSSCs with four FTO glass (b) T1/T2 tandem DSSCs: TCO-less tandem DSSCs architecture with 1nm thick Pt sputtered ITO glass in conjunction with FTO glass/Ti foil as bottom cell counter electrode (c) T3 tandem DSSCs: TCO-less tandem DSSCs consisting of 1nm thick semitransparent Pt nanoparticle on ITO-PET film with Ti foil as counter electrode of bottom cell, Ref [15].

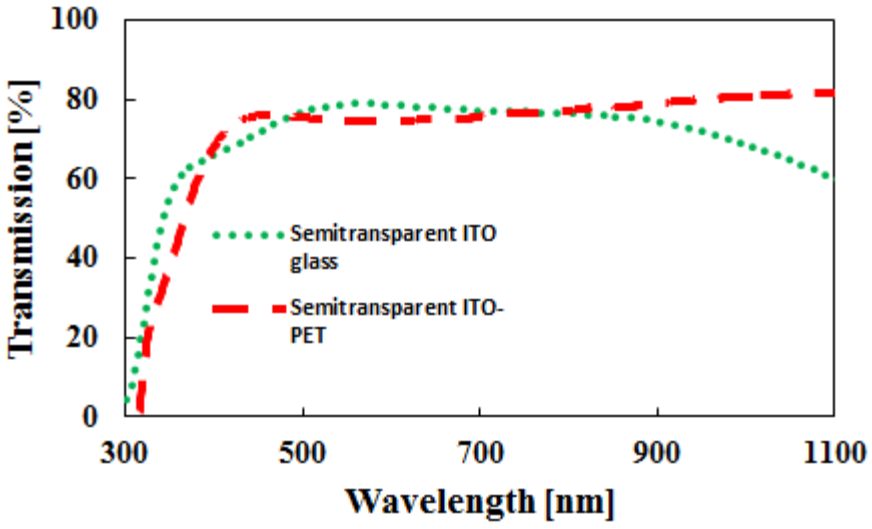

Figure 12. The optical transmittance spectra of 1nm thick coated semitransparent ITO glass and ITO-PET film showing the photon advantage after 750nm wavelength.

Tandem DSSCs with TCO-less back contact bottom electrode:

To achieve the optimal performance of the tandem DSSC under investigation, proper matching of short circuit current density (Jsc) of respective single cells were performed by optimizing their active layer thicknesses. Attempts have been made to attain the enhanced photovoltaic performance of TCO-less tandem DSSCs (Fig. 7,8) by enabling improved incident light to the bottom electrode which was realized by utilizing light efficient TCO-less back contact bottom electrode. Photovoltaic characteristics with photocurrent action spectra of tandem DSSCs with TCO-less back contact bottom electrode (architecture T1 of Fig. 7) fabricated in this work are shown in the Fig. 13. TCO-less tandem architecture (T1) and its sub cells (top and bottom) show photovoltaic performance with efficiency (η) of 6.58%, Voc 1.20 V, FF 0.63, Jsc 8.65 mA/cm^2, Top cell: η 4.47%, Voc 0.76 V, FF 0.73, Jsc 8.11 mA/cm^2 and Bottom cell: η 2.10%, Voc 0.44 V, FF 0.67, Jsc 7.11 mA/cm^2. Though bottom cell of architecture T1 shows around 14% enhanced light (700-900 nm), obtained Jsc is comparable and little lower than bottom cell of TCO tandem DSSC Jsc which is due to poor collection of electrons in back contact bottom cell architecture [28].

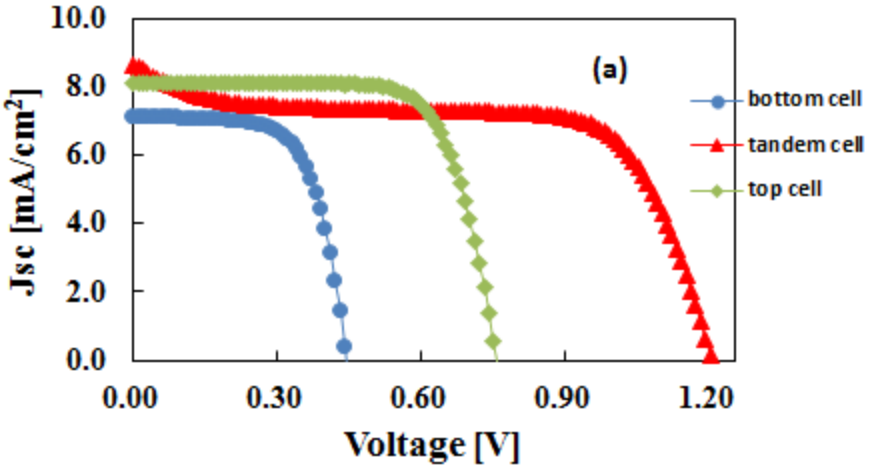

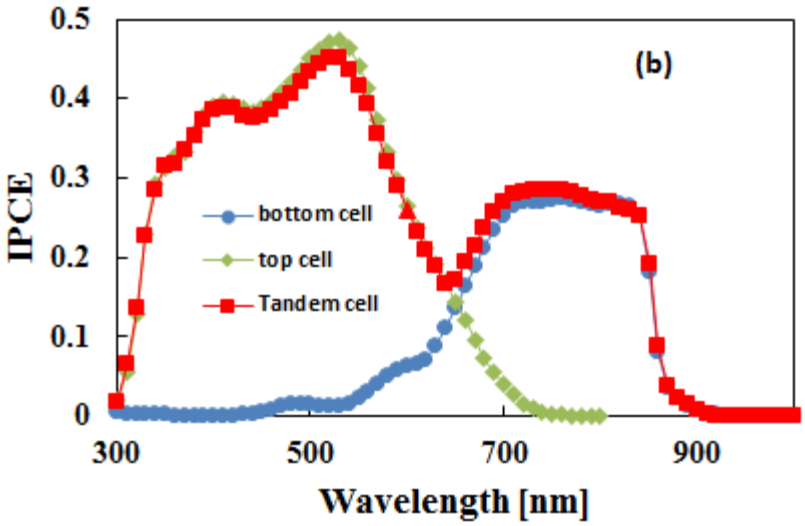

Figure 13. Exhibiting the (a) I-V characteristics under simulated condition (b) photocurrent spectra of TCO-less Tandem DSSCs employing ITO glass as intermediate layer (Fig. 7, T2 architecture), Ref [15].

The tandem DSSCs with flexible bottom cell as Ti foil counter electrode architecture (architecture T2, Fig. 7) have shown the efficiency (η) of 6.33%, Voc 1.22 V, FF 0.53, Jsc 9.18 mA/cm^2, Top cell: η 5.48%, Voc 0.80 V, FF 0.75, Jsc 9.15 mA/cm^2 and Bottom cell: η 1.54%, Voc 0.42 V, FF 0.48, Jsc 7.72 mA/cm^2. I-V characteristics and IPCE spectra have been shown in Fig. 13.

The energetic mismatch of TiO_2 and PC25 envisge to change the electrolyte composition in bottom cell. The bottom electrolyte composition was rich of LiI and additional Li^+ causes positive shift of the TiO_2 conduction band energy (CB) relative to previous energy levels resulting in increase in electron injection efficiency from dye to TiO_2 [29,30]. The additive 4-tert butyl pyridine in electrolyte has nature to passify the TiO_2 surface by blocking free space on it and causes the negative shift of CB of TiO_2 level yielding low electron yield and here energy constraint avoided to use it leading to relatively poor FF of bottom cell [29, 31, 32].

TCO-less tandem DSSC architecture T3 (Fig. 8) consisting ITO-PET film as an intermediate layer and Pt/Ti foil as bottom cell counter electrode exhibits the photovoltaic performance (Fig. 15) as η 7.19%, Voc 1.19V, FF 0.65, Jsc 9.34 mA/cm^2. At the same time photovoltaic performance

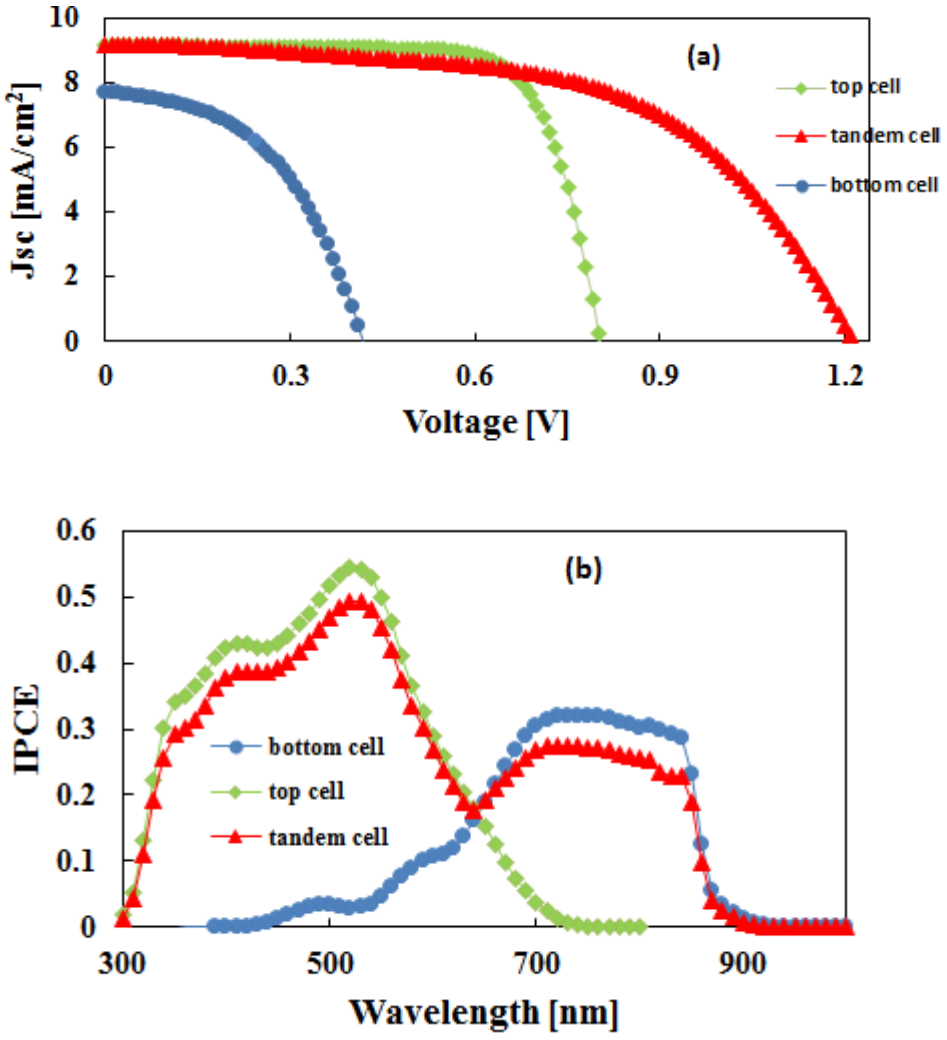

Figure 14. Figure showing the (a) I-V characteristics (b) photocurrent action spectra of TCO-less tandem DSSCs employing ITO glass as intermediate layer and Pt coated Ti foil as bottom cell counter electrode (T2 architecture, Fig. 5), Ref [15].

exhibited by Top cell: η 4.82%, Voc 0.75V, FF 0.67, Jsc 9.65 mA/cm^2 and Bottom cell: η 2.04%, Voc 0.40V, FF 0.62, Jsc 8.13 mA/cm^2 indicate the advantage of tandem device architecture. Flexible TCO-less tandem DSSC architecture T3 in which bottom cell receives around 25 % more light than architecture T1 in region (700-900nm) shows considerable Jsc improvement. FF of T3 architecture slightly decreases and it could be considered as dependency on increased light intensity as with intense light, high carriers available in the device are more prone to recombination

and leakage current will occur leading to increase in shunt resistance [33]. Bottom cell Voc should slightly increase due to charge generation rate increasing more strongly with intense light [34] and here in T3 architecture is almost constant probably due to atmospheric effect on the photovoltaic performance of the DSSC [35].

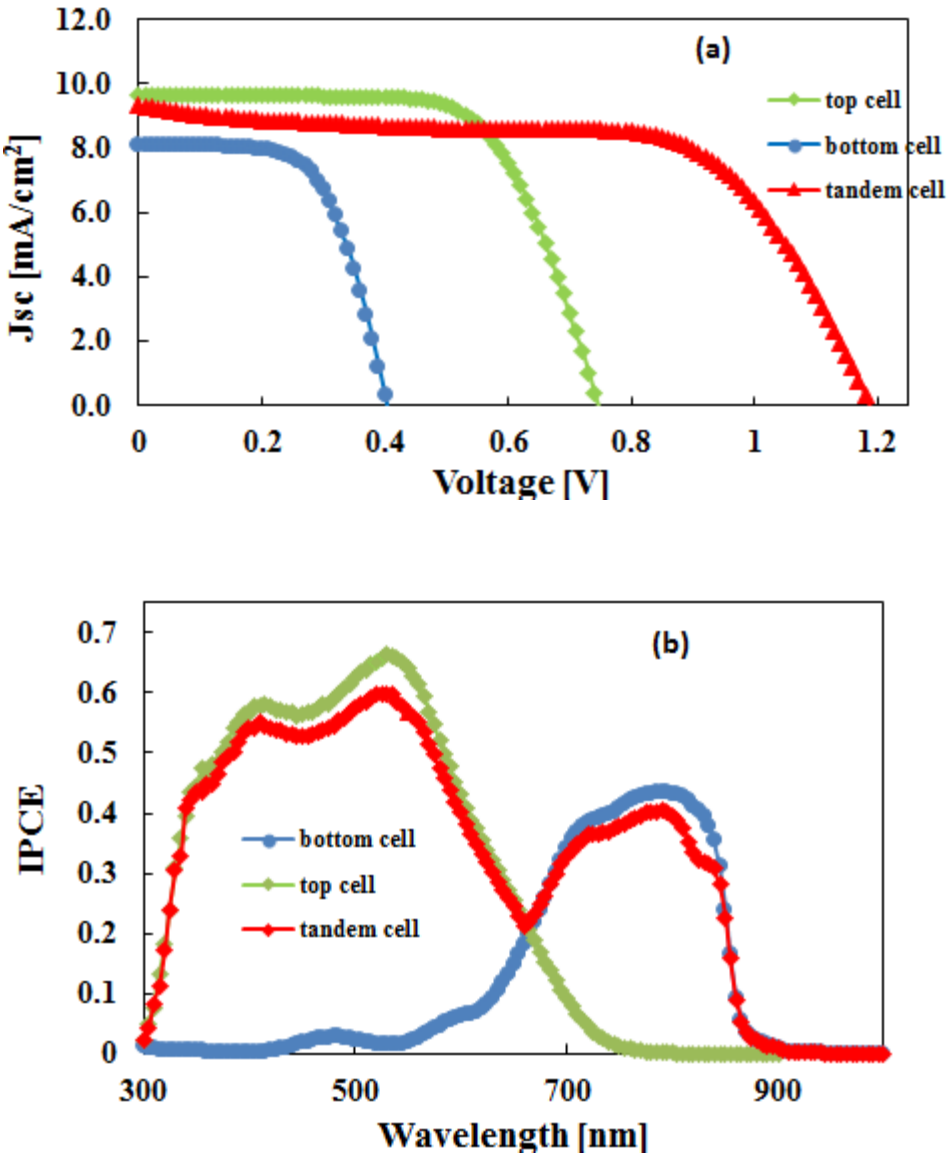

Figure 15. Figure exhibiting the (a) I-V characteristics (b) photocurrent current action spectra of TCO-less tandem DSSCs employing 1nm Pt coated ITO/PET film as intermediate layer and 60 nm thick Pt coated Ti foil as bottom cell counter electrode (T3 architecture, Fig. 6), Ref [15].

Enhanced light received by bottom cells in different tandem architectures (T1, T2 and T3) is supported by enhancement in the observed incident photon to current conversion efficiency (IPCE) in the 700-900 nm (Fig. 9,10,11,12) [36]. The efficiency reported is greater than the sum of top cell and bottom cell efficiencies and the open circuit voltage (Voc) of fabricated TCO-less tandem cell is equal to the sum of corresponding bottom cell and top cell Voc, justifying the tandem formation. Energetics mismatch of TiO_2 conduction band and LUMO energy level of PC25 leads to the removal of 4-t-butylpyridine and addition of excess LiI in the electrolyte of bottom cell and is responsible for lower Voc of the bottom cell which ultimately affects the tandem cell performance. Thus enhanced light intensity at bottom cell (architecture T3 with ITO-PET film as intermediate layer) leads to improved short circuit current (Jsc) with better current matching resulting into enhanced photo conversion efficiency.

4.4 Conclusion:

We demonstrated and proved the proof concept of flexible TCO-less tandem DSSC bearing semitransparent ITO-PET film as an intermediate layer with novel phthalocyanine dye (PC25) as NIR region harvesting dye having initial efficiency of 7.19% at 1 sun condition. It was proved that the architecture possess addition of around 30% photon (700-1100nm) towards bottom electrode as compared to conventional TCO tandem DSSCs. We expect to exploit this flexible TCO-less tandem architecture by harvesting wavelength region up to 1100 nm with suitable energetically matched sensitizing dye collaborating Co based top cell DSSCs.

4.6 References:

1. B. O. Regan and M. Gratzel, *Nature*, 1991, **353**,737.
2. M. Gratzel, *Progress in Photovoltaics Research and Applications*, 2006, **14**, 429.
3. H. S. Jung and J-K Lee, *Journal of Physical Chemistry Letters*, 2013, **4**, 1682.
4. T. Kinoshita, J. T. Dy, S. Uchida, T. Kubo and H. Segawa, *Nature Photonics*, 2013, **7**, 535.
5. M.Durr, A. Bamedi, A. Yasuda and G. Nelles, *Applied Physics Letters*, 2004, **84**, 3397.
6. A. Hagfeldt, G. Boschloo, L. Sun, L. Kloo and H. Pettersson, *Chemical Review*, 2010, **110**, 6595.
7. W. Shockley and H. J. Queisser, *Journal of Applied Physics*, 1961, **32**, 510.
8. M. Yanagida, N. O.-Komatsuzaki, M. Kurashige, K. Sayama and H. Sugihara, *Solar Energy Materials & Solar Cells*, 2010, **94**, 297.
9. P. Loper, S.-J. Moon, S. M. D. Nicolas, B.Niesen, M. Ledinsky, S. Nicolay, J. Bailat, J.-H. Yum, S. D. Wolf and C. Ballif, *Physical Chemistry Chemical Physics*, 2015, **17**, 1619.
10. C. D. Bailie, M. G. Christoforo, J. P. Mailoa, A. R. Bowring, E. L. Unger, W. H. Nguyen, J. Burschka, N. Pellet, J. Z. Lee, M. Gratzel, R. Noufi, T. Buonassisi, A. Salleo and M. D. McGhee, *Energy & Environmental Science*, 2015, **8**, 956.
11. A. Nattestad, A.J. Mozer, M.K.R. Fischer, Y.-B. Cheng, A. Mishra, P. Bauerle and U. Bach, *Nature Materials*, 2010, **9**, 31.
12. H. Choi, T. Hwang, S. Lee, S. Nam, J. Kang, B. Lee and B. Park, *Journal of Power Sources*, 2015, **274**, 937.
13. J. P. Mailoa, C. D. Bailie, E. C. Johlin, E. T. Hoke, A. J. Akey, W. H. Nguyen, M. D. McGehee and T. Buonassisi, *Applied Physics Letters*, 2015, **106**, 121105.
14. S. Wenger, S. Seyrling, A. N. Tiwari and M. Gratzel, *Applied Physics Letters*, 2009, **94**, 173508.
15. A.K. Baranwal, T. Shiki, Y. Ogomi, S.S. Pandey, T. Ma and S. Hayase, *RSC Advances*, 2014, **4**, 47735.

16. M. Yanagida, N.O. Komatsuzaki, M. Kurashige, K. Sayama and H. Sugihara, *Solar Energy Materials & Solar Cells*, 2010, **94**, 297.

17. T. Yamaguchi, Y. Uchida, S. Agatsuma and H. Arakawa, *Solar Energy Materials & Solar Cells*, 2009, **93**, 733.

18. M. Murayama and T. Mori, *Thin Solid Films*, 2008, **516**, 2716.

19. S. Ito, T. N. Murakami, P. Comte, P. Liska, C. Gratzel, M. K. Nazeeruddin, and M. Gratzel, *Thin Solid Films*, 2008, **516**, 4613.

20. K. Zhu, E. A. Schiff, N.-G. Park, J. Van de Lagemaat and A. J. Frank, *Applied Physics Letters*, 2002, **80**, 685.

21. S. Ito, P. Liska, R. Charvet, P. Comte, P. Pechy, M. K. Nazeeruddin, S. M. Zakeeruddin and M. Gratzel, *Chemical Communications*, 2005, **4351**.

22. A. K. Kulkarni, T. Lim, M. Khan and K. H. Schulz, *Journal of Vaccum Science Technology A*, 1998, **16**, 1636.

23. V. Zardetto, T. M. Brown, A. Reale and A. D. Carlo, *Journal of Polymer Science B: Polymer Physics*, 2011, **49**, 638.

24. T. P. Chou, Q. Zhang, B. Russo, G. E. Fryxell, G. Cao, *Journal of Physical Chemistry C*, 2007, **111**, 6296.

25. H. G. Yun, J. H. Park, B. S. Bae and M.G. Kang, *Journal of Materials Chemistry*, **2011**, 21, 3558.

26. (26) M. Ye, D. Zheng, M. Lv, C. Chen, C. Lin and Z. Lin, *Advanced Materials*, 2013, **25**, 3039.

27. W. Q Wu, Y. F. Xu, H.-S. Rao, C.-Y. Su and D.-B Kuang, *Journal of Physical Chemistry C*, 2014, **118**, 16426.

28. N. Fuke, A. Fukui, A. Islam, R. Komiya, R. Yamanaka, L. Han and H. Harima, *Journal of Applied Physics*, 2008, **104**, 064307.

29. S.A. Haque, E. Palomares, B. M. Chao, A.N.M. Green, N. Hirata, D. R. Klug and J.R. Durrant, *Journal of American Chemical Society*, 2005, **127**, 3456.

30. S. Altobello, R. Argazzi, S. Caramori, C. Contado, S. Fre Da, P. Rubino, C. Chone, G. Larramona and C.A. Bignozzi, *Journal of American Chemical Society*, 2005, **127**, 15342.

31. M. Yanagida, T. Yamaguchi, M. Kurashige, K. Hara, R. Katoh, H. Sugihara and H. Arakawa, *Inorganic Chemistry*, 2003, **42**, 7921.

32. G. Boschloo, H. Lindstrom, E. Magnusson, A. Holmberg and A. Hagfeldt, *Journal of Photochemistry and Photobiology A*, 2002, **148**, 11.

33. B. Qi and J. Wang, *Physical Chemistry Chemical Physics*, 2013, **15**, 8972.

34. H. J. Snaith, L.S.-Mende, M. Gratzel and M. Chiesa, *PHYSICAL REVIEW B*, 2006, **74**, 045306.

35. S. Ito, I.M. Dharmadasa, G. J. Tolan, J.S. Roberts, G. Hill, H. Miura, J.-H.. Yum, P. Pechy, P. Lisca, P. Comte, M. Gratzel, *Solar Energy*, 2011, **85**, 1220.

36. J. Halme, G. Boschloo, A. Hagfeldt and P. Lund, *Journal of Physical Chemistry C*, 2008, **112**, 5623.

Chapter 5

Conclusions

The work carried on during this thesis consist of the feasibility and optimization study of mechanically stack tandem DSSCs in various photon efficient novel architectures. The fabricated tandem cell have shown the compatibility in harvesting the broader wavelength region and covering up to 900nm wavelength region. The feasibility and optimization of tandem devices are carried out by three strategies: The mechanically stacked top cell DSSC and TCO-less back contact DSSC facilitated light efficient tandem architecture and further modification to flexible bottom cell, the flexible tandem architecture with conductive PET film as intermediate layer exhibiting more photon efficient, visible region harvesting dye in tandem architecture and extending the harvesting region by utilizing novel Si-Phthalocyanine PC25 dye covering wavelength region up to 900nm.

Human life is driven by the energy and this necessitates the continuous inclination and research in solar cell. Existing and mature solar cell technology advancement are discussed in broadened way with their outcome in current scenario. Earth temperature is rising due to global warming effect and dye sensitized solar cells (DSSCs) have overpower the existing technology due to its low carbon emission properties. DSSCs have known limitation in terms of light harvesting efficiency and further efficiency enhancement with cost reduction are possible by tandem architecture. The tandem DSSCs exploit the broader wavelength spectra and increased photovoltage promotes the better photovoltaic efficiency. Conventional tandem DSSC architecture have known limitation of light transmission loss due to existence of superfluous transparent conductive oxide (TCO) layers. The new and novel tandem architectures are needed to cope the risen effect of TCO layers with better transmission and conductivity properties.

Solar cell measurements have a set of standards and various parameters related to it are described. The solar cell efficiency and its interrelationship with variant of FF, Jsc, Voc are discussed. The solar cell characteristics parameters are described and explained with AM 1.5 context. Instruments utilized in this thesis work have elaborated with their basic working principle.

The conventional tandem architecture consist of TCO glass/D131-TiO_2/transparent Pt-TCO glass/TCO glass/N719-TiO_2 /Pt-TCO glass. The fabricated stack architecture of top cell DSSC and TCO-less back contact have the device architecture of TCO glass/D131-TiO_2/ transparent Pt-TCO glass /N719-TiO_2/protected sus-mesh/ Pt-FTO glass. The resulting device architecture have assisted around 20% added light transmission to bottom cell and this paves the room for enhanced efficiency. Bottom cell active layer and top cell active later thickness have been optimized to achieve proper current matching. The resulting open voltage 1.45V justifies the proof concept of tandem cell formation. To achieve better catalytic action towards the bottom cell, new architecture TCO glass/D131-TiO_2/ transparent Pt-TCO glass /N719-TiO_2/protected sus-mesh/ Pt-Ti foil has been projected and 7.10% efficiency under 1sun condition has been achieved which is better than the conventional tandem DSSC 6.28% efficiency.

The electrical and optical arrangement of the aforesaid tandem architecture have shown proof of concept with complementary visible region harvesting dye. A novel stable organic sensitizer Si Phthalocyanine (PC25) covering 900nm wavelength region have utilized in various architectures to harvest incident photon flux on bottom cell. PET films are getting attention in roll to roll device futuristic fabrication. The tandem cell architecture have explored in better light efficient (around 30%) way with flexible bottom cell in TCO glass/N719-TiO_2/ transparent Pt-ITO-PET film /PC25-TiO_2/sus-mesh/ Pt-Ti foil architecture. The resulting flexible tandem DSSC shows proof of concept with Voc 1.19 V and 7.19% initial efficiency at AM 1.5 condition. The obtained performance is greater than its individual subcell as well as combined subcell efficiency and is better than conventional tandem DSSC efficiency also. The dye PC25 energetic mismatching is responsible for lower Voc in bottom cell and ultimately affecting the tandem cell performance.

Future Prospects:

For future development and commercialization purposes flexible DSSCs show high synergistic potential. Mechanically stacked tandem DSSCs have shown the prominent behavior of easy fabrication process than monolithic tandem cell and are viable alternative for commercialization. The hindrance in tandem performance are found to be induced by intermediate layers making obstacle with light transmission. TCO layers, a costly components are associated with fabrication of DSSCs as intermediate layer need to be avert. PEDOT:PSS have profound catalytic activity and could be used on flexible PET film with more than 90% transmission properties. Impressive mechanical, electrical and transparent properties of Graphene layer places it at outstanding equivalence in application of intermediate layers for high performance tandem DSSC. Carbon nanotube sheets are other plausible intermediate catalytic layer to implement as flexible intermediate film to achieve the appealing tandem DSSC performance. We have utilized the Si-phthalocyanine dye as novel NIR region harvesting medium with low open voltage and low IPCE. Further efforts are directed to achieve the higher open voltage with higher IPCE covering around 1000nm wavelength region. Perovskite solar cell are the most talk 3rd generation dye sensitized solar cell with 20% efficiency and could be implemented as bottom electrode to cover the NIR photo harvesting.

To further conclude it, I would stress the intermediate layer engineering facilitated profit of photon harvesting at bottom cell in cooperation with efficient and energetic sensitizer, could travel a mile stone tandem DSSC photovoltaic performance. These are the challenges to follow and I hope the content and finding of this thesis pave the path for further optimization and understanding of reduction of losses fundamental to DSSCs.

Appendix

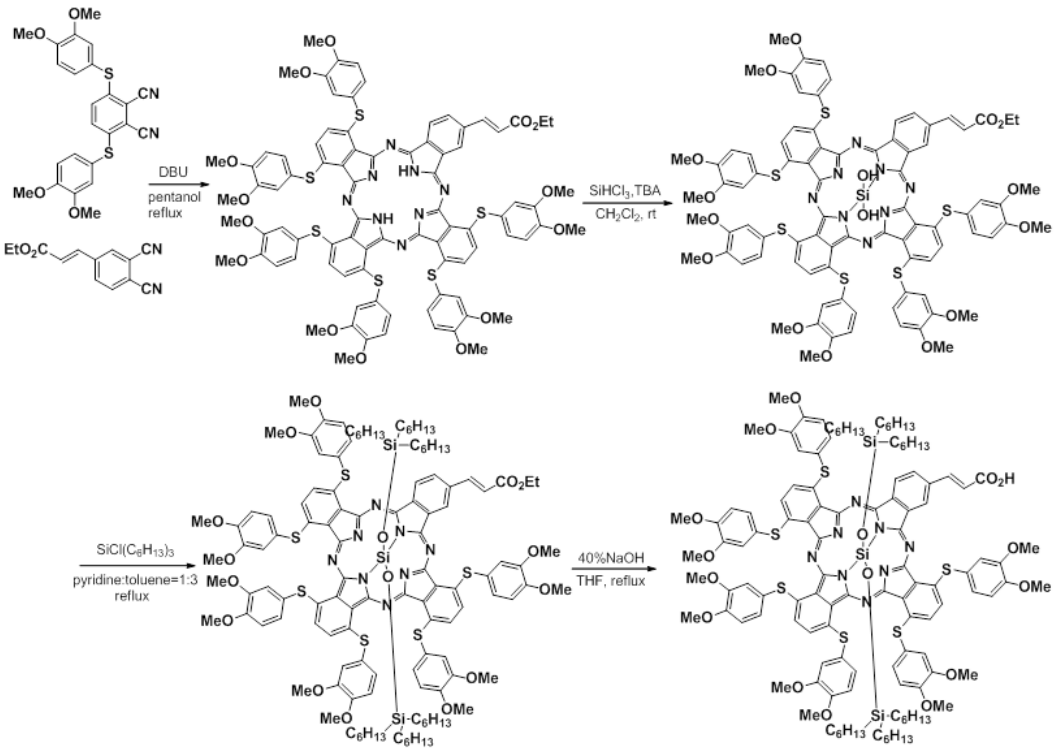

Figure 1: Scheme of synthesis of sensitizer PC25 used in bottom cell of various tandem DSSCs architectures.

ACHIEVEMENTS

PUBLICATIONS (*Corresponding Author)

1. **Ajay K. Baranwal***, N. Fujikawa, A. Hayat, S.S. Pandey, Y. Ogomi, T. Ma and S. Hayase*,"Combining Novel device architecture and NIR dye towards the fabrication of transparent conductive oxide-less tandem dye sensitized solar cell", **Applied Physics Express**, 2015,8,102301. (**Impact factor: 2.365**)

2. **A.K. Baranwal***, T. Shiki, Y. Ogomi, S. S. Pandey, T. Ma and S. Hayase*,"Tandem dye-sensitized solar cells with a back contact bottom electrode without a transparent conductive oxide layer " , **RSC Advances,** 2014, **4**, 47735-47742. (Cited in Progress in Photovoltaics: Research & Applications: Photovoltaics literature survey (No. 115)) (**Impact factor: 3.84**)

CONFERENCE PRESENTATIONS

1. **Oral: Ajay K Baranwal,** Naotaka Fujikawa, Yuhei Ogomi, Shyam S. Pandey, Tingli Ma and Shuzi Hayase; Tandem Dye-Sensitized Solar Cells based on back contact bottom electrodes; **IJEGMBE-2015, 22-25 December 2015, Nakamura Centenary Memorial Hall, Kyutech, Japan.**

2. **Oral: Ajay K Baranwal**, Naotaka Fujikawa, Yuhei Ogomi, Shyam S. Pandey, Tingli Ma and Shuzi Hayase; TCO-less Tandem DSSC with ITO-PET as an Intermediate Layer Featuring Enhanced Spectra; **ICMAT2015 & IUMRS-ICA2015, 28 June-03 July 2015, SunTec Singapore.**

3. **Oral: Ajay K Baranwal**, Naotaka Fujikawa, Yuhei Ogomi, Shyam S. Pandey, Tingli Ma and Shuzi Hayase; TCO-less Tandem dssc featuring enhanced spectra with new architectures; The **62nd JSAP spring meeting, March 11-14, 2015, MatsuyamaTokai University, Shonan campus, Tokyo, Japan.**

4. **Oral**: **Ajay K Baranwal,** Naotaka Fujikawa, Yuhei Ogomi, Shyam S Pandey, Tingli Ma and Shuzi Hayase; Extended Spectral Photo Response utilizing TCO-less Tandem DSSC; The **75th JSAP autumn meeting, Sept. 14-20, 2014, Hokkaido University, Sapporo campus, Hokkaido, Japan.**

5. **Oral: Ajay K Baranwal**,Tsubasa Shiki, Yuhei Ogomi, Shyam S. Pandey, Tingli Ma, and Shuzi Hayase;Tandem dye sensitized solar cells utilizing back contact transparent conductive oxide-less (TCO-less) bottom electrodes; **The 15th IUMRS-International confrence in Asia (IUMRS-ICA 2014), Aug. 24-Aug. 30, 2014, Fukuoka University, Fukuoka, Japan.**

6. **Poster**: Ajay K Baranwal, Tsubasa Shiki, Yuhei Ogomi, Shyam S. Pandey, Tingli Ma and Shuzi Hayase,Tandem Dye Sensitized Solar Cells based on TCO-less Bottom Electrodes, **The 51th Kyushu Branch Chemical Society Meeting, June 28, 2014, Kitakyushu, Japan.**

Acknowledgement

First of all, I would like to thank Prof. Shuzi Hayase for giving me opportunity to work under him as PhD scholar. His immense depth of knowledge and insight into the work have pave the excellent background in this work. His charming personality always motivate to tackle the challenges very easily.

I would like to thank Prof Pandey for his valuable suggestions and fruitful discussion. His enthusiasm and faith in me have created a true passion for work in this field and inspired me to see through all the setbacks I experienced along the way. I would like to add on that his kind and supportive nature has make my stay in Japan very lively. My truthful thank to Prof Ma for fruitful suggestions and discussions regarding my carried research work on. My sincere thanks to Prof Takashima, Prof Ogomi for their support in experiments carried out.

I am very thankful of Mr. Naotaka Fujikawa for synthesizing the dye for my research work. I acknowledge Dr Temuri Nishimura, Mr Takuya Morimoto, Mr Moriya Sohei, Mr Sakamoto for their helping nature and making the lab atmosphere very healthy and charming.

I would also like to thank my lab colleague Dr Kapil, Dr Zaman, Dr Hayat and Dr Tarun for their nice company during my PhD work.

I express my sincere thanks to Mr Gyanendra, Mr Balbeer, Mr Reeturaj making my Japan stay pleasant.

I am very greatful to Kyushu Institute of Technology for making my stay in Japan pleasant and memorable. Particularly I would like to thank Ms Yasuko Nagamatsu for kind support provided.

Moreover, I heartily thank to my parents (Mr Ramniwas, Mrs Shanti Devi), elders (Mr Krishn, Mr Sanjay), Sister in laws (Mrs Amita, Mrs Parul), Brother in laws (Mr Madhuresh, Mr Pawan, Mr Vikash), sisters (Mrs Krishna, Mrs Sadhna, Mrs Sony) and nephew (Aasta, Ekansh, Chhoti) for their support and trust on me.